

**Collective Effects of Particle
Dynamics in the Planetary Rings**

THESIS SUBMITTED FOR THE DEGREE
OF
DOCTOR OF PHILOSOPHY (SCIENCE)
OF JADAVPUR UNIVERSITY

SUBMITTED BY
ABHIJIT BHATTACHARYYA

DEPARTMENT OF PHYSICS
JADAVPUR UNIVERSITY
CALCUTTA - 700 032

Collective Effects of Particle Dynamics in the Planetary Rings

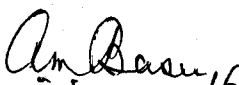
THESIS SUBMITTED FOR THE DEGREE
OF
DOCTOR OF PHILOSOPHY (SCIENCE)
OF JADAVPUR UNIVERSITY

SUBMITTED BY
ABHIJIT BHATTACHARYYA

DEPARTMENT OF PHYSICS
JADAVPUR UNIVERSITY
CALCUTTA - 700 032


CERTIFICATE

This is to certify that the thesis entitled "Collective Effects of Particle Dynamics in the Planetary Rings" submitted by Abhijit Bhattacharyya who got his name registered on Aug 06, 1998 for the award of Ph. D.(Science) degree of Jadavpur University, is absolutely based upon his own work under supervisions of Dr. A. M. Basu of Department of Physics, Jadavpur University and Prof. Sandip K. Chakrabarti of the S. N. Bose National Center for Basic Sciences, and that neither this thesis nor any part of it has been submitted for any degree/diploma or any other academic award anywhere before.


Dr. A. M. Basu 16.8.01
Signature of Supervisor

Date with Official Seal

DR. A. M. BASU
ASSISTANT PROFESSOR IN PHYSICS
JADAVPUR UNIVERSITY
CALCUTTA—700 032

 16.8.2001

**Prof. Sandip K.
Chakrabarti**

Signature of Supervisor

Date with Official Seal

Prof. Sandip K. Chakrabarti
Associate Professor
S. N. Bose National Centre
FOR BASIC SCIENCES
Block, Salt Lake, Calcutta-700 098

Dedicated to my Parents

Abstract

Planetary Rings consist of particles of size ranging from micron to a few meters. These particles are under a large number of forces: 1. gravity of the planet pulling the particles toward the center, 2. gravity of the moons pulling the particles outward and often upward or downward from the plane of the ring, 3. self-gravity of the ring which pulls the matter down to the plane etc. apart from collisional effects. We write down the equations of motion of a particle in a rotating frame as well as on the inertial frame and solve these equations both numerically and analytically using perturbative methods. We find that there is a considerable shear in the vertical direction even within the ring itself and the dissipation it causes can damp excitations due to moons within a couple of hundreds of kilometers. We concentrate on the damping property of the vertical bending waves which are excited by nearby moons orbiting in inclined orbits and show that for reasonable parameters of the ring, the damping of the bending wave due to Titan in Saturn's C ring could be explained. Our procedure is general and could be applicable to all the planetary rings. For micron sized particles Lorentz force should also be included since this force becomes comparable to other force components.

In this thesis, the Chapter 1 describes an introduction to the subject of planetary ring, narrating the types of rings observed in astrophysics, the chronological description of planetary ring study and the motivation of choosing the subject.

The Chapter 2 describes the origin of planetary ring systems using two most popular models accepted by the scientists and some basic principles like the Roche limit and the coagulation of particles. It also describes some basic features ringed planets including their information on rings and satellites. Lastly a comparative study is given.

The Chapter 3 describes the resonance and the spiral waves observed in the planetary rings. Since the planetary ring has a close resemblance with the galactic disk, a brief comparative analysis is discussed. Basic physics behind the resonance is given. Spiral waves are of two types like density waves and spiral bending waves. A brief mathematical description of density wave is given. Later spiral bending wave is discussed. Since our work is on the bending wave, the description of bending wave is discussed in two categories. At first the bending wave is studied using the particle dynamics

and the locus of a particle in the warped ring is measured with reference to the coordinate system attached to the midplane of the warped ring. Then the shear developed is measured. Here particle collision is not considered. However, the shear observed in this study is due to the choice of the coordinate reference frame in the midplane of the warped ring. The damping length of the bending wave matches to some extent on the observational data. However, some discrepancies are observed where the source of error creeps in due to insufficient data obtained on the surface mass density, wave amplitude etc. Next, the fluid dynamics is used assuming the disk having thickness as infinitesimally small and a dispersion relation is obtained.

The Chapter 4 describes the study of Titan -1:0 resonance using our numerical modeling using FORTRAN codes and then comparing data with the analytical studies. Titan -1:0 resonance is considered as our object of study as it is the the only known one-armed bending wave that propagates outwards, away from the Saturn, and yet observed in which the wave pattern rotates opposite to the orbital direction of the ring particles. The analytical studies are done in two ways, with and without binning. Binning in the phase-space indicates the population of particles visited a particular bin. Since one may study N-particle simulation to get a realistic picture of the ring, one has to solve equations for those N particles and which is a very time and memory consuming thereby limiting on the maximum number of particles for study. Hence, in that respect, the idea of using a single particle and later introduction of bins in the phase space will literally produce the effect of N particles. However, the problem lying with the binning is how to fix the walls of the bins in the phase-space?

The Chapter 5 describes the result of analytical study considering damping length as a function of surface mass density with ring height as a parameter for Titan -1:0 resonance and comparison with observed data is also provided.

The Chapter 6 describes the main conclusion of the thesis on the bending wave observed in the planetary ring.

Acknowledgment

The starry night sky is an attraction to mankind since the Stone age. The distance from our Earth, gradual change of starry curtain in every night etc. acted as catalysts to sustain the quest for celestial objects through ages even till today. Today, our computer systems may get flooded with the data about celestial objects using space-probes. We are just thriving to see the wall of the Universe speculating the distance of the farthest object. Though we are just probing for most distant and enigmatic objects, the most interesting point to note is that still we have lots of unsolved mysteries regarding our nearest neighbors like planets in our Solar system. One of these problems relate to the existence of the planetary ring systems. I tried to study only a small fraction of the problems on the planetary ring systems. I am grateful to my guides to allow me to work on this astrophysical problem.

I am grateful to Dr. Anandamohan Basu, one of my co-guides, for allowing me to study on this interesting feature while I was also working to set-up one experimental plasma research laboratory at the Department of Physics, Jadavpur University.

The interest to the problem which we addressed in this thesis has grown by my other co-guide Prof. Sandip K. Chakrabarti. Being an astrophysicist, he tried to let me understand the basic problem and the physics associated with it. He also permitted me to use the computer facility at the S. N. Bose National Center for Basic Sciences.

It would not have been possible to write this thesis without kind help from my guides.

I sincerely thank Dr. Manoranjan Khan, Faculty of Science, Jadavpur University who has constantly inquired to me about the progress of my work and also extended his kind cooperation beyond certain limits to ease my work with less tension.

I thank Samiran Ghosh, Tushar Chaudhuri and Indrajit Sadhukhan for their valuable suggestions given to me while preparing the manuscripts.

I am earnestly grateful to Debuda (Debajit Kundu) who solved some of my unending problems in my personal life while I was working as fellow. I also thank sincerely Prasanto-da and Kartick-da of our departmental library who helped me to access books beyond limits.

I am grateful for ever to my mother who managed to tackle all the problems at our home without disturbing me in spite of her sever illness. I could complete my work earnestly only with her blessing. I thank my

little sister Roma constantly watched me to avoid my forgetfulness. It was impossible for me to finish my work without their constant help and inspiration.

I thank all with my heartiest gratitude.

Contents

1	Introduction	1
1.1	Historical Background	5
1.2	Types of Astrophysical Disks	7
1.2.1	Galactic Disks	7
1.2.2	Stellar disk - the accretion disk	8
1.2.3	Planetary disk system	8
1.3	Motivation of the Present Study	9
2	The Planetary Rings	11
2.1	The Origin of the Rings	11
2.1.1	The Roche limit	12
2.1.2	The Coagulation Model	16
2.1.3	The Break-up Model	19
2.2	Ring Characteristics	22
2.2.1	The Jovian system	23
2.2.2	The Saturnian system	25
2.2.3	The Uranian ring	29
2.2.4	The Neptunian ring	29
2.2.5	Comparative Analysis	30
3	Resonance and the spiral waves	33
3.1	Basics of Orbits and Resonances	34
3.2	Galactic disks and planetary ring	36
3.3	Spiral Density Waves	38
3.4	Spiral Bending Waves	42
3.4.1	The Particle Dynamics	43
3.4.2	The Fluid Dynamics	56

4	The Numerical modeling	63
4.1	Introduction	63
4.2	Observed features at the -1:0 nodal bending wave . . .	64
4.3	Numerical Simulation Procedure	66
4.4	Results of numerical simulation	68
4.5	Numerical modeling of analytical expressions	71
4.6	Results for binning of analytical expressions	72
4.7	Concluding Remarks	72
5	Analytical Studies	83
5.1	Introduction	83
5.2	Model Equations	84
5.3	Computation of the Shear components	87
5.4	Results for various ring conditions	89
5.5	Conclusion	90
6	Conclusion	93

List of Figures

2.1	Nature of tidal force acting on the satellite	12
2.2	Saturn's ring as taken from Hubble's space telescope	27
3.1	Geometry of bending waves	44
4.1	Simulation for Titan -1:0 resonance	69
4.2	Damping length vs Optical depth for Titan -1:0 resonance simulation	70
4.3	Shear vs. Position along Z-axis for Titan -1:0 resonance simulation for $h = 500, \sigma = 0.4$	73
4.4	Population vs. Position along Z-axis for Titan -1:0 resonance simulation for $h = 500, \sigma = 0.4$	74
4.5	Shear vs. Position along Z-axis for Titan -1:0 resonance simulation for $h = 750, \sigma = 0.4$	75
4.6	Population vs. Position along Z-axis for Titan -1:0 resonance simulation for $h = 750, \sigma = 0.4$	76
4.7	Shear vs. Position along Z-axis for Titan -1:0 resonance simulation for $h = 750, \sigma = 0.4 \epsilon$ fed in	77
4.8	Population vs. Position along Z-axis for Titan -1:0 resonance simulation for $h = 750, \sigma = 0.4\epsilon$ fed in	78
4.9	Shear vs. Position along Z-axis for Titan -1:0 resonance simulation for $h = 750, \sigma = 4.5$	79
4.10	Population vs. Position along Z-axis for Titan -1:0 resonance simulation for $h = 750, \sigma = 4.5$	80
5.1	Surface mass density (σ) [gm/cm^2] vs damping length [cm] for different ring heights h . Observed damping length of 85km is shown for comparison.	91

5.2 Surface mass density (σ) [gm/cm^2] vs log(damping length [cm]) [cm] for different ring heights h . Observed damping length of 85km is shown for comparison. 92

List of Tables

2.1	Numerical models of primitive circumplanetary disk . . .	15
2.2	Coagulation time scale	18
2.3	Summary of dynamical time scales	18
2.4	Useful physical parameters for Jupiter	23
2.5	The Jovian satellite system	24
2.6	Ring characteristics of Jovian system	24
2.7	Useful physical parameters for Saturn	25
2.8	The Saturnian satellite system	26
2.9	Main physical properties of Saturn's ring system	28
2.10	Useful physical parameters for Uranus	30
2.11	The Uranian satellite system	31
2.12	Useful physical parameters for Neptune	32
2.13	The Neptunian satellite system	32
4.1	Results of analytical expressions after binning	81

Chapter 1

Introduction

In the Universe practically everything rotates and every rotating self gravitating object flattens to become a disk. The flattening of the rotating system is basically due to the opposite action of two major dynamic forces - the gravitational and the centrifugal forces. To maintain the equilibrium, the system is forced to flatten along the axis of rotation. However, exceptions are observed for systems having large velocity dispersion or a large pressure like spherical star clusters, star themselves etc. It is to be noted here that collisional and collisionless systems are totally different. In spherical systems with dissipation or inelastic collisions, the high thermal velocities of the particles decrease through friction or shocks leading to formation of disks. This process is much slower in almost collisionless stellar system. If the collisionless stellar systems have a relatively large rotational angular momentum, theoretically it is possible for them to become a disk provided various instabilities develop naturally on a dynamical time scale. This means that stable systems do not evolve into a flat disk.

Theoretical calculations regarding disk modeling [4, 13, 14, 21, 22, 44, 70], usually, consider thin disk approximation which signifies that the ratio of disk height ' h ' to its distance ' R ' from the central gravitating object like planet should be very much smaller than unity *i.e.* $h/R \ll 1$. This approximation, in general, holds true for all galactic, circumstellar and circumplanetary rings. However, hot and thick accretion disk are observed for accretion disks of black holes and other binary systems. Physically the approximation ' h/R ' signifies

that the disk considered by us behaves as “cold” disk and the pressure gradient is comparatively much smaller than two main dynamic forces - the gravitational and the centrifugal forces. To understand the effect of pressure gradient, let us consider the Euler equation as,

$$\frac{d\mathbf{v}}{dt} = \frac{\partial\mathbf{v}}{\partial t} + (\mathbf{v}\cdot\nabla)\mathbf{v} = -\frac{1}{\rho}\frac{\partial P}{\partial\mathbf{r}} + \mathbf{F}. \quad (1.1)$$

where \mathbf{F} is the force per unit mass acting on the disk particles such that,

$$\mathbf{F} = \mathbf{F}_{grav} + \mathbf{F}_{centrifugal} = -\nabla\Phi(\mathbf{r}, t) + \mathbf{F}_{centrifugal}. \quad (1.2)$$

If $h/R \ll 1$, $\frac{1}{\rho}\frac{\partial P}{\partial r} \ll F$. Also the condition $h/R \ll 1$ limits the characteristic scale length L of spatially regular structures such that $L : h \leq L \leq R$. Hence the smaller the ratio h/R , the more characteristic scales one can fit into the range between h and R and the richer will be the possibilities for the formation of structures in an astrophysical disk system.

Besides the gravitational and centrifugal force terms, other actively operating forces include thermal and viscous mechanisms, self-gravity of the disk itself and the electromagnetic effects. At the equilibrium gravitational attraction by the central gravitating object and the outward centrifugal force balance each other resulting in the interesting features of weaker mechanisms playing in the disk make it dynamical and evolving which make study of the disks as important.

The astrophysical disks become more interesting due to presence of differential rotation [28] within the disk itself. At equilibrium, the gravitational attraction between the disk and the massive central body balances the centrifugal force originated due to rotation, following Kepler’s law. In that case, the angular velocity of the disk is $\omega = \sqrt{\frac{GM}{r^3}}$ i.e. $\omega \propto r^{-3/2}$ where r is the distance between the disk and the central object. The disk is then termed as “Keplerian disk”. The effect of differential rotation originates for a ring of width δr such that angular velocity for the portion of the disk nearer the central object $\omega_1 \propto r^{-3/2}$ while that for the portion furthest from the central object is $\omega_2 \propto (r + \delta r)^{-3/2}$. The differential rotation $\delta\omega = \omega_1 - \omega_2$ produces a shear on the particles within the disk causing deformation. Physically, this means a large scale flow of shear .

Circumstellar and circumplanetary ring systems have viscosity. Viscosity, in conjunction with the rotational shear of disk, is a constant energy source within the disk and transfers energy from this large-scale shear flow *i.e.* the orbital energy of the disk into heat which is manifested as random motion of particles within the disk. The power of energy source, for example, in case of Saturnian ring system is about $100kW$. This production of energy by viscous dissipation in the disk makes it possible to develop various instabilities and formation of regular spatial structures - "Self - organization" of the systems.

The effect of viscosity means effect of collision among particles. In a planetary ring with a moderate optical depth, a particle usually travels over a distance comparable to the circumference of an orbit between successive collisions. However, most of this journey is traveled in the tangential direction. Since our primary interest is on the efficiency of diffusion in the radial direction, the typical radial excursion between successive collisions may be regarded as the relevant scale for the mean free path. If a typical particle experiences at least two collisions per orbit around the central planet *i.e.* $\omega_c \geq \Omega/\pi$ *i.e.* $\tau \geq 1$, the radial mean free path may be approximated as $\lambda = c/\omega_c$, where c is the velocity of dispersion. If the number of particles in a ring is relatively sparse *i.e.* $\tau \ll 1$, the collisional frequency may be assumed to be small compared with the orbital frequency. Here the radial movement of the particle is bounded by the orbital eccentricity e so that the mean free path approaches the upper limit $ae \simeq c/\Omega$ where a is the semi-major axis of the orbit. For arbitrary value of τ both limiting values of λ [16, 28] may be given as,

$$\lambda^2 = \frac{c^2}{\Omega^2(1 + \tau^2)}. \quad (1.3)$$

For a typical particle, the mean radial excursion after n such collisions may be approximated by the random walk expressions, $\Delta r = n^{1/2}\lambda$. Thus the time scale t_{rw} required for a typical particle to randomly walk over a distance Δr is given by,

$$t_{rw} = \frac{n}{\omega_c} = \frac{1 + \tau^2}{\tau} \left(\frac{\Delta r}{c} \right)^2. \quad (1.4)$$

In combined presence of viscosity and differential rotation, a viscous stress is developed that leads to an outward transfer of angular momentum and a general radial spreading of the ring. The efficiency of angular momentum transfer is determined by the magnitude of the viscosity ν . If $\nu = f(r)$, the timescale for spreading in the radial direction [47] is $t_v \simeq (\Delta r)^2 / \nu$, as long as the radial spreading is small enough so that there is no substantial change in ν . In general, viscosity is given by $\nu = \omega_c \lambda^2$ so that the time scale for radial spreading is given as,

$$t_v \simeq \frac{1 + \tau^2}{\omega_c} \Omega^2 \left(\frac{\Delta r}{c} \right)^2. \quad (1.5)$$

The kinetic and fluid treatments of diffusion process indicate the dependency of ν on both τ and c . Consider two neighboring particles having nearly circular orbits separated by a radial mean free path. The difference between their pre-collisional circular velocities is of the order $\lambda\Omega$. After a collision, they will each acquire an orbital eccentricity of the order of $\lambda/c = c/\Omega a$. The energy change per unit mass associated with this gain in the eccentricity is of the order of $(\lambda/a)^2 = \lambda^2\Omega^2$. As the kinetic energy per unit mass associated with eccentric motions i.e. c^2 , its rate of change may be determined as $\dot{E}_t \simeq c^2\omega_c \simeq \lambda^2\Omega^2\omega_c$. In a fluid mechanical theory, this tendency for increasing c is normally attributed to the effect of viscous stress. In a differentially rotating disk, this viscous stress continually converts energy from that stored in the systematic shearing motion into that associated with random motion

$$\dot{E}_t = \nu \left(r \frac{\partial \Omega}{\partial r} \right)^2 \quad (1.6)$$

at a rate per unit mass given by Eq. 1.6, which is of the order $\nu\Omega^2$ for the Keplerian orbits. In the absence of any dissipative process, the particles would be “heated up” in the sense that the dispersion velocity would increase indefinitely. However, typical collisions between particles within the ring are partially inelastic, resulting in the dependence of the coefficient of restitution of the matter of the ring grains.

Also the last but not the least interesting fact about the disk systems is that they have very long life time. It is natural to see that the ring should disperse, while in reality rings have distinct boundaries.

In the present work, let us discuss only the planetary ring system. Especially, the collective behavior of ring particles will be addressed using numerical and analytical modeling.

1.1 Historical Background

The physics of planetary ring system is interesting for its classical dynamic and evolving nature. Rings and disks became a part of astronomical discussion only in the seventeenth century. In 1644, René Descartes introduced the idea that the whole space in the Universe is filled with vortices of invisible matter and there is no space left without vortex. Therefore the Earth had a vortex extending to and including the Moon. Galileo discovered four Jovian satellites in 1610. In 1655, Christian Huygens discovered a satellite of Saturn about which he published in 1659 [37].

Huygens, believing on the Cartesian model, compared the vortices of the Earth and the Saturn. In case of Earth, rotational period about its own axis is one day while for the Moon, the orbital period about is slightly more than 28 days. Huygens also measured that the orbital period of Saturn's moon is about 16 days. He concluded that the rotational period of Saturn is around half-a-day. Hence, all the matter between the Saturn and its moon had to rotate with the period between half-a-day and 16 days. But, it has been observed that the "handles" or ansae, although show slow changes over many years, remain unaffected over a period of 16 days. Huygens then concluded that Saturn must be surrounded by a ring system [37]. Huygens wrote "It is girdled by a thin flat ring, nowhere touching, inclined to the ecliptic". He even predicted the future dates for disappearance of the rings: July 1671, March 1685 and December 1700. The rings properly disappeared in accordance with Huygens' predictions, confirming the correctness of his theory.

The structure of Saturn's ring system was again questioned as sometimes the ansae was observed as handles and sometimes not. A solid thick ring structure could not explain all those phenomena. At last the debate between Fabri and Huygens concluded that the ringlike structure of Saturn could be either due to vapor/fluid or collection of

dust particles of varying sizes [77]. In 1675, J. D. Cassini observed that the ring system was divided by a dark band which was later named after name as *Cassini's gap*. In 1785, Laplace showed that a solid ring, in uniform rotation, would break apart under the action of *centrifugal forces* and the system would probably have to consist of a large number of independent "ringlets" [41].

In 1847, Roche discovered an important analysis for stability of ring system – the Roche Limit [58]. Roche determined that within a certain limit from the planet, any satellite and presumably also any ring would be torn apart by the tidal forces. Saturn's ring system lie within that limit [19]. In 1848, C ring was discovered. It was observed that Saturn was visible even through the C ring. Saturnian ring system provided one of the best classical system to study leading to Maxwell's classic essay in 1857 that conjecture that Saturn's ring system could only consist of an indefinite number of very small particles [2]. The theory also conjectures that the stability of the system also requires countless independently orbiting satellites. Also, later, Keeler and Campbell spectrographically measured the Doppler shift and thus the Keplerian orbital velocities of constituent particles.

In 1866, Kirkwood initially suggested resonant perturbations by Jupiter caused the radial gaps and clumps in the asteroid belts. In 1867 he extended his theory to the Cassini division and in 1871 to Encke's division [55]. During the late nineteenth century, observers visually noted many elusive subdivisions in both the A ring and B rings, and also numerical extensions of Goldsborough [27] who extended it to the outer edge of the A ring and the inner edge of the B ring [21, 22].

Observations of the brightness attributable to the rings [52] has clearly demonstrated a strong brightening with decreasing phase angle, the so called *opposition effect*. Seeliger [62, 63] explained the effect in the light of Maxwell's many-particle ring as due to variations in mutual shadowing by these many particles in a layer significantly thicker vertically than the size of a typical particle. This concept has come to be known as the classical, or many-particle -thick, ring model.

Improved ground-based observations gradually revealed structural and orbital details, like topologically flat but spread out structures, op-

tical transmission through the rings, structural variation with radius, different reflectivity depending on wavelength and observational geometry. It was easy to model theoretically for the smooth and continuous ring structures. However, since 1977, the idea changed abruptly as nine narrow black ringlets were discovered around Uranus. Prof. J. C. Bhattacharyya discovered [6] rings as they occulted a star observed from the Earth. In March and July 1979, very diffuse thick rings were discovered around Jupiter by the Voyager spacecraft. Even waves developed in rings have also been observed. At present we have swarms of data obtained from spacecrafts like Cassini, Voyager 1 and Voyager 2, Pioneer 10, 11, Ulysses etc.

1.2 Types of Astrophysical Disks

In general, astrophysical disks may be classified into three classes: (1) galactic disks, (2) disks around stars and (3) planetary disks. Though the main theme of this thesis is the planetary ring systems, other systems are reviewed for comparative analysis as far as physical processes are concerned.

1.2.1 Galactic Disks

The history of galaxies starts with Galileo in 1610, when he described in his "Stellar Herald" that "The Milky Way is an accumulation of countless stars". In 1750, Wright in his booklet "Original Theory or New Hypothesis of the Universe" interpreted the Milky Way as a disk-shaped galaxy as seen from inside and bright nebulae as accumulations of faraway stars like our own Galaxy. In 1845, Lord Rosse discovered M51 galaxy and found it to be a spiral galaxy. In 1929, Hubble discovered the recession of galaxies, i.e., the expansion of the Universe. He also became the father of the present-day galactic classification systems.

From the whole range of galaxies, our interest is only to those galaxies which have disk-shaped components. A typical spiral galaxy is a set of disks of stars, gas and dust embedded in a spherical halo. Further discussions on galactic disk will be found in Page 36.

1.2.2 Stellar disk - the accretion disk

The disk around a star is basically an accretion disk formed in a binary system. The evolution of a component in a close binary system often leads to one of the stars increasing in size to become a *red giant* and filling its Roche lobe. This means that matter from the surface of that red giant starts to flow out in the form of a jet – mainly through the inner Lagrangian point – into the attraction sphere of the second star. The non-vanishing angular momentum of the outflowing matter leads to the formation of an accretion disk around the second star [36, 57]. Study of accretion process started with Bondi [7].

An analysis of the luminosity curve of a binary star makes it possible to establish accurately the geometry of the binary system and to detect whether there is a disk within it [15]. In the binary system, the viscosity of gaseous accretion disk is very large due to turbulence [23].

The shape of the accretion disk depends on the balance between heating and cooling. The disk is heated by the incident jet of matter from the companion which possesses a large amount of kinetic energy, the viscous dissipation of orbital energy, and the radiation of stars in the system. It is cooled by the emission from its surface. Efficient cooling leads to the formation of a thin disk. The dynamics of thin accretion disk becomes more interesting due to launching of spiral waves by the resonating action of neighboring star(s). If the heating source turns out to be more powerful, the disk becomes thick and looks like a torus [36].

Accretion disks are also observed for more compact objects like *black hole* [64]. There are also more exotic variants of accretion disks of stars themselves which surround massive black holes in *Active Galactic Nuclei*(AGN). An accretion disk in such a system is a powerful source of radiation, processing an appreciable fraction of the rest mass of matter falling onto the black hole into quanta and it is one of the most efficient energy sources of our Universe.

1.2.3 Planetary disk system

It is very curious that only four planets in the Solar system have rings. They are Jupiter, Saturn, Uranus and Neptune. It is also interesting

to note that these planets have higher numbers of satellites. Rings observed are, generally very distinct, containing particles of varying size. Particles having size of the order of micron are subjected to forces like gravitational, centrifugal, Lorentz force, radiation pressure, background dragging, self gravity of the disk and satellite forcing while for particles of larger size, the locus of the particle is determined by the gravity alone. Hence, in general, all the ring structures around the planets may be divided into two categories: “primary” and “secondary” rings. Primary category contain dense rings with rather large particles – upto several meters in size. These rings have a rather longer life time. They include A, B and C rings of Saturn, nine dense Uranian ring, the primary Neptunian rings including Adams ring with segments and the main Jovian ring with larger particles. The secondary ring type are rarefied gaseous dusty rings which need a constant influx of matter in order to exist for a long time. The E and G ring of Saturn, the gaseous torus on the orbit of Io and the rarefied Jovian rings - the halo and the gossamer and faint rings belong to the secondary category. A detailed view will be given in Chapter 2.

1.3 Motivation of the Present Study

The astrophysical disk systems are the practical experiences of complex systems of classical mechanics. Especially, the planetary rings are not only the most complex, they are also nearest so that we may get a large amount of data using space and ground-based probes. The planetary rings are also similar to larger systems like galactic disks except that they have smaller scales. Theories made on the structures of planetary ring systems can be safely applied on other systems. One of the fundamental problem of the physics of the planetary rings is to find the dynamics of a typical particle within the ring. This motivates us to work on the planetary ring system. In this thesis, particle dynamics within the planetary ring to produce collective effects – especially the formation of waves. Our main attention is for the spiral bending wave in the planetary ring systems has been discussed. We analysed the bending wave for Titan -1:0 resonance. The importance of studying this mode is that it is the only known bending wave that

propagates outward, away from the Saturn having only one arm and the wave pattern rotates opposite to the orbital direction of the ring particles. In the C ring, there is no other observed bending wave till today. However, the thickness of the C ring is not yet determined with accuracy as far as the damping length of the wave is concerned. The damping length observed from Voyager radio occultation data indicates outside the wave region, the surface mass density is of the order of $\sim 0.4 \text{ gm} - \text{cm}^{-2}$ and a local ring thickness is of the order [59] of ≤ 5 meters. Still there is some discrepancy in theoretical modeling and observed data. However, we analysed this case with first numerical simulation with the FORTRAN codes and then we analysed with the analytical models to tally the physics behind the ring problem.

Chapter 2

The Planetary Rings

So far, it was clear to some extent that rings are formed from particles of varying sizes and mass. However, it was not clear how and why the rings were formed. So, at present there are three basic questions those come to mind, namely:

- Where does the matter come from to form the rings?
- Why are the particles limited in size, and, why do the rings not agglomerate into satellites?
- What determines the boundaries of the rings?

To seek the answers to these questions, let us discuss the origin of planetary rings.

2.1 The Origin of the Rings

In the early days, date back to early seventeenth century, it was a common belief to consider the planetary ring as the uncoagulated remnant of a circumplanetary disk from which the regular satellites were formed, In 1847, Roche [58] considered the equilibrium condition between tidal forces and the self-gravitation of a satellite and put forward the hypothesis that the Saturnian rings would be the result of the break-up of a large body through the tidal pull near the planet. To realize the hypothesis, let us turn back to review the classical Roche limit.

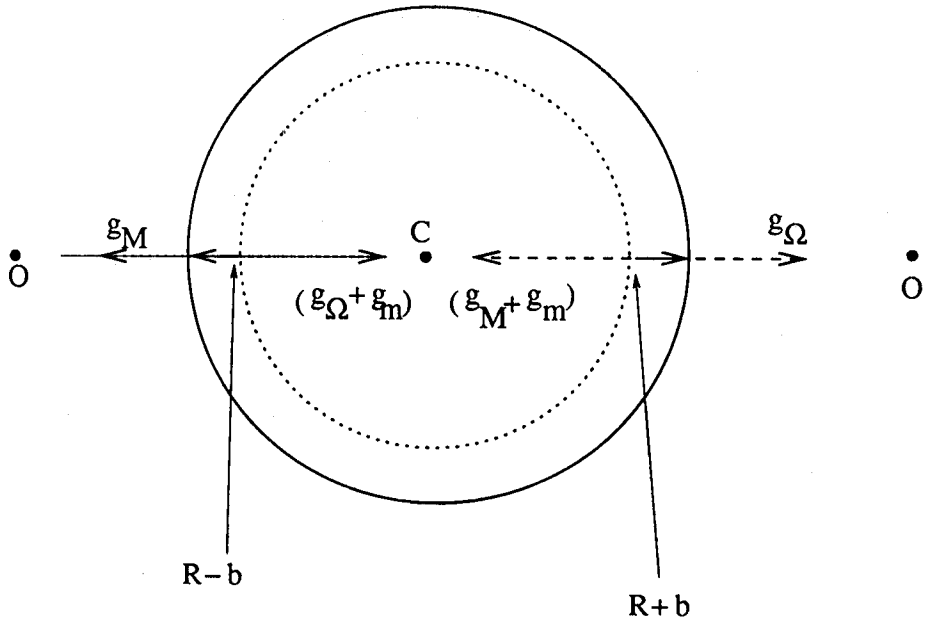


Figure 2.1: Nature of tidal force acting on the satellite

2.1.1 The Roche limit

Roche considered a satellite rotating synchronously with hydrostatic equilibrium around a planet and its main distortion is due to the tidal force and the centrifugal force.

Let us consider that the planet of mass M , radius R_p and density ρ_p is situated at the point O in the Fig.2.1. Let R be the orbital radius of the center of the mass of the satellite. Let $R \pm b$ are arbitrary points on line $\overline{OCO'}$. Let the satellite has a uniform density ρ having a spherical shape with radius r_s .

Now the gravitational acceleration is given by,

$$g = \frac{GM}{R^2}. \quad (2.1)$$

which opposes the centrifugal acceleration

$$f = \Omega^2 R. \quad (2.2)$$

Hence for any pair of interior points of satellites $R \pm b$ lying on $\overline{OCO'}$,

the resulting acceleration becomes

$$\begin{aligned} g_{\Omega} + g_M + g_{m(b)} &= \Omega^2 (R \pm b) - \frac{GM}{(R \pm b)^2} \mp \frac{Gm(b)}{b^2} \\ &= \pm \left(3\Omega^2 - \frac{4}{3}\pi G\rho \right) b, \end{aligned} \quad (2.3)$$

where, g_{Ω} =the centrifugal acceleration, g_M =the gravitational acceleration in the field of the planet, $g_{m(b)}$ =the gravitational acceleration due to the central part of the mass of the satellite inside the (constant) radius b , $m(b) \equiv \frac{4}{3}\pi\rho b^3$, $b \leq r_s$ and r_s is the radius of the satellite.

From Eq. 2.3, it is clear that the left hand side must be positive and so from the right hand side we observe that,

$$3\Omega^2 > \frac{4}{3}\pi G\rho \quad (2.4)$$

should be satisfied and the resulting acceleration at the points $R \pm b$ is directed away from the sphere b =constant. Hence the condition given by the Eq. 2.4 is the necessary and sufficient condition for the break-up of the hydrostatically stable “fluid” satellite when the intermolecular cohesive forces are not considered.

Let us consider the outer limit for Roche zone be R_R inside which a self-gravitating satellite is broken up by the tidal forces. Then in the equilibrium condition,

$$\begin{aligned} \frac{Gm}{4r_s^2} &= 2\pi G \left(\frac{R_p}{R_R} \right)^3 \rho_p \times 2r_s + 2\pi G \left(\frac{r_s}{4r_s} \right)^3 \rho \times 2r_s \\ \text{or, } R_R &= 2.4535 \left(\frac{\rho_p}{\rho} \right)^{\frac{1}{3}} \end{aligned} \quad (2.5)$$

$$\text{or, } R_R = 1.52 \left(\frac{M}{\rho} \right)^{\frac{1}{3}}. \quad (2.6)$$

The Roche model provided by Eq. 2.5 is interesting and also provides answer to all questions asked at the beginning of this Chapter. The replies may be given as: the material of the broken-up satellite accidentally reached the danger zone could construct the rings; the tidal forces prevent the existence of satellites within the ring zone and boundary of the rings may be given by Eq. 2.5 and Eq. 2.6 such that at that radius the tidal forces are sufficiently decreased to become comparable to the self-gravitation force.

In 1947, Jeffreys [39] showed that the intermolecular cohesive force, which was neglected in the computation of Roche, becomes significant for small satellites and becomes dominating over self-gravitation and as a result he found an additional condition for the break-up of the satellite:

$$P_{max} < 1.68\rho r_s^2\Omega^2. \quad (2.7)$$

The Eq. 2.7 may be understood by considering a simple case of ice. A body of ice having tensile strength of 10^7 dyne/cm^2 will not be broken up in the Saturnian ring zone, if its radius $r_s < 200 \text{ km}$. This means, that the ring particles which are much smaller cannot be the result of a tidal break-up of a large satellite: fragments of a satellite are already stable against tidal break-up. Hence Roche hypothesis is challenged by the condensation model according to which the rings are the remnants of a circumplanetary proto-satellite cloud. The tidal force becomes one of the controlling factors to prevent accretional growth of particles by intermolecular cohesion and the resulting formation of satellites. Here it is to be noted that, even till today, it is not exactly clear whether tidal force prevents accretion or breaks up the growing particle.

It has been understood that the formation of ring and satellite is affected by the processes of formation of planets which may be grouped into two categories.

If the planets were formed by large scale gravitational instabilities like Jeans instability with rotational effects, then the entire mass of the planetary disk would collapse into a giant gaseous protoplanet on a time scale of the order of the period [11].

The second class of model requires solid core of 1 to $10 M_\oplus$ that trigger gas accumulation [51, 61]. Based on hydrostatic models, one could say that if the time scale of gas accumulation were $\leq 10^6 \text{ yrs}$, the protoplanet would be too hot to allow condensed ice to exist as close to Saturn as the present rings, and the ring material would have to be preserved as a gaseous disk for $\sim 10^6 \text{ yrs}$ after formation, or else be transported inward from a larger radius after that period of time. On the contrary, if gas accumulation took $\geq 10^6 \text{ yrs}$, ice may have been stable at the ring radius during the time of planet growth, and the storage problem would not exist.

From all these aspects, it is clear that two important cases may

Zone	Type	σ_k	R (10^{10}) cms	M (g)	σ_s (gm cm^{-2})	h (10^{10}) cm	σ_g — σ_s	ρ (g/cc)
Jupiter								
rings-V	rock	1000	1.8	10^{22}	10	0.3	100	3.10^{-5}
I-II	rock	1000	7	10^{26}	10^4	1.5	100	7.10^{-5}
III-IV	ice	250	20.0	3.10^{26}	3.10^3	3	25	3.10^{-6}
Saturn								
rings	ice	250	1.5	10^{24}	10^3	0.1	20	2.10^{-5}
I-V	ice	250	5	5.10^{24}	10^3	0.6	20	3.10^{-6}
Titan	(CH_4)	100	12	$1.4.10^{26}$	3.10^3	3	5	5.10^{-7}
Uranus								
rings	(ice)	250	0.5	10^{19}	10^{-1}	0.1	3	3.10^{-10}
I-IV	(ice)	250	6	3.10^{24}	3.10^2	1.5	3	7.10^{-8}

Table 2.1: Numerical models of primitive circumplanetary disk. Here 'zone' = Planet zone, 'Type' = types of solids, ' R ' = orbital radius, ' M ' = mass of solids, ' σ_s ' = surface density of solids, ' h ' = equivalent thickness of gas disk, ' σ_g/σ_s ' = ratio of solid to gas surface density, ' ρ ' = mid-planet gas density.

happen. If satellite formation is an efficient process, then the disk masses may have been much greater. On the other hand, if the satellite formation was concurrent with the slow growth of the planets, then the instantaneous mass of the disk may have been much less. Hence an optimum case may be considered which is presented in Table 2.1 [34].

The primary issue debated in the origin problem is, therefore, whether they represent a failure of the innermost portion of a circumplanetary disk to accumulate into satellites, or whether they are the result of the disruption of pre-existing satellites.

2.1.2 The Coagulation Model

After Jeffrey's work Eq. 2.7, people started to think that coagulation of particles by accretion process was actually responsible for ring formation. This is because the ring particles which were much smaller could not form by satellite break-up model. To verify the validity of this doctrine one needs to check time scales of various dynamical processes acting on the planetary ring/disk system.

- A proto-satellite disk is subjected to viscous shear leading to disk spreading. Ideally disk must not have any turbulence and hence timescale for viscous spreading would be $\sim 10^9$ yrs. However, in reality, due to presence of sufficient matter in the circumplanetary disk with the surface mass density $\geq 10^4$ g/cm² (cf. Table 2.1), disk would be optically thick leading to unstable disk and hence turbulence [43]. The time scale to migrate over a distance of the order of orbital radius due to viscous shear is $t \sim a^2/\nu_e$. Here, ν_e = effective kinematic viscosity $\sim (\Delta v)(\delta)/R_e$, where Δv is the turbulent velocity and is on the order of the product of the eddy scale δ times the radial gradient of the orbital velocity which is about $\Omega/2$ for Keplerian motion and R_e is the effective Reynolds number. Hence $\nu_e \sim (\delta)(\Omega/2)(\delta)/R_e = (1/2)(\delta^2\Omega/R_e)$. If the turbulence is driven by thermal convection in the vertical direction, then δ will be on the order of the vertical scale height: $\delta \sim h \equiv v_T/\Omega$. The value for the R_e is expected to be ~ 1000 [43]. The time scale in years of viscous spreading of a turbulent disk becomes,

$$t \sim R_e \frac{\Omega a^2}{v_T^2} \sim 10^5 \left(\frac{m_p}{m_\odot} \frac{a}{a_\oplus} \right)^{\frac{1}{2}} \left(\frac{100K}{T} \right), \quad (2.8)$$

where, (m_p/m_\odot) is the mass of central body in solar units, (a/a_\oplus) is the orbital radius in AU, T is the temperature of the gas disk. The dissipation time for the solar nebula itself is thus on the order of 10^5 years; while for a circumplanetary disk about Jupiter or Saturn, $t \sim 100$ year. Hence, it is questionable whether the protoplanetary accretion disk could exist as a steady state feature under these circumstances.

- If a planet experiences infall of matter from the solar nebula, both solid and gaseous components would feel drag [35]. The infalling matter may have a very little angular momentum. Harris [35] derived the rate of inward spiraling of a satellite for the case of matter arriving with no preferred angular momentum with respect to the planet, and infalling from the solar nebula with originally negligible velocity relative to the planet. Hence the rate of inward spiraling is,

$$\frac{da}{a} \cong -3 \frac{\rho_p}{\rho_s} \frac{r_p^2}{ar_s} \frac{dm_p}{m_p}, \quad (2.9)$$

where, ρ , r and m are the density, radius and mass of the planet (p) or satellite (s). The flux of mass on the satellite is

$$\frac{dm_s}{m_s} \cong -\frac{2}{5} \frac{da}{a}. \quad (2.10)$$

Harris [35] also obtained similar equations for the rate of mass gain and orbital evolution of an optically thick ring (r) subjected to mass infall as,

$$\frac{dm_p}{m_p} \cong 1, \quad (2.11)$$

$$\frac{da}{a} \cong 2 \frac{dm_r}{m_r} \cong 2 \frac{dm_p}{m_r}. \quad (2.12)$$

If such a ring existed throughout the growth of the planet, then approximately half of the total planetary mass would have arrived via the ring infall. This mass would have arrived with orbital angular momentum and hence would over-spin the planet. Thus the scenario of a growing planet continuously surrounded by an optically thick ring is contradictory to the observed spins of the planets.

- Next let us view the time scale of coagulation of the solid particles through mutual collisions [61]. The time scale for growth, assuming that all the particles stick on contact is given by,

$$t \sim \frac{m_s}{\dot{m}_s} \sim \frac{2\rho_s r_s}{\sigma_s \Omega}. \quad (2.13)$$

The coagulation time scales in the various zones of the disk models of Table 2.1 are given in the Table 2.2.

Planet	Time scale (yr) ($r_s \text{ km}^{-1}$)
Jupiter	
ring/V	3
I - II	0.05
III - IV	0.3
Saturn	
Rings	0.02
I - V	0.02
Titan	0.3
Uranus	
Rings	100
I - IV	2

Table 2.2: Coagulation time scale in models of circumplanetary disks

Therefore, we can write-up a summary of all sorts of dynamical time scale appropriate within the context as Table 2.3.

Processes	Time Scales(yr)
Viscous spreading (gas)	≥ 100
Gas drag on particulate disk	10 - 1000
Gas drag on satellite	$\sim 200 (r_s \text{ km}^{-1})$
Infall of circumsolar matter on disk	$\geq 10^{-3}$ (planet growth time)
Infall of circumsolar matter on satellites	$\geq r_s/r_p$ (planet growth time)
Coagulation/fragmentation	$\sim 0.1 (r_s \text{ km}^{-1})$

Table 2.3: Summary of dynamical time scales

In a turbulent disk, coagulation may be abandoned, although viscous spreading would help to dissipate very rapidly. For a quiescent gas, aerodynamic drag would remove a particulate disk from inside the Roche limit while small particles outside the Roche limit would coagulate with shorter time scales. Hence it is not comprehensible to

assume solid particles as small as those of the present Saturnian or Uranian rings have survived either within the Roche zone or outside for time scale of the order of 10^5 yrs should be appropriate.

The model of ring origin in which the ring mass is preserved in the form of satellites until after planet growth is complete is believed to be the correct model.

2.1.3 The Break-up Model

Harris conjectured that satellites were formed or were captured into orbits about giant planets and then spiraled inward when the planet growth was completed, and/or any circumplanetary gas was dissipated, the inward migration ceased, leaving the presently observed satellite systems, plus additional small satellites in the regions presently occupied by the rings. Such satellites would not necessarily be disrupted [1, 39], but may have persisted intact for sometime, much as the case for Phobos today [20]. However, if subsequently disrupted by a large meteoritic collisions, these small satellites would be unable to re-accumulate into larger ones, due to the planetary tidal forces, and could instead evolve collisionally into the presently observed ring system.

The time scale for the process of mutual collisions may be estimated by Eq. 2.13 where r_s should be taken to be on the order of that of the parent body ($\sim 200km$ for Saturn or $\sim 10km$ for Jupiter and Uranus). The time scales for Jupiter, Saturn and Uranus are 30 yrs, 4 yrs and 1000 yrs respectively. The collision depends on the size of the particles such that as the size of the particles become smaller and smaller, collisions become more and more gentle. Since the impact velocity between the particles should be at least on the order of the escape velocity of the larger fragments from the surface, the kinetic energy of such an impact can be equated with the limiting energy for fragmentation to define the size [32, 33], to which the largest fragments to be reduced as,

$$r \sim \left(\frac{3E_c}{4\pi G} \right)^{1/2} \approx 20 \left(\frac{E_c}{\rho_s} \right)^{1/2} m, \quad (2.14)$$

where, E_c is the critical specific energy for fragmentation in ergs/s,

$E_c \sim 10^7$ for solid rock and $E_c \sim 2 \times 10^5$ for ice.

However, the particle velocity v in a protoplanetary disk with a power-law mass distribution: $dN(m) = cm^{-q}dm$ is determined by the mass m and the radius a of the largest particle: $v = \sqrt{Gm/\Theta a}$, where, Θ is the Safronov parameter [61] which, for the case $q < 2$, would be a few units so that v turns out to be less than the characteristic velocity $v \simeq \sqrt{Gm/a}$ — the escape velocity at the surface of a larger particle.

So the above values for E_c , indicate that rapid collisional fragmentation should cease when the largest fragments are for ice ring $\sim 5km$ in radius, for a rocky ring no longer than $40km$ in radius, though observation indicate this number to be around $\sim 10km$. The main reason for this discrepancy lies in – a) *not considering the differential rotation of the disk*, b) *large shear velocities near the planet*.

Nowadays, it is considered also that the collisional break-up model must accompany the usual accretional growth such that two particles after collision may stick together [24, 26]. According to them, the enhanced destructibility of the particles in the rings is convected with the large magnitude of the shear velocities due to the differential rotation of the rings. Quasi-grazing collisions have the largest relative velocities in which case the semi-major axes of the colliding particles differ approximately by twice the radius of the particles. The break-up in quasi-grazing collisions decreases the volume of a large particle at the rate

$$\left(\frac{dV}{dt}\right)^- \approx \delta V \omega_c, \quad (2.15)$$

where, δV is the volume of the layer swept away in a single collision and ω_c is the frequency of the grazing collisions. It has been assumed that a cylindrical segment of height H_s is swept away resulting in $\delta V \approx \pi a H_s^2$. Here, ω_c may be estimated as,

$$\begin{aligned} \omega_c &\approx \left(\frac{2aH_s}{a^2}\right) \omega_0 = \left(\frac{2H_s}{a}\right) \omega_0, \\ \omega_0 &= \frac{3\Omega\sigma(a)}{\rho a} \left(1 + \frac{v^2}{u^2}\right), \end{aligned}$$

where, ω_0 is the total collisional frequency, u is the relative velocity of the particles and $\sigma(a)$ be the surface density of a particle of size a .

Assuming that in each grazing collision a volume element

$$\delta V \sim \frac{m(\Omega a)^2}{\epsilon_v},$$

breaks up as

$$\left(\frac{dV}{dt}\right)^- = 4\pi a^2 \left(\frac{da}{dt}\right)^-, \quad (2.16)$$

and we get the rate of decrease of particle radius as,

$$\left(\frac{da}{dt}\right)^- \approx \frac{4\sqrt{\rho}}{\sqrt{3}(\epsilon_v)^{3/2}} \Omega^4 a^3 \sigma(a) \left(1 + \frac{v^2}{u^2}\right), \quad (2.17)$$

where, ϵ_v is the break-up energy of particles per unit volume.

Using $\sigma(a) = (4/3)a\rho\tau(a)$, $\tau(a) = n(a)\pi a^2$, where, $\sigma(a)$ is the surface (number) density of particles of size a , $\tau(a)$ is the optical depth, we rewrite the loss equation as:

$$\left(\frac{da}{dt}\right)^- \approx \frac{16\pi}{3^{3/2}} \left(\frac{\rho}{\epsilon_v}\right)^{3/2} \Omega^4 a^6 n(a) \left(1 + \frac{v^2}{u^2}\right). \quad (2.18)$$

In case of the accretional growth of particle of size a , if it moves with velocity v in a medium of volume density ρ_s , mass increase rate will be,

$$\left(\frac{dm}{dt}\right)^+ \approx v\rho_s\pi(a+l)^2 \left(1 + \frac{v^2}{u^2}\right), \quad (2.19)$$

where, $m (= \frac{4}{3}\pi\rho a^3)$ is the mass of the particle and l is the characteristic size of the particles in the accreting medium. Using the relations $v \cong h/\Omega$ and $\sigma \cong h\rho_s$, where h is the thickness of the disk and σ the integral surface density of the disk, one may write the rate of growth for particle radius as:

$$\left(\frac{da}{dt}\right)^+ \approx \frac{\sigma\Omega}{4\rho} \left(1 + \frac{l}{a}\right)^2 \left(1 + \frac{v^2}{u^2}\right), \quad (2.20)$$

with

$$\sigma = \int_0^{a_{max}} \sigma(a) da \quad (2.21)$$

where, a_{max} is the maximum size of the particles in the ring.

From Eqs. 2.17, 2.18, 2.20 and 2.21, it is clear that there exists one critical particle size a_{cr} for which there is a balance between accretion

and break-up, i.e., $(da/dt)^+|_{a=a_{cr}} = (da/dt)^-|_{a=a_{cr}}$. Using this, we can obtain an expression for the break-up energy particles per unit volume (for $l \approx a$) as:

$$\epsilon_v \cong 4.4\rho\Omega^2 a^2 \left(\frac{\sigma_a}{\sigma}\right)^{2/3} \quad (2.22)$$

If we take $\sigma_a/\sigma \cong 1$, from Eq. 2.7, it follows that tidal force break up a $10m$ sized object, if $P_{max} \sim \rho\Omega^2 a^2 \sim 10^{-2} \text{ dyne} - \text{cm}^{-2}$.

From Eq. 2.22 using collisional break-up mechanism with $a \sim 10m$: $\epsilon_v \sim \rho\Omega^2 a^2 \sim 10^{-2} \text{ erg/cc}$. Though both the cases provide identical numbers, the physics is different. The break-up energy depends on the size of the particles and can be very small since the tensile strength is governed by another phenomenon called *self - adhesion*.

Hence it is considered that planetary rings are the relics of a circumplanetary proto-satellite disk and only this model provides correct answers to the first three questions, which were addressed at the beginning of this Chapter.

2.2 Ring Characteristics

In the last Section the origin models of the ring were reviewed. Due to variation in masses, spins, orbital distance from the Sun, magnetic field etc., rings of different planets show different characteristics. Let us now study the basic ring characteristics of the four outer planets – Jupiter, Saturn, Uranus and Neptune for which rings have been observed. Basically the planetary ring comprises of particles of varying size ranging from sub-microns length to few kilometers. Usually the forces acting on these particles include gravitational force due to the planet itself, the centrifugal force due to rotation in the orbit, the gravitational forcing due to satellites of the planet, Lorentz forces due to magnetic field field of the planet and the charge develop in the planetary magnetosphere, radiation loss as Poynting - Robertson drag, aerodynamic drag and the implicit collisional forces. Lorentz force is active in case of particles of micron and sub-micron sized particles [3] like those in Jovian magnetosphere, Saturn's E and F ring, Uranian rings etc.

2.2.1 The Jovian system

The Jovian ring system was the only one to have been discovered by spacecrafts. The ring system was detected from back-scattered light from Voyager - 1 (V1) as V1 passed through the Jovian equatorial plane [56, 72] (observed in narrow angle frame FDS 16368.19) in 1979.

Some physical parameters for Jupiter is given in Table 2.4. The physical parameters concerning the satellites are given in Table 2.5, while parameters concerning ring system is given in Table 2.6.

Mass ($1 M_J$)	$317.8M_{\oplus} = 1.901 \times 10^{27}kg$
Equatorial radius ($1 R_J$)	7.14×10^4km
Polar radius	6.68×10^4km
Heliocentric distance	$5.20AU = 7.78 \times 10^8km$
Sidereal period	$11.86yrs$
Synodic period	$398.88days$
Mean orbital speed	$13.06km/s = 15.7R_J/day$
Main magnetic dipole moment	$4.2 \times 10^{-4}TR_J^3$
Magnetic dipole tilt	$9.8^{\circ} \pm 0.3^{\circ}$

Table 2.4: Useful physical parameters for Jupiter

New results on morphology of Jovian ring system appeared after analysis of 25 images captured by Voyager 2 (V2) [56, 65, 66]. Using the images, a limited range of viewing geometries were sampled with about 50% taken in the back-scattered (low solar phase angles) light and the rest in front-scattered. It was observed that the Voyager images of the Jovian ring was much brighter in forward than in back-scattered light. Observations in forward scattered light are sensitive mainly to micrometer / sub-micrometer sized grains, while measurements in back-scattered light give information on grains of larger size and macroscopic bodies.

Interpretations of the Jovian ring data have evolved gradually. The most prominent feature is the narrow main ring itself which is dubbed as 'The main ring' [38]. All investigations noted the presence of some additional scattered light inward from the ring's normal boundaries [38]. This extra brightness is apparent in every image taken at high phase angles (FDS 20691.27 - 3.02). It was conjectured that a con-

Satellite	R (R_J)	e [$\times 10^3$]	i (deg)	R_s (km)	A
Sinope	331.93	275	153	20	-
Pasiphae	329.13	378	148	35	-
Carme	316.53	207	163	22	-
Ananke	296.92	169	147	15	-
Elara	164.38	207	28	40	0.03
Lysithea	164.15	107	29	20	-
Himalia	160.78	158	28	90	0.03
Leda	155.38	148	27	8	-
Callisto	26.37	7	0.281	2400	0.2
Ganymede	14.99	0.6/1.5	0.195	2631	0.4
Europa	9.40	10.1/0.1	0.470	1569	0.6
Io	5.90	4.1/0.01	0.040	1815	0.6
Thebe	3.11	15	0.8	?x55x45	0.05-0.1
Amalthea	2.54	3	0.40	135x82x75	0.06
Adrastea	1.81	0	0	12.5x10x7.5	0.05-0.1
Metis	1.79	4	0	?x20x20	0.05-0.1

Table 2.5: The Jovian satellite system. Here ' R ' = Orbital radius of satellite, ' e ' = eccentricity, ' i ' = inclination, ' R_s ' = radius of the satellite, ' A ' = Albedo.

Ring	Radius (R_J)	Width (R_J)	Thickness (km)	optical depth (τ)
The gossamer ring	1.72-2.94	1.22	< 4000	10^{-7}
The bright ring	1.72-1.81	0.09	< 30	4×10^{-6}
The faint ring	1.00-1.72	0.72	< 1000	7×10^{-6}
Halo	1.00-1.72	0.72	> 10,000	5×10^{-6}

Table 2.6: Ring characteristics of Jovian system

tinuous disk of material extends from the main ring's inner edge all the way down to Jupiter's atmosphere. Finally, the third component - the Halo was recognized as a vertically extended cloud of material which envelops the entire system. Later, Showalter *et al* [65] discov-

ered another ring called the Gossamer ring from the V2 image (FDS 20693.02). The main Jovian ring is probably defined by a population of macroscopic bodies visible in back-scattered light. This population has an optical depth of about 3×10^{-6} corresponding to a total cross-sectional area of $2 \times 10^4 km^2$. Adrastea and Metis have about one-tenths of this area. Hence, either these two moons are largest ring bodies or the macroscopic bodies may have originated as the ejecta from a major impact into one or both of the ring moons. Still there are lots of physical aspects of the ring which remain unexplained.

2.2.2 The Saturnian system

The Saturn's ring system is the most studied ring system. Some physical parameters related to Saturn is given in Table 2.7 and ring-satellite system in Table 2.8.

Mass ($1 M_S$)	$5.685 \times 10^{29} g$
Equatorial radius ($1 R_S$)	$60330 km$
Polar radius	$6.68 \times 10^4 km$
Heliocentric distance	$5.20 AU = 7.78 \times 10^8 km$
Sidereal period	$11.86 yrs$
Synodic period	$398.88 days$
Mean orbital speed	$13.06 km/s = 15.7 R_S/day$
Main magnetic dipole moment	$4.2 \times 10^{-4} T R_S^3$
Magnetic dipole tilt	$9.8^\circ \pm 0.3^\circ$

Table 2.7: Useful physical parameters for Saturn

Saturn's ring is classically divided into ring systems like A, B, C, D, E, F and G ring systems. Rings A, B and C contain far more material than the peripheral D, E, F and G rings and measured as normal optical depth:

$$\tau(\lambda) = \int \int n(r, z) Q_e(r, \lambda) \pi r^2 dr dz, \quad (2.23)$$

where z is the direction perpendicular to the rings, $n(r, z)$ is the number density per radius increment (cm^{-4}) of particles of radius r , and $Q_e(r, \lambda)$ is the extinction efficiency of the particles at wavelength λ .

Satellite	R (R_S)	e [$\times 10^3$]	i (deg)	R_s (km)	A
Phoebe	214.686	163	175.3	115x110x105	0.06
Iapetus	59.030	28.3	7.52	730 \pm 8	0.5/0.04
Hyperion	1481.1	104.2	0.43	175x120x100	0.2
Titan	20.253	29.2	0.33	2575 \pm 2	0.2
Rhea	8.736	1.0-0.3	0.35	765 \pm 4	0.6
Dione	6.256	2.2	0.02	559 \pm 5	0.55
Helene	6.256	5	0.2	18x?x?	0.6
Tethys	4.884	0.0	1.09	524 \pm 5	0.8
Telesto	4.884	-	-	15x12x8	0.6
Calypso	4.884	-	-	?x12x11	0.9
Enceladus	3.945	4.5	0.02	251 \pm 5	1.0
<i>E ring</i>	3-8	-	-	[302 000]	?
Mimas	3.075	20.2	1.53	197 \pm 3	0.7
<i>G ring</i>	2.819	-	-	[1000]	?
Janus	2.511	7	0.14	110x95x80	0.5
Epimetheus	2.510	9	0.34	70x58x50	0.5
Pandora	2.349	4.2	0.0	55x43x33	0.5
<i>F ring</i>	2.324	2.6 \pm 0.6	0.0	45	?
Prometheus	2.310	2.4	0.0	70x58x50	0.5
Atlas	2.282	2	0.3	19x?x14	0.5
<i>A ring</i>	2.025-2.267	-	-	[14610]	0.5
Pan	2.214	?	? 10	0.5	?
<i>Cassini division</i>	1.948-2.025	-	-	[4650]	0.2
<i>Huygens ringlet</i>	1.953	0.40 \pm 0.17	-	[43]	?
<i>B ring</i>	1.525-1.948	-	-	[25520]	0.5
<i>C ring</i>	1.235-1.525	-	-	[17490]	0.2
<i>Maxwell ringlet</i>	1.450	0.34 \pm 0.04	-	[64]	?
<i>Titan ringlet</i>	1.291	0.26 \pm 0.02	-	[25]	?
<i>D ring</i>	1.110-1.235	-	-	[7450]	?

Table 2.8: The Saturnian satellite system. Here ' R ' = Orbital radius of satellite, ' e ' = eccentricity, ' i ' = inclination, ' R_s ' = radius of the satellite, ' A ' = Albedo.

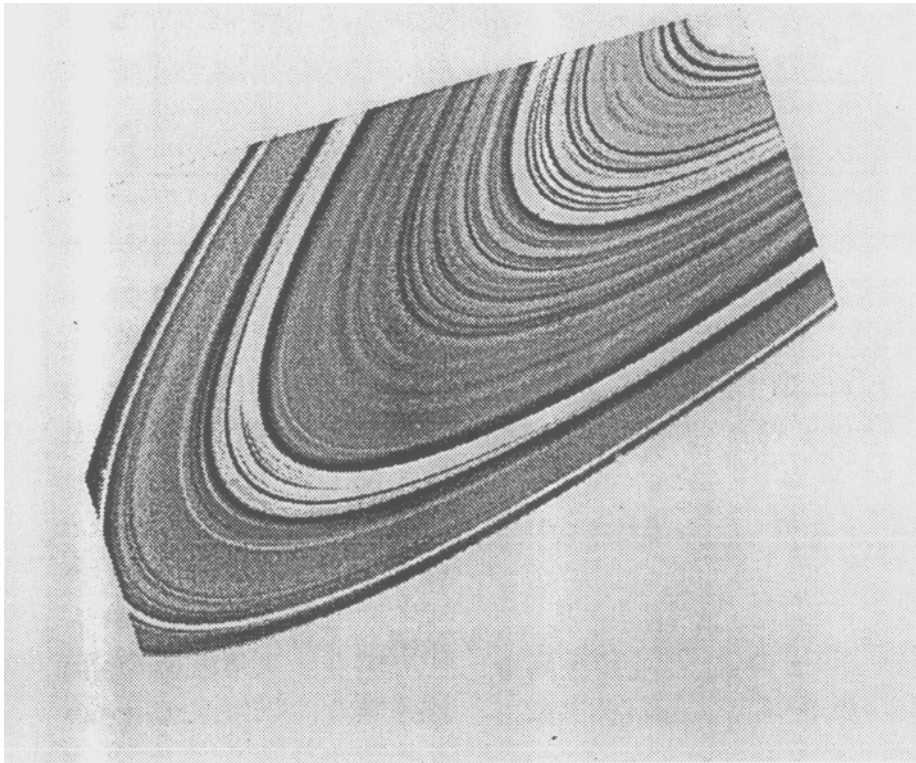


Figure 2.2: Saturn's ring as taken from Hubble's space telescope

Though Saturn's rings were studied from terrestrial telescopes, the significant analysis was done using the spacecraft data. The three main spacecraft contributor to the program were Pioneer-11, Voyager 1 (V1) and Voyager 2 (V2) and still we are waiting for Cassini to send data around 2004. The main physical characteristics of the Saturnian rings are given in Table 2.9. The main methods of the study by the spacecraft were:

- direct photography – the visible range of the spectrum;
- measurement of the light of a star eclipsed by a ring – ultraviolet region;
- radio-occultation of Voyager signal by the rings – when the ring happens to be between the spacecraft and the Earth.

Ring parts	$2h$ [m]	$\bar{\tau}$	σ [g/cm^2]		r_g^{max} [m]
			Radio occultation	Resonance theories	
<i>C ring :</i>					
interior	5	0.08	3.2 ± 1.8	1.5	4.5
exterior	5	0.12	4.3 ± 2.5	1-5	2.4-5.3
<i>B ring:</i>					
interior	5-10	1.21	-	70 ± 4	-
central	5-10	1.76	-	(99 ± 6)	-
exterior		1.84	-		
Cassini division	20	0.12	18.8 ± 0.5	16 ± 3	7.5
<i>A ring:</i>					
interior	10-30	0.70	34 ± 6	40 ± 2.5	5.4
exterior	10-30	0.57	24.4 ± 7.2	34 ± 20	8.9-11.2
<i>G ring:</i>	10^5	$10^{-6} - 10^{-4}$	-	-	-
<i>E ring:</i>	10^7	$10^{-6} - 10^{-5}$	-	-	-

Table 2.9: Main physical properties of Saturnian ring system. Here $2h$ = total ring height, $\bar{\tau}$ = average optical depth, σ = surface mass density, r_g^{max} = maximum size of particles.

The important points discovered from satellite data include:

- Rings seemed to have divisions into ringlets. Regional boundaries are defined by significant and fairly abrupt changes in optical depth.
- Existence of spiral waves due to satellite resonances. Spiral waves are divided into two types, namely – *density* and *bending* waves. The strongest spiral waves are due to the lower order resonance.
- The existence of eccentric rings.
- “Spokes”. In B ring one could observe spokes which extend along the radius and situated on the “corotation radius” where

the orbital period is equal to the rotational period of the planet. The particle sizes are usually very small.

- Characteristic features of the particle size spectrum. Data from V2 Photopolarimeter (PPS) [67] and radio-occultation data [76], particle size has been estimated. Tyler has shown that the particle varies from few millimeters to tens of meters. The particle size spectrum $n(a) = na^{-q}$ has an index $q = 2.8$ to 3.4 in the range of sizes upto the maximum $a_{max} = 5$ to $10m$. However, Showalter *et al* [67] observed that PPS data shows non-Poisson behavior, specially in the A ring.

2.2.3 The Uranian ring

The ring system of Uranus was discovered during observation of occultation of star SAO 158687[6]. The important characteristics observed for the Uranian rings were:

- Narrow rings
- sharp edges
- Long lived structures in the radial direction
- eccentric rings
- Rings inclined to the equator
- uniform apsidal and nodal precession
- adjacent broad and narrow ring components
- low albedo ring particles

The physical parameters for Uranus is given in Table 2.10 and the physical properties for Uranian system is given in Table 2.11.

2.2.4 The Neptunian ring

In 1980, Nicholson and Jones [54] communicated that they had observed the occultation of a star by a Neptunian ring on Aug 21st,

Mass ($1 M_U$)	$8.686 \times 10^{28}g$
Equatorial radius ($1 R_U$)	$25559km$
Polar radius	$24973km$
Heliocentric distance	2.872×10^9km
Sidereal period	$84.02yrs$
Magnetic Dipole field strength	$0.228gauss - R_U^3$
Dipole tilt to rotational axis	58.6°

Table 2.10: Useful physical parameters for Uranus

1978. The peculiar feature of the Neptunian rings is the absence of a second occultation, as if the ring behaves as an arc. Moreover, the results of the observation of a star at the same time by two telescope indicated that the density of an arc drops abruptly over a distance of a few hundred kilometers along the orbit.

2.2.5 Comparative Analysis

Planetary ring system consists of particles of varying size and number density. The primary rings [26] contain larger particles and hence ring has longer life-time. Usually observed around twice the planetary radii. In general, satellites are observed beyond the limits of the primary rings. On the other hand, secondary rings contain grains of micron / sub-micron size and hence they need a continuous influx of matter in order to exist for a long time. The main Jovian ring, A, B C rings for Saturn, denser Uranian rings, primary Neptunian rings belong to the primary ring category while the E ring, the G ring, dusty Uranian rings and the rarefied Jovian rings belong to the secondary ring category.

Satellite	R (km)	e [$\times 10^3$]	i (deg)	R_s (km)	A
Oberon	582596 \pm 71	0.8	0.10	775 \pm 10	0.24
Titania	435844 \pm 86	2.2	0.14	805 \pm 5	0.28
Umbriel	265969 \pm 48	5.0	0.36	595 \pm 10	0.19
Ariel	191239 \pm 57	3.4	0.31	580 \pm 5	0.40
Miranda	129783 \pm 66	2.7	4.22	242 \pm 5	0.34
Puck	86006 \pm 25	(0.1)	0.3	77 \pm 3	0.07
Belinda	75256 \pm 29	(0.1)	0.0	34 \pm 4	-
Rosalind	69942 \pm 26	(0.1)	0.3	29 \pm 4	-
Portia	66090 \pm 34	(0.2)	(0.1)	55 \pm 6	-
Juliet	64350 \pm 27	0.6	(0.1)	42 \pm 5	-
Desdemona	62675 \pm 24	(0.2)	0.2	29 \pm 3	-
Cressida	61776 \pm 27	(0.2)	0.0	33 \pm 4	-
Bianca	59172 \pm 26	0.9	(0.2)	22 \pm 3	-
Ophelia	53794 \pm 39	10.1	(0.1)	16 \pm 2	-
ϵ ring	51149	7.94	0.000	[20/96]	[1.2/4]
1986U1R	50023	(0.0)	(0.0)	[1-2]	[0.1]
Cordelia	49771 \pm 17	0.5	0.1	13 \pm 2	-
δ ring	48299	(0.04)	(0.002)	[3/9]	[0.3/0.4]
γ ring	47627	(0.10)	(0.006)	[1/4]	[1.3/2.3]
η ring	47176	(0.00)	(0.001)	[1-2]	[0.1-0.4]
β ring	45661	0.44	0.005	[7/12]	[0.2]
α ring	44718	0.76	0.015	[7/12]	[0.3/0.4]
ring 4	42571	1.06	0.032	[2-3]	[0.3]
ring 5	42235	1.90	0.054	[2-3]	[0.5-0.6]
ring 6	41837	1.01	0.062	[1/3]	[0.2/0.3]
1986U2R	37 - 39.5 $\times 10^3$	-	-	[2500]	[0.001-0.0001]
ring 1	50660 \pm 30	-	-	[16]	[0.1]
arc 1	41760 \pm 30	-	-	[2]	[0.2]
arc 2	41470 \pm 30	-	-	[4]	[0.2]
arc 3	38430 \pm 50	-	-	[2]	[0.2]
ring 2	38280 \pm 50	-	-	[1]	[0.2]

Table 2.11: The Uranian satellite system. Here ' R ' = Orbital radius of satellite, ' e ' = eccentricity, ' i ' = inclination, ' R_s ' = radius of the satellite, ' A ' = Albedo.

Mass ($1 M_N$)	$1.025 \times 10^{29}g$
Equatorial radius ($1 R_N$)	$24764km$
Polar radius	$24341km$
Heliocentric distance	4.498×10^9km
Sidereal period	$164.8yrs$
Magnetic Dipole field strength	$0.142gauss - R_N^3$
Dipole tilt to rotational axis	46.9°

Table 2.12: Useful physical parameters for Neptune

Satellite	R ($10^3 km$)	e [$\times 10^3$]	i (deg)	R_s (km)	A
Nereid	5510	750	27.6	170 ± 25	0.14-0.035
Triton	354.8	< 0.5	158.5	1353 ± 3	0.6-0.9
Proteus	117.6	?	< 1	200 ± 10	0.06
Larissa	73.6	?	< 1	95 ± 10	0.056
Adams ring	62.9	0.47	0.06	[15-50]	[0.01-0.1]
Galatea	62.0	?	< 0.1	79 ± 12	-
1989N4R	53.2-59	-	[5800]	[0.0001]	
Le Verrier ring	53.20	-	-	[100]	[0.01]
Despina	52.5	?	< 1	75 ± 15	0.054
Thalassa	50.0	?	< 1	40 ± 8	-
Naiad	48.0	?	4.5	27 ± 8	-
1989N3R	41.9	-	-	[1700]	[0.0001]

Table 2.13: The Neptunian satellite system. Here ' R ' = Orbital radius of satellite, ' e ' = eccentricity, ' i ' = inclination, ' R_s ' = radius of the satellite, ' A ' = Albedo.

Chapter 3

Resonance and the spiral waves

Saturn's ring system occulted Voyager-I spacecraft on Nov 13, 1980. The spacecraft transmitted dual frequency monochromatic radio signals directly down to Earth through the Saturn's ring system. These signals interacted with ring particles. The attenuation, phase-shift and broad-band frequency content of the received signals revealed considerable structure in the ring along the occulted track [49, 50, 74, 75]. The radio occultation data provide detailed optical depth and phase-shift measurements over the radial extent of the rings at 3.6- and 13-cm wavelengths.

One of the most intriguing observed phenomena is the formation of the spiral waves. Observational data analysis and dynamical theoretical modeling of ring system have identified two kinds of spiral waveforms – density waves and bending waves. Density waves are spiral patterns of enhancement and depletion of ring material, formed by particles coerced into coherently nested *eccentric* orbits. In-plane periodic forcing due to satellites at resonant locations in the rings can excite density waves. Bending waves are vertical corrugations of the disk, formed by particles in coherently nested *inclined* orbits. Satellites in inclined orbits supply the necessary resonant vertical perturbations to ring particles to excite bending waves. The study of waves in planetary ring got importance as a diagnostic tool for local ring properties such as surface mass density, viscosity of ring and thickness. By mod-

eling the radial dispersion of wavelength in a wave, it is possible to infer the local surface mass density of the ring in the wave regions and the radial location of the resonant forcing. The shape and extent of the wave can provide upper bound of ring thickness and the mass of the perturbing satellite.

3.1 Basics of Orbits and Resonances

Let us consider the basic equations and physics of orbits around a planet. Let us consider cylindrical coordinates (r, θ, ϕ) . Let us also consider a free particle orbiting in a circle of radius r with the angular speed $\Omega(r)$ in the equatorial plane $z = 0$ of the planet assumed axisymmetric with an associated potential $\phi_p(r, z)$.

At the equatorial plane, centrifugal equilibrium is obtained from,

$$r\Omega^2(r) = \left. \frac{\partial \phi_p}{\partial r} \right|_{z=0}, \quad (3.1)$$

where, $\Omega(r) = \left[\frac{GM_p}{r^3} \right]^{\frac{1}{2}}$ M_p being the mass of the planet, G being universal gravitational constant.

Ideally, the particle will move around the planet in a Keplerian orbit, assumed to be our reference orbit. . If the test particle is displaced by an arbitrarily small amount, it will oscillate freely in the horizontal and vertical directions about the Keplerian orbit with epicyclic frequency $\kappa(r)$ and vertical frequency $\mu(r)$ respectively. The expressions for those frequencies are given by Lindblad's theory of epicyclic motion given as,

$$\kappa^2(r) = r^{-3} \frac{d}{dr} \left[(r^2 \Omega)^2 \right], \quad (3.2)$$

$$\mu^2(r) = \left. \left[\frac{\partial^2 \phi_p}{\partial z^2} \right] \right|_{z=0}. \quad (3.3)$$

Hence, $\mu(r)$ and $\kappa(r)$ are related to $\Omega(r)$ as,

$$\mu^2(r) + \kappa^2(r) = 2\Omega^2(r). \quad (3.4)$$

If we consider planet as a spherical one then, $\mu(r) \sim \kappa(r) \sim \Omega(r)$. In reality, planet such as Saturn, is oblate, e.g. Saturn, $\mu(r) > \Omega(r) > \kappa(r)$.

Consider now a satellite of mass M orbiting the said planet with a small eccentricity e_M in a plane inclined by a small angle i_M with respect to the planetary equatorial plane $t = 0$. For small perturbations from a satellite, the particle residing in a Keplerian orbit around the planet responds as a multi-dimensional, forced linear harmonic oscillator. The direct contribution of the satellite to the total gravitational potential is:

$$\begin{aligned} \Phi_M(r, \phi, z, t) = \\ -GM \left[r_M^2(t) + r^2 - 2r_M r \cos(\phi_M(t) - \phi) + (z_M(t) - z)^2 \right]^{-\frac{1}{2}}. \end{aligned} \quad (3.5)$$

Here suffix ' M ' corresponds to terms for moon and the other terms are for test particle. The most important point is that $r_M(t) - a_M$, $\Theta_M(t) = \phi_M(t) - \Omega_M t$ and $z_M(t)$ are small quantities and are periodic functions, where a_M is moon-orbit radius, Ω_M is Keplerian local velocity of moon. To a sufficient degree of approximation, $r_M(t)$ and $\Theta_M(t)$ have period $2\pi/\kappa_M$, while $z_M(t)$ has period $2\pi/\mu_M$. Since $\Phi_M(r, \phi, z, t)$ is periodic in time t and angle ϕ , one may Fourier decompose in these variables. The result can be written in elementary form in general as,

$$F_M = \mathcal{R}e [\Phi_M(r, z) \exp(i(\omega t - m\phi))], \quad (3.6)$$

where, the disturbance frequency due to forcing due to the moon is ω . This perturbation frequency ω at which perturbation is launched at the inner vertical resonance as seen from the inertial frame is given by

$$\omega = m\Omega_M \pm n\mu_M \pm p\kappa_M, \quad (3.7)$$

where, m, n, p are non-negative integers. In general n is even for horizontal forcing and odd for vertical forcing. Actually for $n=\text{odd}$ and $p=0$ or even for vertical forcing and $n=0$ or even and $p=\text{odd}$ for horizontal forcing [68]. The forcing amplitude associated with disturbance frequency ω of Eq. 3.7 is proportional to $e_M^{|p|} \sin^{|n|} i_M$ [30, 68].

Now the test particle will undergo horizontal(Lindblad) resonance at $r = r_L$, where,

$$\omega - m\Omega(r_L) = \pm\kappa(r_L) \quad (3.8)$$

and it will suffer vertical (inclination) if its radial position is at $r = r_V$ satisfies,

$$\omega - m\Omega(r_V) = \pm\mu(r_V). \quad (3.9)$$

Large satellites exist exterior to the main ring system, and hence $\Omega_M < \Omega$. So inner resonances are important than outer ones. The satellite forcing associated with the resonances characterized by a ratio of integers which contain a difference N between numerator and denominator must be proportional to a product of $(N - 1)$ factors of small quantities, e_M and $\sin i_M$. Thus the strongest inner horizontal resonances correspond to the ratio $m : m - 1$, involving only the circular part of the satellite motion, while the strongest inner vertical resonances correspond to the ratio $m + 1 : m - 1$ involving one factor of the inclination of the satellite orbit.

3.2 Galactic disks and planetary ring

Before discussing waves in detail let us explore possibility of any resemblance of galactic disks with planetary ring. In spite of a difference in scale length by a factor of a trillion, spiral galactic disk structure and Saturn's ring system seem to have many superficial similarities. Both of these structures are spatially thin structures supported primarily by centrifugal equilibrium between gravitational and centrifugal forces. Both consist of innumerable discrete objects whose random motions are very small compared to their Keplerian speed. Both of them have varieties in internal structure. Collective gravitational effects can explain much of the internal structures of these objects.

However, there is a crucial difference in the relative scale of collective processes which operate in galactic disk and in Saturn's rings. The natural scale of self-gravitational disturbances in flattened distributions of matter with surface mass density σ and angular rotation

speed Ω is roughly given by [73],

$$L = \frac{2\pi G\sigma}{\kappa^2},$$

where, κ is the epicyclic frequency related to Ω as,

$$\kappa^2(r) = r^{-3} \frac{d}{dr} \left[(r^2 \Omega)^2 \right], \quad (3.10)$$

In spiral galaxies, the scale L is comparable to the radius r of the disk, whereas in planetary ring system $L \ll r$. For example, in Saturn's ring $\sigma \sim 50\text{g/cm}^2$, $\kappa \sim 2 \times 10^{-4}\text{s}^{-1}$, $L \sim 500\text{cms}$ where $r \sim 10^{10}\text{cms}$. The reason for the difference in the ratio of L to r is that the ratio of mass in the disk to that in the rest of the system is much smaller for Saturn than for spiral galaxies.

Next comes the role of physical collisions in galaxies and planetary rings. Physical collisions play an important role in galaxies only for the dynamics of the interstellar gas. Interstellar gas is a minor component of total galactic mass. On a large scale, physical collisions are responsible for galactic shocks [25, 69, 78] and therefore spiral structure is observed.

In planetary rings, inelastic collisions between ring particles affect the large scale structure more directly [31]. First, in the absence of the perturbing effects, collisions ultimately settles ring particles in the equatorial plane of the planet. Second, collisions quickly dissipate random motions of all but the smallest ring materials as smallest ring materials are subjected to strong electro-magnetic forces. Third, collisions lead to friction, which generally works to destroy structure in the ring system.

The physical collisions must be accompanied by shear for dissipative effects. The level of shear friction in the rings is characterized by the kinematic viscosity ν . Let us consider ring material of normal optical depth τ near to unity. Let us also consider that ring materials are made up of particles with characteristic size R possessing RMS random speed c in a typical direction. Their kinetic theory yields formulas for kinematic viscosity [8] as,

$$\nu = \Omega R^2 \tau, \quad c < 2\Omega R, \quad (3.11)$$

$$\nu = \left(\frac{c^2}{2\Omega} \right) \left(\frac{\tau}{1 + \tau^2} \right), \quad c > 2\Omega R. \quad (3.12)$$

The typical vertical displacement of a particle from the central ring plane is c/Ω . Now Eq. 3.11 is applied when vertically sweep of a ring particle, i.e. the characteristics ring thickness, become comparable to or smaller than the size of the ring particles. In case of Saturn's rings, the random speed c has been found to be so small that the non-circular excursions of ring particles are atmost tens of meters, much less than the scale of resolvable collective phenomena [17, 42]. Hence to a high degree of approximation, the effects of non-circular motion for contribution to pressure may be ignored. Also in usual cases of spiral waves of planetary ring, the study is restricted to "long waves" only ignoring "short waves" while "short waves" play a prominent role in the theories of spiral structure of disk galaxies [46]. The non-zero random speed is considered only in so far as they contribute to the gradual damping of density waves and bending waves through the viscosity Eq. 3.12.

3.3 Spiral Density Waves

As discussed earlier, the density wave is basically a collective response of a planetary ring to horizontal forcing by an external satellite. For small amplitude assumption, the theory can be linearized for simplicity. In the linear approximation, horizontal and vertical motions decouple from each other and hence these two effects may be treated separately.

The dynamics is usually studied assuming a two dimensional gas disk and treated with Boltzmann equation. Shu[70] considered a kinetic treatment with encounter-less Boltzmann equation which is identical to fluid treatment using the gas-dynamical equations with zero pressure and viscosity. However, Goldreich and Tremaine [29] also considered a two dimensional gas disk having pressure p acting only in the horizontal plane and is related to the surface mass density σ by,

$$p = K\sigma^\gamma. \quad (3.13)$$

The enthalpy η and sound speed c satisfy the relation

$$(\gamma - 1)\eta = c^2 = \frac{dp}{d\sigma}. \quad (3.14)$$

Here we are discussing the analysis of density waves following Shu's treatment which uses the fluid treatment. The disk is considered as an infinitesimally thin disk of matter of surface mass density $\sigma(r, \vartheta, t)$. Let $\varphi_D(r, \vartheta, z, t)$ be the potential due to self-gravity and must satisfy Poisson's equation

$$\frac{1}{r} \frac{\partial}{\partial r} \left(r \frac{\partial \varphi_D}{\partial r} \right) + \frac{1}{r^2} \frac{\partial^2 \varphi_D}{\partial \vartheta^2} + \frac{\partial^2 \varphi_D}{\partial z^2} = 4\pi G \sigma \delta(z), \quad (3.15)$$

where, $\delta(z)$ is the Dirac delta function.

Now let us consider a satellite of mass M which orbits the planet with a small eccentricity e_M in a plane inclined by a small angle i_M with respect to the planet's equatorial plane $z = 0$. Let (r_M, ϑ_M, z_M) be the time-dependent cylindrical coordinates of this satellite. The direct contribution to the total gravitational potential is given by Eq. 3.5. Let $u(r, \vartheta, t)$ and $v(r, \vartheta, t)$ be the r and ϑ components of fluid velocity. The equations of compressible fluid dynamics for purely horizontal motions in a pressureless inviscid disk may be written as

$$\frac{\partial \sigma}{\partial t} + \frac{1}{r} \frac{\partial}{\partial r} (r \sigma u) + \frac{1}{r} \frac{\partial}{\partial \vartheta} (\sigma v) = 0, \quad (3.16)$$

$$\frac{\partial u}{\partial t} + u \frac{\partial u}{\partial r} + \frac{v}{r} \frac{\partial u}{\partial \vartheta} - \frac{v^2}{r} = -\frac{\partial}{\partial r} [\varphi_P + \varphi_D + \varphi_M], \quad (3.17)$$

$$\frac{\partial v}{\partial t} + \frac{u}{r} \frac{\partial}{\partial r} (rv) + \frac{v}{r} \frac{\partial v}{\partial \vartheta} = -\frac{1}{r} \frac{\partial}{\partial \vartheta} [\varphi_D + \varphi_M]. \quad (3.18)$$

The system as a whole is considered to have balanced centrifugal force with some small perturbations. To consider the linear response of satellite forcing Eq. 3.5 second order perturbation terms are neglected. This makes

$$\begin{aligned} \sigma(r, \vartheta, t) &= \sigma_0(r) + \mathcal{R}e [S(r) \exp(i(\omega t - m\vartheta))], \\ u(r, \vartheta, t) &= 0 + \mathcal{R}e [U(r) \exp(i(\omega t - m\vartheta))], \\ v(r, \vartheta, t) &= r\Omega(r) + \mathcal{R}e [V(r) \exp(i(\omega t - m\vartheta))], \end{aligned} \quad (3.19)$$

where, strictly speaking, one must consider $\Omega(r)$ to satisfy the relation

$$r\Omega^2(r) = \left[\frac{\partial}{\partial r} (\varphi_P + \varphi_{D0} + \sum \varphi_{M0}) \right]_{z=0} \quad (3.20)$$

To relate the Lindblad resonance with the galactic disk, one may use Oort parameter $B(r)$ to relate Keplerian angular velocity $\Omega(r)$ as,

$$\begin{aligned} B(r) &= \Omega(r) + \frac{r}{2} \frac{d\Omega}{dr}, \\ \kappa^2(r) &= 4B(r)\Omega(r), \end{aligned} \quad (3.21)$$

where, $2B(r)$ is the estimate of the amount of vorticity in the disk i.e. $\nabla \times \mathbf{v}$.

Here φ_{D0} is the potential that corresponds to the equilibrium disk of surface density σ_0 and $\sum \varphi_{M0}$ is the time-independent axisymmetric part of the potential due to all of the planet's satellites. The equation Eq. 3.20 is more accurate than Eq. 3.1 and is generally used for more general case like that of closed binary stars, the solar nebula etc.

Using Eq.3.19 in Eqs. 3.16, 3.17 and 3.18, we may derive linearized sets as

$$i(\omega - m\Omega)S + \frac{1}{r} \frac{d}{dr} (r\sigma_0 U) - \frac{im}{r} \sigma_0 V = 0, \quad (3.22)$$

$$i(\omega - m\Omega)U - 2\Omega V = -\frac{\partial}{\partial r} (\Phi_D + \Phi_M), \quad (3.23)$$

$$i(\omega - m\Omega)V + \frac{\kappa^2}{2\Omega} U = \frac{im}{r} (\Phi_D + \Phi_M), \quad (3.24)$$

Here Eqs. 3.23 and 3.24 provide $\Phi_D(r, z = 0)$ and $\Phi_M(r, z = 0)$ for $z = 0$ plane in the ring, and Φ_D can be written in linearized form of Poisson's equation from Eq. 3.15 as shown below which may be derived from integrating Eq. 3.15 in the closed neighbourhood of $z = 0$ under the assumption that Φ_D is continuous across $z = 0$ while its derivative along z axis reverses sign.

$$\frac{1}{r} \frac{\partial}{\partial r} \left(r \frac{\partial \Phi_D}{\partial r} \right) + \frac{\partial^2 \Phi_D}{\partial |z|^2} - \frac{m^2}{r^2} \Phi_D = 0 \text{ for } |z| > 0, \quad (3.25)$$

$$S(r) = \frac{1}{2\pi G} \left(\frac{\partial \Phi_D}{\partial |z|} \right)_{|z|=0+} \quad (3.26)$$

solving Eqs. 3.22, 3.23 and 3.24 we obtain

$$\begin{aligned} U &= i\Lambda_U(\Phi_D + \Phi_M), \\ V &= \Lambda_V(\Phi_D + \Phi_M), \\ S &= \Lambda_S(\Phi_D + \Phi_M), \end{aligned} \quad (3.27)$$

where, $\Lambda_U, \Lambda_V, \Lambda_S$ are the real differential operators given by,

$$\begin{aligned} \Lambda_U &= \frac{1}{D} \left[-(\omega - m\Omega) \frac{d}{dr} + \frac{m}{r} 2\Omega \right], \\ \Lambda_V &= \frac{1}{D} \left[\frac{\kappa^2}{2\Omega} \frac{d}{dr} - \frac{m}{r} (\omega - m\Omega) \right], \\ \Lambda_S &= \left(\frac{1}{\omega - m\Omega} \right) \left(\frac{1}{r} \frac{d}{dr} r \sigma_0 \Lambda_U + \frac{m}{r} \sigma_0 \Lambda_V \right), \end{aligned} \quad (3.28)$$

where, D is the determinant of the coefficient matrix associated with Eqs. 3.23 and 3.24 :

$$D = \kappa^2 - (\omega - m\Omega)^2. \quad (3.29)$$

The equation Eq. 3.29 is clearly understood as a discriminant for the difference in frequency from the Lindblad resonances Eq. 3.8. The equations also provide some physical significances. Singularities may be observed in the Eq. 3.28 for $D = 0$ in case of Lindblad resonance $r = r_L$ and corotation resonance $r = r_C$ for $m\Omega - \omega = 0$. Away from the resonances, the general solution to the Eq. 3.25 breaks into two parts - wave and non-wave zones. The individual waves satisfy homogeneous equations and are free density waves as per Lin-Shu theory. The non-wave part is particular solution of the nonhomogenous equation. It must be noted that the division into these wave and non-wave parts is applicable for zones excluding resonances.

If we assume,

$$\Phi_D(r, z = 0) \equiv F(r), \quad (3.30)$$

where, $F(r)$ is rapidly varying function

we get,

$$\frac{\partial^2 \Phi_D}{\partial r^2} + \frac{\partial^2 \Phi_D}{\partial |z|^2} = 0 \text{ for } |z| > 0. \quad (3.31)$$

This leads to the nonhomogenous equation,

$$r \frac{d\Phi_D}{dr} - \frac{isrD}{2\pi G\sigma_0} \Phi_D = -r \frac{d\Phi_M}{dr} + \frac{m2\Omega}{(\omega - m\Omega)} \Phi_M. \quad (3.32)$$

To drive the free spiral density wave part, one may consider free solution in the WKBJ form as,

$$\Phi_D(r, 0) = \Phi(r) \exp \left[i \int^r k dr \right], \quad (3.33)$$

where, Φ , k is real and $|kr| \gg 1$ and hence this solution becomes rapidly oscillating.

We reach to the dispersion relation as [45],

$$D + (kc)^2 - 2\pi G\sigma |k| = 0. \quad (3.34)$$

and its solutions are given by

$$|k| = \frac{\pi G\sigma}{c^2} + \epsilon \left[\left(\frac{\pi G\sigma}{c^2} \right)^2 - \frac{D}{c^2} \right]^{\frac{1}{2}}, \quad (3.35)$$

where, $\epsilon = +1$ for “short waves” and $\epsilon = -1$ for “long waves”. Since k may be positive and negative, wave may be leading and as well as trailing.

3.4 Spiral Bending Waves

Analysis of bending waves may be carried out in one of the several ways. Shu [68, 70] analysed the spiral bending waves as the long density waves. In that study Shu analysed the bending waves as a whole as observed from a stationary laboratory frame. However, it may be also interesting to carry out the analysis of motion of each dust grain within the warped ring since it may give us more basic features, though it may be a local description. For global view of bending waves one may refer to Shu [70].

Chakrabarti [13, 14] worked on analysis of equation of motion of a single particle in the warped self-gravitating ring of finite thickness. The approach describes equation of motion of test particle as seen from the frame placed in the warped ring. Since this approach is quite a new approach and provides some more insight about particle

dynamics, we are discussing it first, while later we shall discuss on the fluid dynamics using the *WKBJ* formalism to achieve the dispersion relation.

3.4.1 The Particle Dynamics

Let us choose a right handed Cartesian coordinate system (X, Y, Z) at a radial distance r from the center of the planet. The X axis points radially outwards, the Y axis points towards the azimuthal direction and the Z axis points upwards vertically normal to the equatorial plane of the planet as shown in Fig.3.1. The frame is rotating around the planet with the local Keplerian velocity $\Omega(r)$. Let the amplitude of the vertical oscillation be ϵ . Let m be the mass of the dust grain at (x, y, z) .

Now, let O be origin of reference frame placed at the mid plane of the ring having coordinates (x^*, y^*, z^*) . The projection of normal drawn from the particle to the ring has components $x_1 = x - x^*$, $y_1 = y - y^*$ and $z_1 = z - z^*$. Let phase of the propagating wave be denoted by ϕ^* and that of particle is denoted by ϕ .

Hence,

$$\phi^* = k_x x^* + k_y y^* - \omega t, \quad (3.36)$$

and

$$\phi = k_x x + k_y y - \omega t. \quad (3.37)$$

Thus,

$$\Rightarrow \phi - \phi^* = k_x (x - x^*) + k_y (y - y^*) = k_x x_1 + k_y y_1. \quad (3.38)$$

As per Fig.3.1, $X'Y'Z'$ frame is on the warped-ring system, O' (x^*, y^*, z^*) is its origin at the mid-plane of the warped ring. Let dust of mass m_d is situated at A (x, y, z) in XYZ frame and (x', y', z') in $X'Y'Z'$ frame of reference.

Hence one may write,

$$\begin{aligned} z' &= h + \epsilon \cos \phi^*, \\ &= h + \epsilon \cos (k_x x' + k_y y' - \omega t), \end{aligned} \quad (3.39)$$

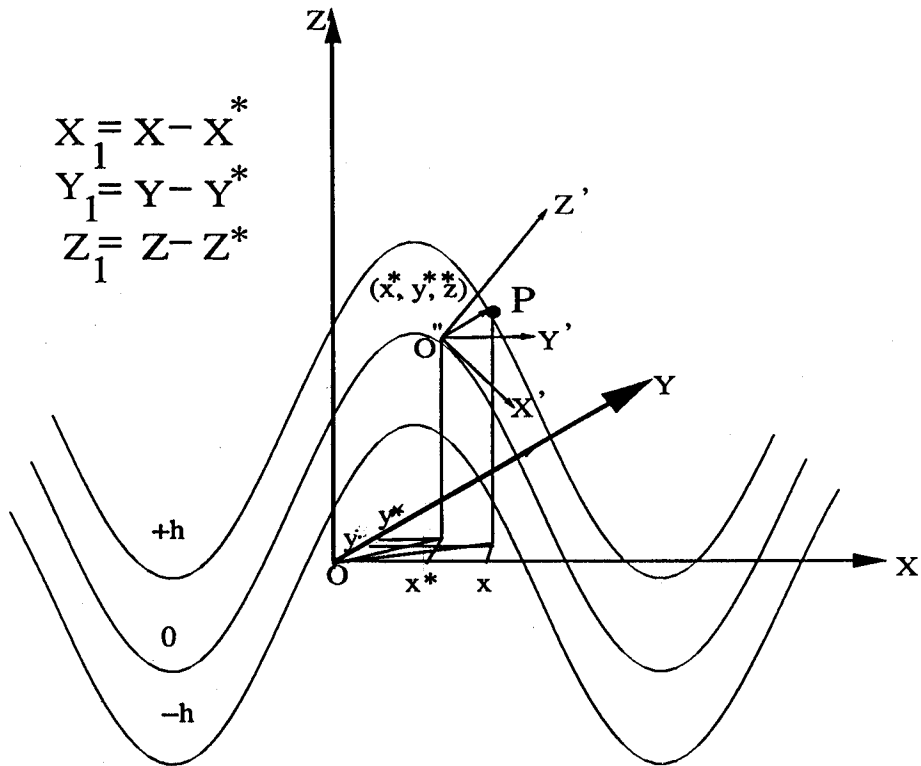


Figure 3.1: Geometry of bending waves. Coordinates are shown schematically. The rotating frame (X, Y, Z) also oscillates vertically with frequency ω of the perturbation due to moon

$$\Rightarrow \frac{\partial z'}{\partial x'} = -\epsilon k_x \sin \phi^*, \quad (3.40)$$

$$\frac{\partial z'}{\partial y'} = -\epsilon k_y \sin \phi^*, \quad (3.41)$$

$$\frac{\partial z'}{\partial z'} = 1. \quad (3.42)$$

Now unit vector normal to Eq. 3.39 surface is given as,

$$\hat{k}' = \frac{1}{\sqrt{(\partial z'/\partial x')^2 + (\partial z'/\partial y')^2 + (\partial z'/\partial z')^2}} \left[\hat{i} \frac{\partial z'}{\partial x'} + \hat{j} \frac{\partial z'}{\partial y'} + \hat{k} \frac{\partial z'}{\partial z'} \right],$$

or,

$$\begin{aligned} \hat{k}' &= \hat{i} \left[-\frac{\epsilon k_x \sin \phi^*}{\sqrt{1 + \epsilon^2 k^2 \sin^2 \phi^*}} \right] + \hat{j} \left[-\frac{\epsilon k_y \sin \phi^*}{\sqrt{1 + \epsilon^2 k^2 \sin^2 \phi^*}} \right] \\ &+ \hat{k} \left[\frac{1}{\sqrt{1 + \epsilon^2 k^2 \sin^2 \phi^*}} \right] \end{aligned} \quad (3.43)$$

From Fig. 3.1,

$$\begin{aligned} \vec{O'A} &= (x - x^*)\hat{i} + (y - y^*)\hat{j} + (z - z^*)\hat{k} \\ &= \hat{i}x_1 + \hat{j}y_1 + \hat{k}z_1, \end{aligned} \quad (3.44)$$

and,

$$|\vec{O'A}| = \sqrt{x_1^2 + y_1^2 + z_1^2}. \quad (3.45)$$

The unit vector is given by,

$$\begin{aligned} \frac{\vec{O'A}}{|\vec{O'A}|} &= \hat{i} \frac{x_1}{\sqrt{x_1^2 + y_1^2 + z_1^2}} + \hat{j} \frac{y_1}{\sqrt{x_1^2 + y_1^2 + z_1^2}} + \hat{k} \frac{z_1}{\sqrt{x_1^2 + y_1^2 + z_1^2}} \\ &= \vec{k}'. \end{aligned} \quad (3.46)$$

Then the transformation components between those two frames of reference become,

$$\frac{x_1}{\sqrt{x_1^2 + y_1^2 + z_1^2}} = -\frac{\epsilon k_x \sin \phi^*}{\sqrt{1 + \epsilon^2 k^2 \sin^2 \phi^*}}, \quad (3.47)$$

$$\frac{y_1}{\sqrt{x_1^2 + y_1^2 + z_1^2}} = -\frac{\epsilon k_y \sin \phi^*}{\sqrt{1 + \epsilon^2 k^2 \sin^2 \phi^*}}, \quad (3.48)$$

$$\frac{z_1}{\sqrt{x_1^2 + y_1^2 + z_1^2}} = \frac{1}{\sqrt{1 + \epsilon^2 k^2 \sin^2 \phi^*}}. \quad (3.49)$$

From Eqs. 3.47 and 3.49,

$$\frac{x_1}{z_1} = -\epsilon k_x \sin \phi^*,$$

or,

$$x_1 = z_1 \epsilon k_x \sin \phi^*. \quad (3.50)$$

From Eqs. 3.48 and 3.49,

$$\frac{y_1}{z_1} = -\epsilon k_y \sin \phi^*,$$

or,

$$y_1 = z_1 \epsilon k_y \sin \phi^*. \quad (3.51)$$

From Eqs. 3.38, 3.50 and 3.51,

$$\begin{aligned} \phi - \phi^* &= k_x (z_1 \epsilon k_x \sin \phi^*) + k_y (z_1 \epsilon k_y \sin \phi^*) \\ &= z_1 \epsilon (k_x^2 \sin \phi^* + k_y^2 \sin \phi^*) \\ &= z_1 \epsilon k^2 \sin \phi^*. \end{aligned} \quad (3.52)$$

This approach physically shows what will happen while an observer is at the mid plane of the warped ring. Hence the local vertical gravitational acceleration g_z can be written as a combination of these contribution if we ignore non-circular motion

$$g_z = g_P + g_M + g_D, \quad (3.53)$$

where, g_P is due to planet, g_M is due to satellite forcing and g_D is due to self-gravity of warped disk.

However, initially for simplicity, let us consider only planetary and contribution from the satellite forcing. Then vertical component of equation of motion is given by,

$$\begin{aligned} \ddot{z} &= -\Omega^2 z + A \cos \phi \\ &= -\Omega^2 z + A \cos(k_x x + k_y y - \omega t). \end{aligned} \quad (3.54)$$

Considering Eq. 3.6. For $|z| \ll r$, the term $g_P = -\Omega^2 z$ as it behaves as a restoring force due to linear harmonic oscillator. The solution can be written as

$$z = -\frac{A}{(\Omega^2 - \omega^2)} \cos(k_x x + k_y y - \omega t) \quad (3.55)$$

Following techniques used by Shu [70], the radial coordinate dependent amplitude can be assumed to have the form as $A(x) = A_0 \exp[i \int k_x dx]$ using WKBJ formalism and considering the free solution. To get the principal Fourier component of the undamped disk, we choose $A_x = A_0 \exp[i k_x x]$. Identifying the wave amplitude with ϵ , one can clearly write A_0 as $A_0 = \epsilon(\Omega^2 - \omega^2)$.

Therefore, from Eqs. 3.55, the force component for satellite forcing is given as,

$$z_{\text{sat}} = \epsilon (\Omega^2 - \omega^2) \cos(k_x x + k_y y - \omega t). \quad (3.56)$$

To get components of satellite forcing from Eq. 3.56 in the frame of reference placed at the mid-plane of warped ring system, one has to multiply proper components from Eq. 3.47-3.49.

The equation of motion of test grain can be written as,

$$\ddot{x} = -2\Omega \dot{y} + 3\Omega^2 x - \nu^2 x_1 - \frac{(\Omega^2 - \omega^2) \epsilon^2 k_x \cos \phi \sin \phi^*}{(1 + \epsilon^2 k^2 \sin^2 \phi^*)^{\frac{1}{2}}}. \quad (3.57)$$

$$\ddot{y} = 2\Omega \dot{x} - \nu^2 y_1 - \frac{(\Omega^2 - \omega^2) \epsilon^2 k_y \cos \phi \sin \phi^*}{(1 + \epsilon^2 k^2 \sin^2 \phi^*)^{\frac{1}{2}}}, \quad (3.58)$$

and

$$\ddot{z} = -\Omega^2 z - \nu^2 z_1 + \frac{(\Omega^2 - \omega^2) \epsilon \cos \phi}{(1 + \epsilon^2 k^2 \sin^2 \phi^*)^{\frac{1}{2}}}. \quad (3.59)$$

Hence, for the mid plane of the warped ring, we may write,

$$z^* = \epsilon \cos(k_x x^* + k_y y^* - \omega t). \quad (3.60)$$

From Fig. 3.1 we can write,

$$\begin{aligned} z_1 &= z - z^* \\ &= z - \epsilon \cos(k_x x^* + k_y y^* - \omega t) \\ &= z - \epsilon \cos \phi^*, \end{aligned} \quad (3.61)$$

or,

$$\dot{z}_1 = \dot{z} + \epsilon \sin \phi^* (\dot{\phi}^*) \quad (3.62)$$

using Eq. 3.36, we get ,

$$\dot{\phi}^* = -\omega \quad (3.63)$$

or,

$$\ddot{z}_1 = \ddot{z} + \epsilon \omega^2 \cos \phi^*. \quad (3.64)$$

We assume that the force due to self gravity of the disk on a particle is that due to a flat disk of constant density ρ . Hence, frequency of vertical oscillations of a particle due to self gravity is,

$$\nu^2 = 4\pi G\rho. \quad (3.65)$$

Let us define,

$$\alpha^2 = \Omega^2 + \nu^2. \quad (3.66)$$

We consider the z -component of acceleration of the test particle acting under centrifugal force, Coriolis force and the moon forcing, i.e., enhancing Eq. 3.54, we write,

$$\ddot{z} = -\Omega^2 z - \nu^2 z_1 + \frac{(\Omega^2 - \omega^2) \epsilon \cos \phi}{(1 + \epsilon^2 k^2 \sin^2 \phi^*)^{\frac{1}{2}}}. \quad (3.67)$$

Since k^2 is very small, we may neglect $\epsilon^2 k^2 \sin^2 \phi^*$ term in the denominator. Hence from Eqs. 3.64 and 3.67,

$$\begin{aligned} \ddot{z} &= \ddot{z}_1 - \epsilon \omega^2 \cos \phi^* \\ &= -\Omega^2 z - \nu^2 z_1 + (\Omega^2 - \omega^2) \epsilon \cos \phi. \end{aligned}$$

Using Eqs. 3.38 and 3.61,

$$\begin{aligned} \ddot{z}_1 &= (\omega^2 - \Omega^2) \epsilon \cos \phi^* - (\Omega^2 + \nu^2) z_1 + \\ &\quad \epsilon (\Omega^2 - \omega^2) \cos [\phi^* + z_1 \epsilon k^2 \sin \phi^*]. \end{aligned} \quad (3.68)$$

Expanding,

$$\cos(\phi^* + z_1 \epsilon k^2 \sin \phi^*) = \cos \phi^* \cos(z_1 \epsilon k^2 \sin \phi^*) - \sin \phi^* \sin(z_1 \epsilon k^2 \sin \phi^*)$$

But since k^2 is very small $\epsilon z_1 k^2 \sin \phi^* \rightarrow 0$, which yields $\cos(z_1 \epsilon k^2 \sin \phi^*) \rightarrow 1$ and $\sin(z_1 \epsilon k^2 \sin \phi^*) \rightarrow z_1 \epsilon k^2 \sin \phi^*$. So, $\cos(\phi^* + z_1 \epsilon k^2 \sin \phi^*) \approx \cos \phi^* - \epsilon z_1 k^2 \sin^2 \phi^*$.

Hence, Eq. 3.68 can be modified from above approximations and Eq. 3.66

$$\begin{aligned} \ddot{z}_1 &= (\omega^2 - \Omega^2) \epsilon \cos \phi^* - (\Omega^2 + \nu^2) z_1 \\ &+ \epsilon (\Omega^2 - \omega^2) (\cos \phi^* - \epsilon z_1 k^2 \sin^2 \phi^*) \\ &= -\alpha^2 z_1 - \epsilon^2 (\Omega^2 - \omega^2) z_1 k^2 \sin^2 \phi^*. \end{aligned} \quad (3.69)$$

Let us transform Eq. 3.69 so that instead of its time dependence, we like to see its phase dependence. Thus from Eq. 3.36, we may derive,

$$\partial \phi^* = \omega \partial t,$$

or,

$$\frac{\partial}{\partial t} \equiv -\omega \frac{\partial}{\partial \phi^*}, \quad (3.70)$$

$$\frac{\partial^2}{\partial t^2} \equiv \omega^2 \frac{\partial^2}{\partial \phi^{*2}}. \quad (3.71)$$

Therefore, modifying Eq. 3.69 using Eq. 3.71, we get,

$$\frac{\partial^2 z_1}{\partial \phi^{*2}} = -\frac{z_1}{\omega^2} \left[\alpha^2 + \frac{\epsilon^2 (\Omega^2 - \omega^2) k^2}{2} \right] + \frac{\epsilon^2 (\Omega^2 - \omega^2) z_1 k^2 \cos 2\phi^*}{2\omega^2}. \quad (3.72)$$

Let us put,

$$\gamma^2 = \frac{\epsilon^2 k^2 (\Omega^2 - \omega^2)}{\omega^2} \quad (3.73)$$

and

$$\begin{aligned} \eta^2 &= \frac{\alpha^2}{\omega^2} + \frac{\epsilon^2 (\Omega^2 - \omega^2) k^2}{2\omega^2} \\ &= \frac{\alpha^2}{\omega^2} + \frac{\gamma^2}{2} \end{aligned} \quad (3.74)$$

Hence Eq. 3.72 reduces to

$$\frac{\partial^2 z_1}{\partial \phi^{*2}} = \eta^2 z_1 + \frac{\gamma^2 \cos 2\phi^*}{2} z_1 \quad (3.75)$$

The first term is simple harmonic. Hence we may assume the second term to be a source of perturbation and so z_1 can be assumed as to be expandable to a series.

$$\begin{aligned} \Rightarrow z_1 &= z_1^{(0)} + \gamma^2 z_1^{(1)} + \gamma^4 z_1^{(2)} + \gamma^6 z_1^{(3)} + \dots \\ &= z_1^{(0)} + \sum_{i=1}^N \gamma^{2i} z_1^{(i)}, \end{aligned} \quad (3.76)$$

or,

$$\frac{\partial^2 z_1}{\partial \phi^{*2}} = -\eta^2 \left[z_1^{(0)} + \sum_{i=1}^N \gamma^{2i} z_1^{(i)} \right] + \frac{\gamma^2 \cos 2\phi^*}{2} \left[z_1^{(0)} + \sum_{i=1}^N \gamma^{2i} z_1^{(i)} \right]. \quad (3.77)$$

It is clear that γ^2 is the perturbing factor. So we may compare coefficients of γ^2 and its higher terms on both sides.

From Eq. 3.77,

$$\frac{\partial^2 z_1^{(0)}}{\partial \phi^{*2}} = -\eta^2 z_1^{(0)}. \quad (3.78)$$

This is the zeroth order approximation and the solution can be approximated as

$$z_1^{(0)} = h \sin \eta \phi^*. \quad (3.79)$$

From Eqs. 3.77 and 3.79, equating the coefficients of γ^2 terms,

$$\frac{\partial^2 z_1^{(1)}}{\partial \phi^{*2}} = -\eta^2 z_1^{(1)} + \frac{\cos 2\phi^*}{2} z_1^{(0)}. \quad (3.80)$$

This gives,

$$z_1^{(1)} = -\frac{h}{16} \left[\frac{\sin(2+\eta)\phi^*}{1+\eta} - \frac{\sin(2-\eta)\phi^*}{1-\eta} \right]. \quad (3.81)$$

From Eqs. 3.77 and 3.81, considering γ^4 terms,

$$\frac{\partial^2 z_1^{(2)}}{\partial \phi^{*2}} = -\eta^2 z_1^{(2)} + \frac{\cos 2\phi^*}{2} z_1^{(1)}$$

$$z_1^{(2)} = \frac{h}{64} \left[\frac{\sin(4+\eta)\phi^*}{8(1+\eta)(2+\eta)} - \frac{4 \sin \eta \phi^*}{(1+\eta)(1-\eta)} - \frac{\sin(4-\eta)\phi^*}{8(1-\eta)(2-\eta)} \right]. \quad (3.82)$$

Hence the Eq. 3.76 can be re-written as,

$$\begin{aligned}
z_1 &= z_1^{(0)} + \gamma^2 z_1^{(1)} + \gamma^4 z_1^{(2)} + \gamma^6 z_1^{(3)} + \dots \\
&\cong h \sin \eta \phi^* - \frac{h\gamma^2}{16} \left[\frac{\sin(2+\eta)\phi^*}{1+\eta} - \frac{\sin(2-\eta)\phi^*}{1-\eta} \right] \\
&+ \frac{h\gamma^4}{64} \left[\frac{\sin(4+\eta)\phi^*}{8(1+\eta)(2+\eta)} - \frac{4 \sin \eta \phi^*}{(1+\eta)(1-\eta)} - \frac{\sin(4-\eta)\phi^*}{8(1-\eta)(2-\eta)} \right].
\end{aligned} \tag{3.83}$$

From Eqs. 3.50 and 3.51, we can again formulate x_1 and y_1 as,

$$\begin{aligned}
x_1 &= h\epsilon k_x \sin \phi^* \sin \eta \phi^* \\
&- \frac{h\gamma^2 \epsilon k_x}{16} \left\{ \frac{\sin \phi^* \sin(2+\eta)\phi^*}{1+\eta} - \frac{\sin \phi^* \sin(2-\eta)\phi^*}{1-\eta} \right\} \\
&+ \frac{h\gamma^4 \epsilon k_x}{64} \left\{ \frac{\sin \phi^* \sin(4+\eta)\phi^*}{8(1+\eta)(2+\eta)} - \frac{4 \sin \phi^* \sin \eta \phi^*}{(1+\eta)(1-\eta)} \right. \\
&\left. - \frac{\sin \phi^* \sin(4-\eta)\phi^*}{8(1-\eta)(2-\eta)} \right\},
\end{aligned} \tag{3.84}$$

and

$$\begin{aligned}
y_1 &= h\epsilon k_y \sin \phi^* \sin \eta \phi^* \\
&- \frac{h\gamma^2 \epsilon k_y}{16} \left\{ \frac{\sin \phi^* \sin(2+\eta)\phi^*}{1+\eta} - \frac{\sin \phi^* \sin(2-\eta)\phi^*}{1-\eta} \right\} \\
&+ \frac{h\gamma^4 \epsilon k_y}{64} \left\{ \frac{\sin \phi^* \sin(4+\eta)\phi^*}{8(1+\eta)(2+\eta)} - \frac{4 \sin \phi^* \sin \eta \phi^*}{(1+\eta)(1-\eta)} \right. \\
&\left. - \frac{\sin \phi^* \sin(4-\eta)\phi^*}{8(1-\eta)(2-\eta)} \right\}.
\end{aligned} \tag{3.85}$$

From Eq. 3.61, we may write z as

$$z = z_1 + \epsilon \cos \phi^*.$$

Using Eq. 3.83,

$$\begin{aligned}
z &= \epsilon \cos \phi^* + h \sin \eta \phi^* - \frac{h\gamma^2}{16} \left[\frac{\sin(2+\eta)\phi^*}{1+\eta} - \frac{\sin(2-\eta)\phi^*}{1-\eta} \right] \\
&+ \frac{h\gamma^4}{64} \left[\frac{\sin(4+\eta)\phi^*}{8(1+\eta)(2+\eta)} - \frac{4 \sin \eta \phi^*}{(1+\eta)(2-\eta)} - \frac{\sin(4-\eta)\phi^*}{8(1-\eta)(2-\eta)} \right].
\end{aligned} \tag{3.86}$$

Now let us consider the cases for x and y from Eqs. 3.57 and 3.58, and since k^2 is very small we can approximate as,

$$\ddot{x} = -2\Omega\dot{y} + 3\Omega^2x - \nu^2x_1 - (\Omega^2 - \omega^2) \epsilon^2 k_x \cos \phi \sin \phi^*, \quad (3.87)$$

and

$$\ddot{y} = 2\Omega\dot{x} - \nu^2y_1 - (\Omega^2 - \omega^2) \epsilon^2 k_y \cos \phi \sin \phi^*. \quad (3.88)$$

From Eqs. 3.50 and 3.51,

$$\ddot{x} = -2\Omega\dot{y} + 3\Omega^2x - \left[\nu^2 + \frac{\epsilon(\Omega^2 - \omega^2) \cos \phi}{z_1} \right] x_1, \quad (3.89)$$

and

$$\ddot{y} = 2\Omega\dot{x} - \left[\nu^2 + \frac{\epsilon(\Omega^2 - \omega^2) \cos \phi}{z_1} \right] y_1. \quad (3.90)$$

Let us put,

$$\delta = \nu^2 + \frac{\epsilon(\Omega^2 - \omega^2) \cos \phi}{z_1}. \quad (3.91)$$

Hence Eqs. 3.89 and 3.90 can be reformed as

$$\ddot{x} = -2\Omega\dot{y} + 3\omega^2x - \delta x_1, \quad (3.92)$$

and

$$\ddot{y} = 2\Omega\dot{x} - \delta y_1. \quad (3.93)$$

Since $k_x \gg k_y$, we may assume $x_1 \gg y_1$. Thus assuming $y_1 \sim 0$, Eq. 3.93 yields

$$\dot{y} = 2\Omega x. \quad (3.94)$$

Using Eq. 3.94 in Eq. 3.92, we get

$$\ddot{x} = -\Omega^2x - \delta x_1.$$

Again, from Eq. 3.91, $\delta \cong \nu^2$, since at the resonance condition $\Omega^2 \cong \omega^2$. Also considering Eq. 3.71

$$\ddot{x} \cong \omega^2 \frac{\partial^2 x}{\partial \phi^{*2}} = \Omega^2 x - \nu^2 x_1, \quad (3.95)$$

or,

$$\begin{aligned}
\frac{\partial^2 x}{\partial \phi^{*2}} &= -\frac{\Omega^2}{\omega^2}x - \frac{\nu^2}{\omega^2}x_1 = -\frac{\Omega^2}{\omega^2}x - \frac{\nu^2 \epsilon k_x h}{\omega^2} \sin \phi^* \sin \eta \phi^* \\
&+ \frac{\nu^2 \epsilon k_x h}{\omega^2} \left[\frac{\gamma^2}{16} \left\{ \frac{\sin \phi^* \sin(2+\eta)\phi^*}{1+\eta} - \frac{\sin \phi^* \sin(2-\eta)\phi^*}{1-\eta} \right\} \right] \\
&- \frac{\nu^2 \epsilon k_x h}{\omega^2} \left[\frac{\gamma^4}{64} \left\{ \frac{\sin \phi^* \sin(4+\eta)\phi^*}{8(1+\eta)(2+\eta)} - \frac{4 \sin \phi^* \sin \eta \phi^*}{(1+\eta)(1-\eta)} \right. \right. \\
&\left. \left. - \frac{\sin \phi^* \sin(4-\eta)\phi^*}{8(1-\eta)(2-\eta)} \right\} \right]. \tag{3.96}
\end{aligned}$$

Thus, we may write again as final differential equation as follows:

$$\begin{aligned}
\left(D^2 + \frac{\Omega^2}{\omega^2}x \right) / \frac{\nu^2 \epsilon k_x h}{2\omega^2} &= -\cos(1-\eta)\phi^* + \cos(1+\eta)\phi^* \\
&+ \frac{\gamma^2 \cos(1+\eta)\phi^*}{16(1+\eta)} - \frac{\gamma^2 \cos(3+\eta)\phi^*}{16(1+\eta)} - \frac{\gamma^2 \cos(1-\eta)\phi^*}{16(1-\eta)} \\
&+ \frac{\gamma^2 \cos(3-\eta)\phi^*}{16(1-\eta)} - \frac{\gamma^4 \cos(3+\eta)\phi^*}{512(1+\eta)(2+\eta)} + \frac{\gamma^4 \cos(5+\eta)\phi^*}{512(1+\eta)(2+\eta)} \\
&+ \frac{\gamma^4 \cos(1-\eta)\phi^*}{16(1+\eta)(1-\eta)} - \frac{\gamma^4 \cos(1+\eta)\phi^*}{16(1+\eta)(1-\eta)} + \frac{\gamma^4 \cos(3-\eta)\phi^*}{512(1-\eta)(2-\eta)} \\
&- \frac{\gamma^4 \cos(5-\eta)\phi^*}{512(1-\eta)(2-\eta)}. \tag{3.97}
\end{aligned}$$

The complementary function for Eq. 3.97 can be written as,

$$x_{CF} = A_x \sin(\delta + \Omega\phi^*/\omega), \tag{3.98}$$

where, A_x and δ are some constants. Since δ is some arbitrary phase, our system in the warped ring may be chosen so as to make $\delta = 0$. A_x is actually the amplitude of the epicyclic motion as we are dealing with x -direction which is along the radial direction. Chakrabarti [14] assumed that A is of the order of the half thickness of the ring and hence we may re-write as

$$x_{CF} = h \sin(\Omega\phi^*/\omega). \tag{3.99}$$

The particular integral may be reduced to,

$$x_{PI} \simeq -\frac{\nu^2 \epsilon k_x h}{2\omega^2} \left[\frac{1 + \gamma^2/16(1-\eta)}{\Omega^2/\omega^2 - (1-\eta)^2} \cos(1-\eta)\phi^* \right]$$

$$\begin{aligned}
& -\frac{1 + \gamma^2/16(1 + \eta)}{\Omega^2/\omega^2 - (1 + \eta)^2} \cos(1 + \eta)\phi^* \\
& + \frac{\gamma^2/16 + \gamma^4/512(2 - \eta)}{(1 - \eta)[\Omega^2/\omega^2 - (3 - \eta)^2]} \cos(3 - \eta)\phi^* \\
& + \frac{\gamma^2/16 + \gamma^4/512(2 + \eta)}{(1 + \eta)[\Omega^2/\omega^2 - (3 + \eta)^2]} \cos(3 + \eta)\phi^* \\
& + \frac{\gamma^4/512(1 - \eta)(2 - \eta)}{[\Omega^2/\omega^2 - (5 - \eta)^2]} \cos(5 - \eta)\phi^* \\
& - \frac{\gamma^4/512(1 + \eta)(2 + \eta)}{[\Omega^2/\omega^2 - (5 + \eta)^2]} \cos(5 + \eta)\phi^* \Big].
\end{aligned} \tag{3.100}$$

Hence combining the Eq. 3.99 and 3.100, the equation the locus of the dust grain is

$$\begin{aligned}
x & = h \sin(\Omega\phi^*/\omega) \\
& + \frac{\nu^2 \epsilon k_x h}{2\omega^2} \left[\frac{1 + \gamma^2/(16(1 - \eta))}{\Omega^2/\omega^2 - (1 - \eta)^2} \cos(1 - \eta)\phi^* \right. \\
& - \frac{1 + \gamma^2/(16(1 + \eta))}{\Omega^2/\omega^2 - (1 + \eta)^2} \cos(1 + \eta)\phi^* \\
& + \frac{\gamma^2/16 + \gamma^4/(512(2 - \eta))}{(1 - \eta)[\Omega^2/\omega^2 - (3 - \eta)^2]} \cos(3 - \eta)\phi^* \\
& + \frac{\gamma^2/16 + \gamma^4/(512(2 + \eta))}{(1 + \eta)[\Omega^2/\omega^2 - (3 + \eta)^2]} \cos(3 + \eta)\phi^* \\
& + \frac{\gamma^4/(512(1 - \eta)(2 - \eta))}{[\Omega^2/\omega^2 - (5 - \eta)^2]} \cos(5 - \eta)\phi^* \\
& \left. - \frac{\gamma^4/(512(1 + \eta)(2 + \eta))}{[\Omega^2/\omega^2 - (5 + \eta)^2]} \cos(5 + \eta)\phi^* \right],
\end{aligned} \tag{3.101}$$

$$\begin{aligned}
y & = 2h \cos\left(\frac{\Omega\phi^*}{\omega}\right) \\
& - \frac{\nu^2 \epsilon k_x h \Omega}{\omega^3} \left[\frac{1 + \gamma^2/16(1 - \eta)}{\frac{\Omega^2}{\omega^2} - (1 - \eta)^2} \frac{1}{(1 - \eta)} \sin(1 - \eta)\phi^* \right. \\
& + \frac{1 + \gamma^2/16(1 + \eta)}{\frac{\Omega^2}{\omega^2} - (1 + \eta)^2} \frac{1}{(1 + \eta)} \sin(1 + \eta)\phi^* \\
& + \frac{\gamma^2/16 + \gamma^4/512(2 - \eta)}{\frac{\Omega^2}{\omega^2} - (3 - \eta)^2} \frac{1}{(1 - \eta)(3 - \eta)} \sin(3 - \eta)\phi^*
\end{aligned}$$

$$\begin{aligned}
& + \frac{\gamma^2/16 + \gamma^4/512(2 + \eta)}{\frac{\Omega^2}{\omega^2} - (3 + \eta)^2} \frac{1}{(1 + \eta)(3 + \eta)} \sin(3 + \eta)\phi^* \\
& + \frac{\gamma^4/512(1 - \eta)(2 - \eta)}{\frac{\Omega^2}{\omega^2} - (5 - \eta)^2} \frac{1}{(5 - \eta)(3 - \eta)} \sin(5 - \eta)\phi^* \\
& - \frac{\gamma^4/512(1 + \eta)(2 + \eta)}{\frac{\Omega^2}{\omega^2} - (5 + \eta)^2} \frac{1}{(5 + \eta)(3 - \eta)} \sin(5 + \eta)\phi^* \Big] \\
& + \frac{\nu^2 \epsilon k_y h}{2\omega^2} \left[\frac{\cos(1 - \eta)\phi^*}{(1 - \eta)^2} - \frac{\cos(1 + \eta)\phi^*}{(1 + \eta)^2} - \frac{\gamma^2 \cos(1 + \eta)\phi^*}{16(1 + \eta)^3} \right. \\
& + \frac{\gamma^2 \cos(3 + \eta)\phi^*}{16(1 + \eta)(3 + \eta)^2} \\
& \left. + \dots \text{other terms of higher perturbations} \right], \tag{3.102}
\end{aligned}$$

$$\begin{aligned}
z = & \epsilon \cos \phi^* + h \sin \eta \phi^* - \frac{h\gamma^2}{16} \left[\frac{\sin(2 + \eta)\phi^*}{1 + \eta} - \frac{\sin(2 - \eta)\phi^*}{1 - \eta} \right] \\
& + \frac{h\gamma^4}{64} \left[\frac{\sin(4 + \eta)\phi^*}{8(1 + \eta)(2 + \eta)} - \frac{\sin \eta \phi^*}{(1 + \eta)(1 - \eta)} - \frac{\sin(4 - \eta)\phi^*}{8(1 - \eta)(2 - \eta)} \right]. \tag{3.103}
\end{aligned}$$

Hence the equations for X , Y and Z components are given by Eqs. 3.101, 3.102 and 3.103. Since $k_y \ll k_x$ the variation along the y axis may be neglected.

This analytical model may be used for calculation of the damping length of the bending wave in the planetary rings [4, 5]. To calculate the damping length, the energy density of the wave is first calculated using Eq. 3.104 and then the dissipation of the wave is calculated as per (3.105)

$$E_w = \frac{1}{2} \epsilon^2 \Omega^2, \tag{3.104}$$

$$\dot{E}_w = \nu_k \left(\frac{\partial \langle v_x \rangle}{\partial z_1} \right)^2, \tag{3.105}$$

where, the kinematic viscosity ν_k is given by

$$\nu_k = \Omega \tau \max \left(R^2, R_{epi}^2 \right). \tag{3.106}$$

Here R is the size of the largest particle and R_{epi} is the amplitude of the epicyclic motion which is similar to half the thickness of the ring

i.e. h . The group velocity is given by,

$$c_g = \frac{\pi G \sigma}{\omega - m \Omega}, \quad (3.107)$$

Hence the damping length is estimated as,

$$\lambda_D = \frac{E_w}{E_w} c_g, \quad (3.108)$$

The numerical simulation based upon this calculation is given in Chapter 4 using Runge-Kutta algorithm. The numerical calculation is totally based on the numerical integration of the Eq. 3.109 by the Runge-Kutta method.

$$\begin{aligned} \frac{d^2 x}{dt^2} &= -2\Omega \frac{dy}{dt} + 3\Omega^2 x - \nu^2 x_1 - (\Omega^2 - \omega^2) \epsilon^2 \kappa_x \cos(\phi) \sin(\phi^*) / Y \\ \frac{d^2 y}{dt^2} &= 2\Omega \frac{dx}{dt} - \nu^2 y_1 - (\Omega^2 - \omega^2) \epsilon^2 \kappa_y \cos(\phi) \sin(\phi^*) / Y \\ \frac{d^2 z}{dt^2} &= -\Omega^2 z - \nu^2 z_1 + (\Omega^2 - \omega^2) \epsilon \cos(\phi) / Y, \end{aligned} \quad (3.109)$$

where,

$$Y = [1 + \epsilon^2 \kappa^2 \sin^2(\phi^*)]^{1/2}. \quad (3.110)$$

Later the numerical simulation results [*vide* Chapter 4] were matched with the analytical results as may be found in Chapter 5. The shear values determined from Chapter 5 matches with that obtained from the numerical simulation which may be seen from Chapter 4.

3.4.2 The Fluid Dynamics

The fluid dynamics treatment uses the WKBJ approximation for the disk perturbation. In general, it is customary to use the infinitesimally thin disk approximation. Also there were some efforts to find the result for finite height of the disk. Initially let us explore the thin disk approximation.

The thin disk approximation

The entire vertical dynamics is valid for the assumption $R \gg h$. The entire vertical dynamics for a small vertical displacement $\xi(r, \phi, z, t)$ is given by,

$$\left[\frac{\partial}{\partial t} + \Omega(r) \frac{\partial}{\partial \phi} \right]^2 \xi(r, \phi, z, t) = g_z, \quad (3.111)$$

where, g_z =local vertical force per unit mass, such as $g_z = g_p + g_s + g_d + g_l + g_{rad} + \dots$ where, g_p for planetary contribution, g_s for satellite forcing, g_d for disk self-gravity, g_l for Lorentz force component, g_{rad} for radiation force component and so on ... However, for the time being we should only consider the effect of gravity and the self gravity of the disk itself. However, we like to consider now the forcing due to planet and the self-gravity in this discussion.

Now the planetary component comes as,

$$g_p = -\mu^2 \xi, \quad \text{for, } |\xi| \ll r \quad (3.112)$$

Next, let us inquire for the contribution that comes from the disk. Whenever a dust grain is pulled above the normal ring plane by the satellite forcing etc., then this grain feels gravitational attraction from the portion of the whole disk which can see it atop. Hence the dusts placed at a distance from the normal to the disk plane also exerts some force on the test dust. Hence, in effect, the test dust particle will feel a smooth surface density profile due to the whole disk and not a localised surface density. The density distribution corresponding to a pure bending of the disk is

$$\rho_d(r, \phi, z, t) = \sigma(r, \phi, t) \delta(z - \xi(r, \phi, z = 0, t)), \quad (3.113)$$

such that the surface density is given by,

$$\sigma(r, \phi, t) = \Sigma(r) \exp [i(\omega t - m\phi)], \quad (3.114)$$

where, $\Sigma(r) =$ unperturbed disk surface density and $\delta(x) =$ Dirac delta function. We assume, with Lin and Shu [44], that in the ring plane modeled with infinitesimal thickness, there exists a gravitational potential term as,

$$\Phi_d(r, \phi, z, t) = \phi_d(r, z) \exp [i(\omega t - m\phi)]. \quad (3.115)$$

Hence the Poisson's equation may be modified as,

$$\nabla^2 \phi_d(r, z) = 4\pi G \Sigma(r) \delta(z - \xi(r, t)). \quad (3.116)$$

Hence just at the ring mid-plane, we may write,

$$\Sigma(r) = \frac{1}{4\pi G} \left[\frac{\partial}{\partial z} \phi_d(r, z) \right]_{z=0^-}^{z=0^+}. \quad (3.117)$$

The Eq. 3.116 can be re-written as

$$\left(\frac{\partial^2}{\partial r^2} + \frac{1}{r} \frac{\partial}{\partial r} + \frac{\partial^2}{\partial z^2} \right) \phi_d(r, z) = 4\pi G \Sigma(r) \delta(z - \xi(r, t)). \quad (3.118)$$

Since the cross-radial components are too small with respect to other terms, it may be neglected from Eq. 3.118. This assumption, in turn, ensures the homogeneity of the thin disk approximation. Hence Eq. 3.118 reduces to

$$\left(\frac{\partial^2}{\partial r^2} + \frac{\partial^2}{\partial z^2} \right) \phi_d(r, z) = 4\pi G \Sigma(r) \delta(z - \xi(r, t)). \quad (3.119)$$

To solve Eq. 3.119 we consider the potential and its Fourier transform as,

$$\phi_d(r, z) = \frac{1}{2\pi} \int_{-\infty}^{+\infty} \tilde{\phi}_d(r, k_z) \exp(ik_z z) dk_z, \quad (3.120)$$

and,

$$\tilde{\phi}_d(r, k_z) = \frac{1}{2\pi} \int_{-\infty}^{+\infty} \phi_d(r, z) \exp(-ik_z z) dz, \quad (3.121)$$

Using Eqs. 3.120 and 3.121, the Fourier transform of Eq. 3.119 becomes

$$\left(\frac{\partial^2}{\partial r^2} - k_z^2 \right) \tilde{\phi}_d(r, k_z) = 4\pi G \Sigma(r) \exp(-ik_z \xi). \quad (3.122)$$

We assume that Σ and ξ vanish if $r \leq 0$ and also $\phi_d \rightarrow 0$ as $(r^2 + z^2) \rightarrow \infty$, *i.e.*, if $r \rightarrow \infty$. Following Mark [48], using the Green's function technique, we write

$$\tilde{\phi}_d(r, k_z) = -\frac{2\pi G}{|k_z|} \int_{-\infty}^{+\infty} \Sigma(\alpha) \exp(-i\xi(\alpha)k_z) \cdot \exp(-|k_z||r - \alpha|) \cdot d\alpha. \quad (3.123)$$

Now, $g_D = -\frac{\partial}{\partial z} \mathcal{R}e(\phi_d) =$ acceleration in z component on the bent disk. Hence, we write

$$-\frac{\partial}{\partial z} [\mathcal{R}e\{\phi_d\}] = Gi \int_{-\infty}^{+\infty} d\alpha \Sigma(\alpha) \left[-\int_{-\infty}^0 dk_z \exp\{ik_z z - i\xi(\alpha)k_z + k_z|r - \alpha|\} + \int_0^{+\infty} dk_z \exp\{ik_z z - i\xi(\alpha)k_z - k_z|r - \alpha|\} \right],$$

or,

$$-\frac{\partial}{\partial z} [\mathcal{R}e\{\phi_d\}] = -2G \int_{-\infty}^{+\infty} d\alpha \Sigma(\alpha) \cdot \frac{z - \xi(\alpha)}{(z - \xi(\alpha))^2 + (r - \alpha)^2}. \quad (3.124)$$

Since α is arbitrarily chosen, the main contribution comes from the region where $\alpha \rightarrow r$. Hence in the linearized limit of smaller height with respect to the radial scale of variation of ξ , we may write using Taylor's series that

$$\xi(r) = \xi(\alpha) + \xi'(\alpha)(r - \alpha) + \dots \quad (3.125)$$

or,

$$(\xi(r) - \xi(\alpha)) = \xi'(\alpha)(r - \alpha) \quad (3.126)$$

In the limiting value, $\alpha \rightarrow r$, $[\xi(r) - \xi(\alpha)]^2 \rightarrow 0$. Let $\epsilon = [\xi(r) - \xi(\alpha)] \rightarrow 0$. Hence Eq. 3.124 reduces to

$$g_D = -2G \lim_{\epsilon \rightarrow 0} \int_{-\infty}^{+\infty} d\alpha \Sigma(\alpha) \frac{\xi'(\alpha)(r - \alpha)}{\epsilon^2 + (r - \alpha)^2}. \quad (3.127)$$

Since we considered infinitesimally thin disk using Eq. 3.115, one may adopt a vertical displacement of the infinitesimally thin disk of the form

$$\begin{aligned} \xi(r, \phi, z = 0, t) &= \mathcal{R}e[h(r, \phi, z = 0, t)] \\ &= \mathcal{R}e[H(r) \exp i(\omega t - m\phi)], \end{aligned} \quad (3.128)$$

where,

$$H(r) = A \exp \left[i \int^r k(r') dr' \right]. \quad (3.129)$$

Here, $k(r)$ and m are the radial and azimuthal wave numbers. The quantities ω , $k(r)$ and A are in general complex.

Thus,

$$\left[\frac{\partial}{\partial t} + \Omega(r) \frac{\partial}{\partial \phi} \right]^2 \xi = -[\omega - m\Omega(r)]^2 h. \quad (3.130)$$

Hence using Eqs. 3.127, 3.129 and 3.130, we may write,

$$[\omega - m\Omega(r)]^2 = 2\pi G\Sigma(r)s_k|k(r)|, \quad (3.131)$$

where, $s_k = \text{sgn}(k(r))$, indicating the leading or trailing pattern of the spiral wave.

Hence, the dispersion relation of the spiral bending wave considering the effects due to the planet and the self-gravity due to the disk becomes,

$$\mu^2 - [\omega - m\Omega(r)]^2 = -2\pi G\Sigma(r)s_k|k(r)|. \quad (3.132)$$

Again,

$$h = H \exp i(\omega t - m\phi) = A \exp \left(i \int^r k(r') dr' \right) \cdot \exp [i(\omega t - m\phi)], \quad (3.133)$$

or,

$$ih|k| = h \frac{d}{dr} (\ln h). \quad (3.134)$$

So, the previous form Eq. 3.132 the dispersion of the spiral bending wave may be written in another convenient form as

$$\left[D - 2\pi Gi\Sigma(r)s_k \frac{d}{dr} \right] h = 0, \quad (3.135)$$

or,

$$D = \mu^2 - [\omega - m\Omega(r)]^2. \quad (3.136)$$

From the dispersion relation of the form Eq. 3.132, we may derive the group velocity as

$$\begin{aligned} c_g &= -\frac{\partial \omega}{\partial k}, \\ &= -\frac{\pi G\Sigma(r)s_k}{(\omega - m\Omega(r))}. \end{aligned} \quad (3.137)$$

The disk with finite thickness

Consider a disk of finite half-thickness h is a set of infinitesimally thin layers at distances z_i from $z = 0$ midplane.

The perturbed surface density for i -th plane

$$d\sigma_{i_1} = \rho_1(z_i)dz. \quad (3.138)$$

Hence the perturbed surface density of the whole disk is

$$\sigma_1 = \int_{-h}^{+h} \rho_1(z)dz. \quad (3.139)$$

Outside the i -th layer, potential generated by the i -th layer is governed by the Laplace equation,

$$\left[\frac{\partial^2}{\partial r^2} + \frac{1}{r} \frac{\partial}{\partial r} + \frac{1}{r^2} \frac{\partial^2}{\partial \phi^2} + \frac{\partial^2}{\partial (z - z_i)^2} \right] \phi_i(r, \phi, z) = 0. \quad (3.140)$$

Using the principle of separation of variables, let us consider

$$\phi_i(r, \phi, z) = R(r)\Phi(\phi)Z_i(z) = R(r)Z_i(z)e^{im\phi}. \quad (3.141)$$

Using Eq. 3.141 in Eq. 3.140,

$$\frac{1}{R} \left[\frac{\partial^2 R}{\partial r^2} + \frac{1}{r} \frac{\partial R}{\partial r} - \frac{m^2}{r^2} R \right] = -\frac{1}{Z_i} \frac{\partial^2 Z_i}{\partial (z - z_i)^2} = -l^2 \text{ (say), } [l^2 > 0]. \quad (3.142)$$

From, Eq. 3.142,

$$\frac{d^2 R}{dr^2} + \frac{1}{r} \frac{dR}{dr} + \left(l^2 - \frac{m^2}{r^2} \right) R = 0.$$

Let $x = lr$, and we get,

$$\frac{d^2 R}{dx^2} + \frac{1}{x} \frac{dR}{dx} + \left(1 - \frac{m^2}{x^2} \right) R = 0.$$

or,

$$R = c J_m(x), \quad (3.143)$$

where, $J_m(x)$ is the Bessel's function of first kind.

Also,

$$\frac{\partial^2 Z_i}{\partial (z - z_i)^2} = l^2 Z_i.$$

$$Z_i(z) = A \exp[-|l| |(z - z_i)|], \quad z \neq z_i. \quad (3.144)$$

Hence the potential for the i -th layer may be written as

$$\phi_i(r, \phi, z) = A_i J_m(r|l|) \exp[im\phi - |l| |(z - z_i)|]. \quad (3.145)$$

Let us consider the contribution in the i -th layer due to the potential generated by the i -th layer itself as,

$$\left[(\nabla^2)_{\perp} + \frac{\partial^2}{\partial(z - z_i)^2} \right] \phi_i^{in} = 4\pi G d\sigma_i \delta(z - z_i). \quad (3.146)$$

Since the finite disk is a continuous substance, the net potential contribution on it must also be continuous for all values of z including $z = z_i$.

This means $\phi_i^{in} = \phi_i$, for $z = z_i$.

Putting Eq. 3.145 which is valid for outside the i -th region to the case for within the i -th region Eq. 3.146,

$$\begin{aligned} -2|l| \delta(z - z_i) A_i J_m(r|l) \exp[im\phi - |l||z - z_i|] \Big|_{z=z_i} = \\ 4\pi G d\sigma_i \delta(z - z_i) \Big|_{z=z_i}. \end{aligned}$$

By summing up the contributions of all the infinitesimally thin layers, the gravitational potential of the original layer of finite thickness:

$$\Phi(r, \phi, z) = -\frac{2\pi G}{|l|} \int_{-h}^{+h} \exp[-|l||z - z_i|] \rho(z_i) dz_i. \quad (3.147)$$

Chapter 4

Numerical modeling of Titan -1:0 resonance¹

4.1 Introduction

There was confusion in the early eighties about the vertical thickness of the Saturn's ring [18]. Extrapolation of the photometric brightness to zero tilt angle yielded a thickness of the order of one kilometer [10, 71]. However, Voyager photo-polarimeter experiment indicated that the height is far less, and this puts an upper limit of 200m to be the local thickness at the outer edge of the A Ring [40]. After identification of oscillatory features as bending waves [68] and after a good fit of the ring profile the effective thickness is now believed to be far lesser, of the order of a few tens of meters [14, 59, 60]. One of the important new ingredients that has gone into the measurement of thickness is a new source of shear which was found to be present during detailed numerical study of dynamics of particles inside the Saturn's ring. This extra source of shear is found to effectively damp out the Mimas 5:3 bending wave within few tens of kilometers and since then is considered to be important [9, 53, 60] to describe particle dynamics inside a ring. In the present paper, we analyse Titan -1:0 nodal bending wave in Saturn's ring and estimate the importance of this new source of shear. Our motivation stems from the fact that this reso-

¹accepted for publication as letters in the Monthly Notices of Royal Astronomical Society (*MNRAS*), v326, pages L23-L26, 11th Sept. 2001, UK

nance occurs much closer to Saturn than the Mimas 5:3 resonance, and therefore the angular frequency Ω , and hence normal shear $\sim -3\Omega/2$ should be much larger. In fact, the damping length for this resonance is also smaller (around 85km to reduce the amplitude to a negligible value) compared to the damping length of about 150km for Mimas 5:3 resonance. We verify through our simulation that indeed, the new shear is weaker compared to what was obtained in the A ring and as a result for all reasonable values of the ring parameters, the damping length is very large. However, pending an accurate knowledge of the parameters, such as the thickness, the amplitude of bending waves, and the surface density, we determine possible limits of these values assuming this to be the only source of shear. We find that in order to have this damping length, the upper limit of the thickness of the ring is likely to be around 40 meters. Apart from this, we note that the distribution of matter inside a C ring is quite different from that of the A ring. In most of the phases of the bending wave, population is highest near the edges of the wave, rather than in the midplane.

In the next Section, we briefly discuss the observed features of the -1:0 bending wave and show that the earlier analysis is not conclusive in determining the thickness of the ring locally. In §3, we describe briefly our numerical simulation procedure to compute particle and velocity distribution in the local vertical direction of the bending wave. From these, we compute local shear and dissipation length. In §4, we present our results. In §5, we discuss on the results obtained from the analytical expressions. Finally, in §6, we draw our conclusions.

4.2 Observed features at the -1:0 nodal bending wave

When a satellite orbits at the same rate as that of the nodal regression of the ring matter, a nodal bending wave is formed with a one-armed spiral. In the case of Titan -1:0 resonance, the wave propagates outward. Its spiral pattern winds in the direction of the motion of the ring particles while the pattern rotates in the retrograde direction. Average optical depth variation at the location of this resonance clearly shows

'W' patterns which are easily interpreted as multiple passages of light through the ring bent out of the equatorial plane. The radio occultation data clearly allows identification of 28 oscillating waves. These waves start at the inner vertical resonance (IVR) $r_v = 77515 \pm 13\text{km}$ and dies out at around 77609km. Near $r = r_v$, constant density (σ) rings have wavelength [68],

$$\lambda(r) = 209 \frac{\sigma}{r - r_v}, \quad (4.1)$$

where, σ is the local surface mass density in the region of the resonance in units of g/cm^2 and r , r_v and λ are in kilometers. An expression for the amplitude of the bending wave is given in [59],

$$|A_v| = \frac{334}{\sigma^{1/2}} m. \quad (4.2)$$

However, fitting of the 'W' shaped features suggests [59] $\sigma = 4.5 \text{g}/\text{cm}^2$, but it requires an amplitude ten times larger than what Eq. 4.2 would predict. The wavelength obtained for these parameters at $r - r_v = 20\text{km}$ is about 47km. One could use a more realistic $\sigma = 0.45\text{g}/\text{cm}^2$ which produces an amplitude of 500m. The wavelength obtained from this at a distance of 20km from the IVR becomes around 4.7km Eq. 4.1, which is not observed. Further fits of varying wavelength suggest that the surface density varies from $\sigma = 0.86 \pm 0.05\text{g}/\text{cm}^2$ near the IVR to $\sigma = 0.39 \pm 0.02 \text{g}/\text{cm}^2$ [59]. According to the standard model of the bending wave the amplitude of the wave should decay as [68],

$$A(r) = \left(\frac{r_v}{r}\right)^{1/2} \frac{\sigma(r_v)}{\sigma(r)} A_v \exp(-|(r - r_v)/\lambda_D|^3), \quad (4.3)$$

where, λ_D is the damping length,

$$\lambda_D = r_v |\epsilon| \left\{ \frac{3|\mathcal{D}|r^2}{\mu\nu} \right\}^{1/3}, \quad (4.4)$$

$$\mathcal{D} \equiv \left(r \frac{dD}{dr} \right)_{r_v}, \quad (4.5)$$

$$\epsilon \equiv \left(\frac{2\pi G\sigma}{rD} \right)_{r_v}, \quad (4.6)$$

$$D \equiv \mu^2 - (\omega - m\Omega)^2. \quad (4.7)$$

Here, μ is the vertical oscillation frequency, and ν is the kinematic shear viscosity. From a linear theory of viscous damping, the viscosity in the region of $-1 : 0$ resonance is given by [59],

$$\nu = 4.76 \times 10^5 \left(\frac{\sigma}{\lambda_D} \right)^3 \frac{\text{cm}^2}{\text{s}}. \quad (4.8)$$

With a fitted $\nu \sim 0.4\text{g/cm}^2$, and a damping length of $l_D \geq 50\text{km}$, one gets an upper limit of $\nu \sim 0.24 \text{ cm}^2/\text{s}$. Using this, the ring scale height becomes less than 2.6 m [59].

These conclusions create more confusion than resolving the problem. Naturally one would ask: (a) Is the amplitude of the wave around 1600m or 500m at the launching site? Is the surface density $\sigma = 0.45\text{g/cm}^2$ or, $\sigma = 4.5\text{g/cm}^2$? Could the height of the ring be so small ($h \sim 2.6\text{m}$)? While we are unable to answer much of these questions, we find that the dynamics of particles is not simple inside the ring and assuming quite reasonable values of the amplitude 1200m, and of the surface density 0.45g/cm^2 , we find that the upper limit of the thickness of the ring is around 40m. We also notice that unlike the case of the A ring, matter the population of the particles is *denser* nearer the edge of the ring. We also find that there is some shear in the vertical direction because of the variation of the radial velocity along the local vertical direction.

4.3 Numerical Simulation Procedure

In this work, we integrate three second order ordinary differential equations by the fourth order Runge-Kutta method. These equations represent the components of accelerations that are experienced by a particle located at x, y, z inside the ring in a Cartesian coordinate whose X-Y plane coincides with the average plane of the ring and Z axis lies along the local normal to the ring. They are given by Chakrabarti [14],

$$\frac{d^2x}{dt^2} = -2\Omega \frac{dy}{dt} + 3\Omega^2 x - \nu^2 x_1 - (\Omega^2 - \omega^2) \epsilon^2 \kappa_x \cos(\phi) \sin(\phi^*) / Y. \quad (4.9)$$

$$\frac{d^2y}{dt^2} = 2\Omega \frac{dx}{dt} - \nu^2 y_1 - (\Omega^2 - \omega^2) \epsilon^2 \kappa_y \cos(\phi) \sin(\phi^*) / Y \quad (4.10)$$

and

$$\frac{d^2 z}{dt^2} = -\Omega^2 z - \nu^2 z_1 + (\Omega^2 - \omega^2)\epsilon \cos(\phi)/Y, \quad (4.11)$$

where,

$$Y = [1 + \epsilon^2 \kappa^2 \sin^2(\phi^*)]^{1/2}.$$

Here, Ω is the angular frequency at the location where damping is being calculated, $\omega = (\Omega_p - \Omega)$ where, Ω_p is the pattern frequency (in this case, equal to the frequency of Titan, with a minus sign.) ϵ is the amplitude of the bending wave described by,

$$z^* = \epsilon \cos(\kappa_x x^* + \kappa_y y^* - \omega t) = \epsilon \sin(\phi^*). \quad (4.12)$$

Here, (x^*, y^*, z^*) denote the co-coordinate on the midplane, κ_x and κ_y denote the wave numbers of the wave along X- and Y- directions respectively: $\kappa^2 = \kappa_x^2 + \kappa_y^2$. The distance of a particle at (x, y, z) from the origin on the midplane is,

$$x_1 = x - x^* = z_1 \epsilon \kappa_x \sin(\phi^*), \quad (4.13)$$

$$y_1 = y - y^* = z_1 \epsilon \kappa_y \sin(\phi^*), \quad (4.14)$$

$$z_1 = z - z^*. \quad (4.15)$$

If the local height of the ring is $2h$, then one can imagine a box of size $x_{1,max} = 2h\epsilon\kappa_x$, $y_{1,max} = 2h\epsilon\kappa_y$ and $z_{1,max} = 2h$ in which the particle moves around at each phase of the wave. We divide this box into $9 \times 9 \times 9 = 729$ bins. We also divide phase ϕ^* of the wave into nine bins. We then count the number of times the particle visits each of these bins and obtain a population weighted average of the radial velocity components over x_1 and y_1 directions. Since v_x is the more dominant component, we concentrate on v_x and fit the values obtained in each bin as a function of z_1 using fifth order polynomial. The shear is then computed by differentiation of this fitted curve for each wave phase. Finally, we average over all the phases and use the shear average for computing the damping length.

The energy density of the wave is given by

$$E_w = \frac{1}{2}\epsilon^2\Omega^2. \quad (4.16)$$

The energy is transferred to neighboring particles through infrequent collisions (order of one per orbit). In the absence of a detailed model the coefficient of kinematic viscosity ν_k is approximated by Brahic[8],

$$\nu_k = \Omega\tau \max(R^2, R_{epi}^2). \quad (4.17)$$

where R is the size of the largest particle and R_{epi} is the amplitude of the epicyclic motion which is similar to half the thickness of the ring. Though $\tau \sim \sigma$, we estimate $\nu_k = \Omega\tau h^2$ from a general τ for generality. The rate of dissipation of energy is,

$$\dot{E}_w = \nu_k (\partial \langle v_x \rangle / \partial z_1)^2 \quad (4.18)$$

The group velocity c_g is given by,

$$c_g = -\frac{\pi G \sigma}{\omega - m\Omega} \quad (4.19)$$

Hence, an estimate of the damping length is obtained from,

$$\lambda_D = \frac{E}{\dot{E}_w} c_g. \quad (4.20)$$

4.4 Results of numerical simulation

To simulate particle behavior near -1:0 resonance of Titan, We chose several sets of parameters. First we start with the following set: the location of the inner vertical resonance is $r_v = 77514.8\text{km}$, the location where the damping length is to be calculated is $r = 77542\text{km}$. The surface mass density of the ring near the resonance $\sigma = 0.45\text{g/cm}^2$. The half-height of the ring is $h = 20\text{m}$, the amplitude of the wave at the resonance $\epsilon = 1200\text{m}$, the average wavelength of the wave in the X-direction at the launching site is $\lambda_x = 2\pi/\kappa_x = 20\text{km}$, the average wavelength in the Y-direction is $\lambda_y = 2\pi/\kappa_y \sim r_v$.

Figs. 4.1(a-c) show the results of the simulations. The solid curve is for phase $\phi^* = 0$, the dotted curve is for phase $\phi^* = \pi/2$, the dashed curve is for $\phi^* = \pi$ and the dot-dashed curve is for $\phi^* = 3\pi/2$ respectively. In (a), we plot the fitted curve of the average x-component of the velocity v_x as a function of the local vertical height z_1 . The

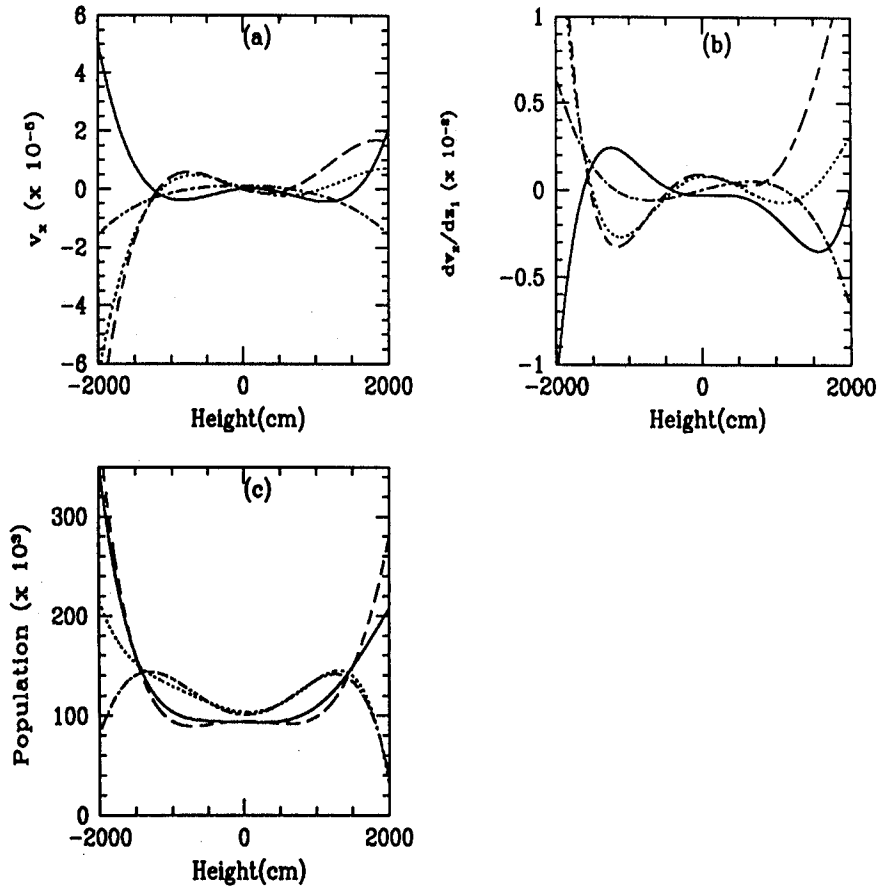


Figure 4.1: Variation of (a) x-component of velocity v_x , (b) shear dv_x/dz_1 and (c) population of matter inside the bending wave of a C-ring near Titan -1:0 resonance. The solid, dotted, dashed and dot-dashed curves are drawn for the wave phases $\phi^* = 0, \pi/2, \pi, 3\pi/2$ respectively. Note that all of these quantities are large close to the upper and lower edges of the wave. For disk parameters, see text.

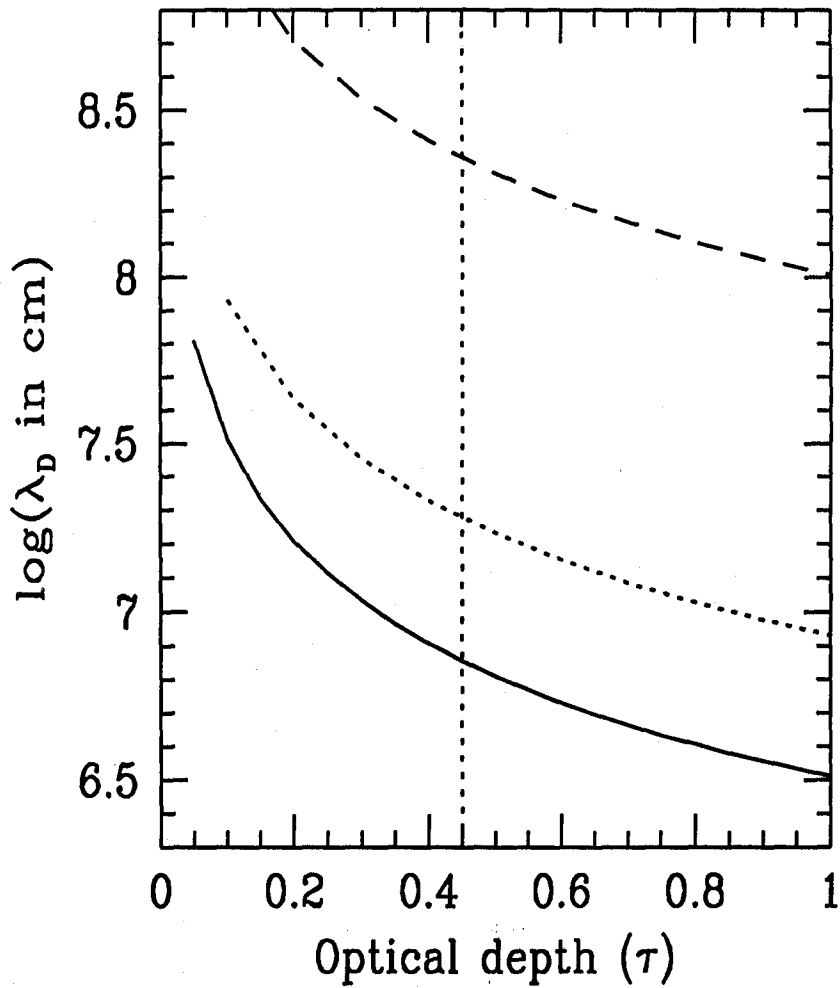


Figure 4.2: Variation of the damping length of the bending wave at the Titan -1:0 resonance assuming that the vertical shear is the only source of damping. Solid, dotted and dashed curves are drawn for $h = 20m$, $h = 16m$, and $h = 7.5m$ respectively. The similarity of the damping length at $\tau=0.45$ with that of the observed damping length indicates that the strict upper limit of the disk height is $40m$.

velocity is measured in units of 10^{-5} cm/s. In (b), the shear dv_x/dz_1 is plotted against local height z_1 . In (c) the population is plotted. We note that towards the edge of the wave in the vertical direction, the population, velocity and shear all are very high. Particularly important is the fact that the population is not highest in the local midplane ($z_1 = 0$) in all the phases. This is to be contrasted with the situation near the Mimas 5:3 resonance of the A-ring. Given that the Saturn's gravity is more important in the C-ring than the A-ring, self-gravity effects are weaker here and this may have caused this modification of the population distribution. We verified that the result is similar for other sets of disk parameters as well.

In Fig. 4.2 we plot the damping length as calculated from Eq. 4.20 as a function of the optical depth τ of the bending wave. The solid curve is drawn for half-thickness $h = 20$ m and the dotted curve and the dashed curve are drawn for $h = 16$ m and $h = 7.5$ m respectively. Other parameters have been kept fixed in the latter two cases of simulations. We note that for $h = 20$ m only the damping length is around 70km when the optical depth $\tau = 0.45$. For other disk heights the damping lengths are far too large. Hence our conclusion is that the strict upper limit of the disk thickness is around $2h = 40$ m.

4.5 Numerical modeling of analytical expressions

Earlier we had shown that the numerical simulation was used to integrate the differential equations over the whole orbit. Here we solve the equation of motion analytically to get expressions for X, Y and Z coordinates for the dust particle like Eqs. 3.101, 3.102 and 3.103. Also we derive \dot{x} , \dot{y} and \dot{z} from those analytical expressions so that those positions in the phase space may be properly binned to get the population in those bins or the number of particles visited those bins. The experiment was continued for a number of times for different values of *half-height*(h) and σ . Also we used the normal formula to compute

the wave amplitude (ϵ) and components of wave vector (k_x, k_y).

$$\epsilon = \frac{334}{\sqrt{\sigma}} \times 100.d0 \text{ cms} \quad (4.21)$$

$$\lambda_x = \frac{209 \times \sigma}{(r - r_v)}, \quad (4.22)$$

$$\lambda_y = 2\pi r_v, \quad (4.23)$$

$$k_x = \frac{2\pi}{\lambda_x}, \quad (4.24)$$

$$k_y = \frac{2\pi}{\lambda_y}. \quad (4.25)$$

Here, r , r_v and $\lambda_{x,y}$ are in kilometers. It has been found out that the values of the amplitude ϵ is observed to have very small order. So a special case has also been studied where the value of the amplitude is supplied from outside for the case of $h = 750\text{cm}$ and $\sigma = 0.4$ and the resulting shear is calculated.

4.6 Results for binning of analytical expressions

It has been found that shear obtained from the results of binning the output from the analytical results are almost 100 times smaller than that numerical simulation. In this analytical study, we used the expression keeping only the hotness of the particles. Hence the binned results contained the hotness of the particle which shows that velocities and hence shear thus obtained are smaller with respected to those from the numerical results. This may be reflected from the tables given below.

4.7 Concluding Remarks

Study of particle dynamics inside the Saturn's ring shows a very complex behavior of matter. We integrate numerically the trajectory of a particle inside the ring and study how it visits different 'bins' in the configuration space. We find that there is a considerable variation of

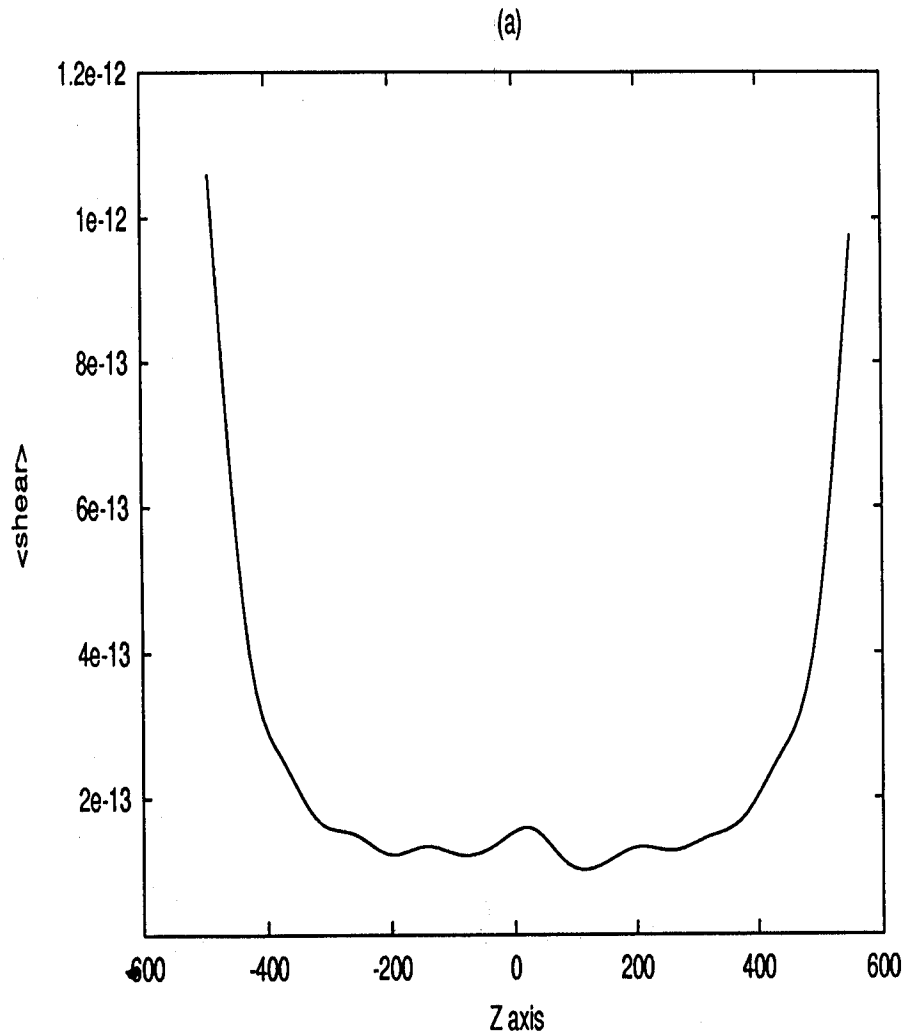


Figure 4.3: Shear vs. Position along Z-axis for Titan -1:0 resonance simulation for $h = 500$, $\sigma = 0.4$

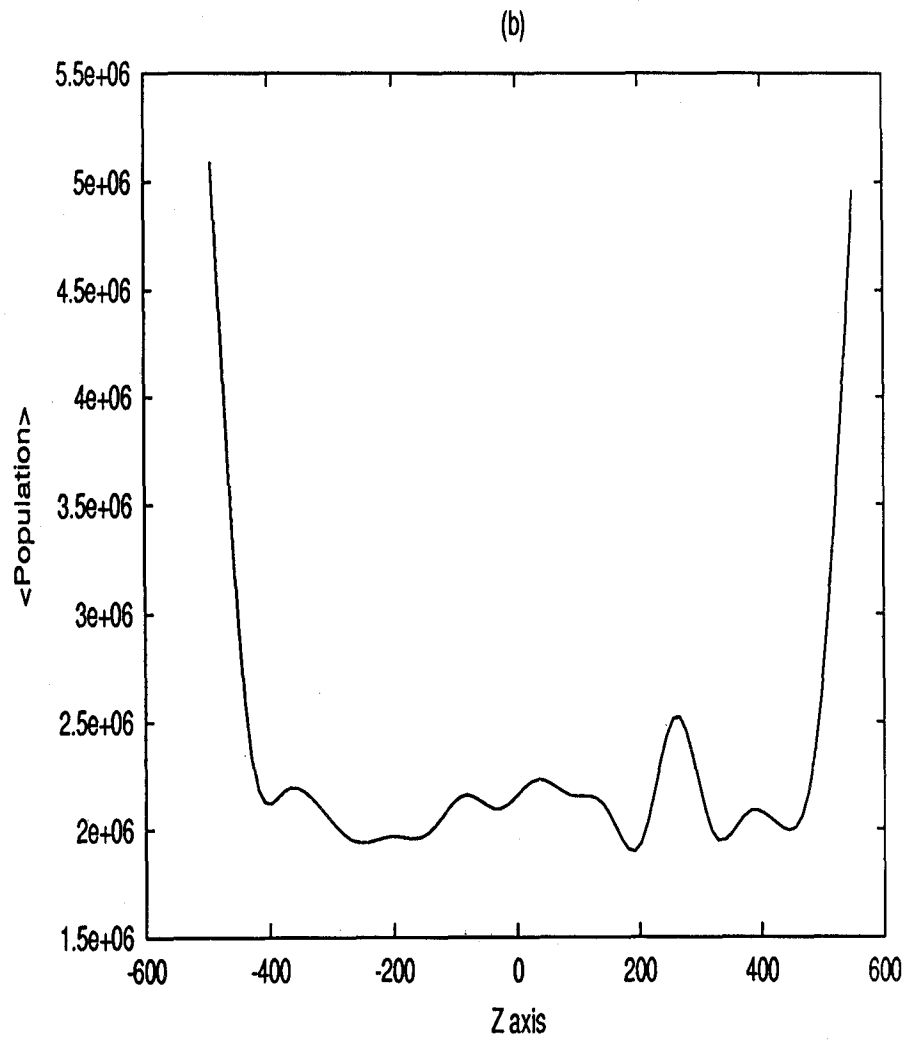


Figure 4.4: Population vs. Position along Z-axis for Titan -1:0 resonance simulation for $h = 500$, $\sigma = 0.4$

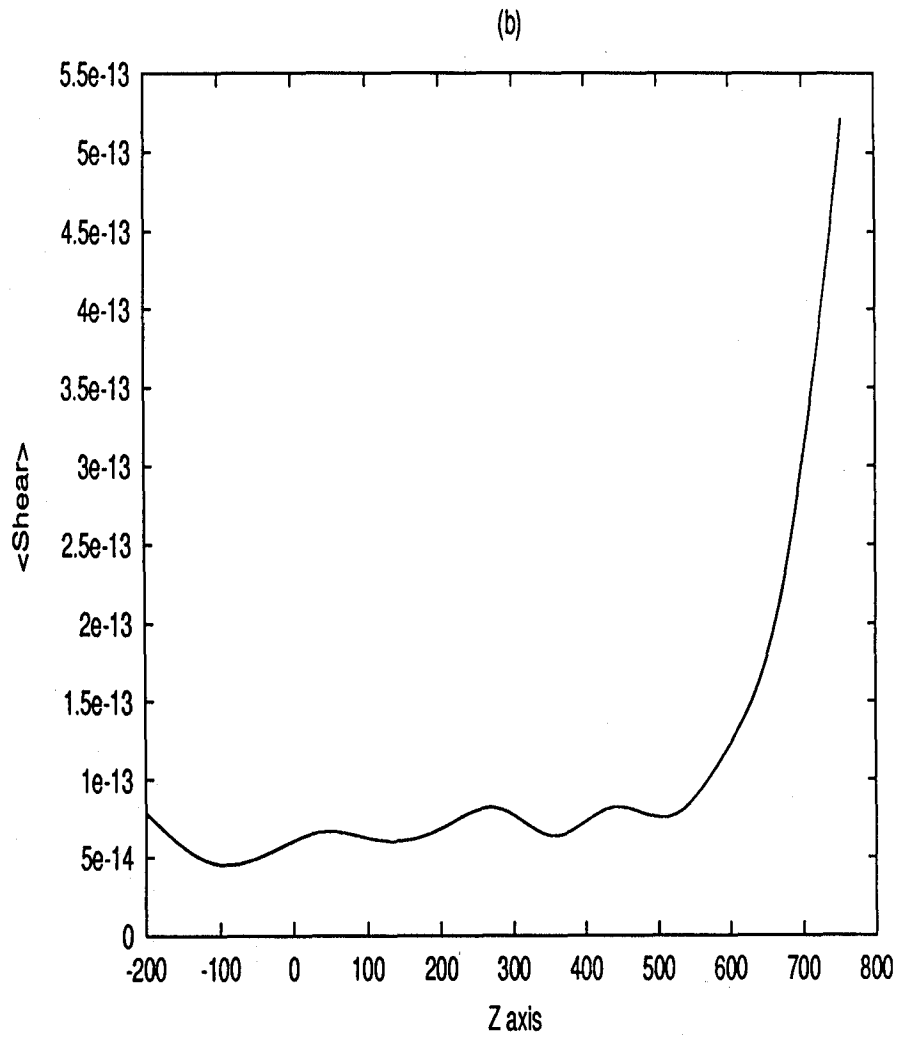


Figure 4.5: Shear vs. Position along Z-axis for Titan -1:0 resonance simulation for $h = 750$, $\sigma = 0.4$

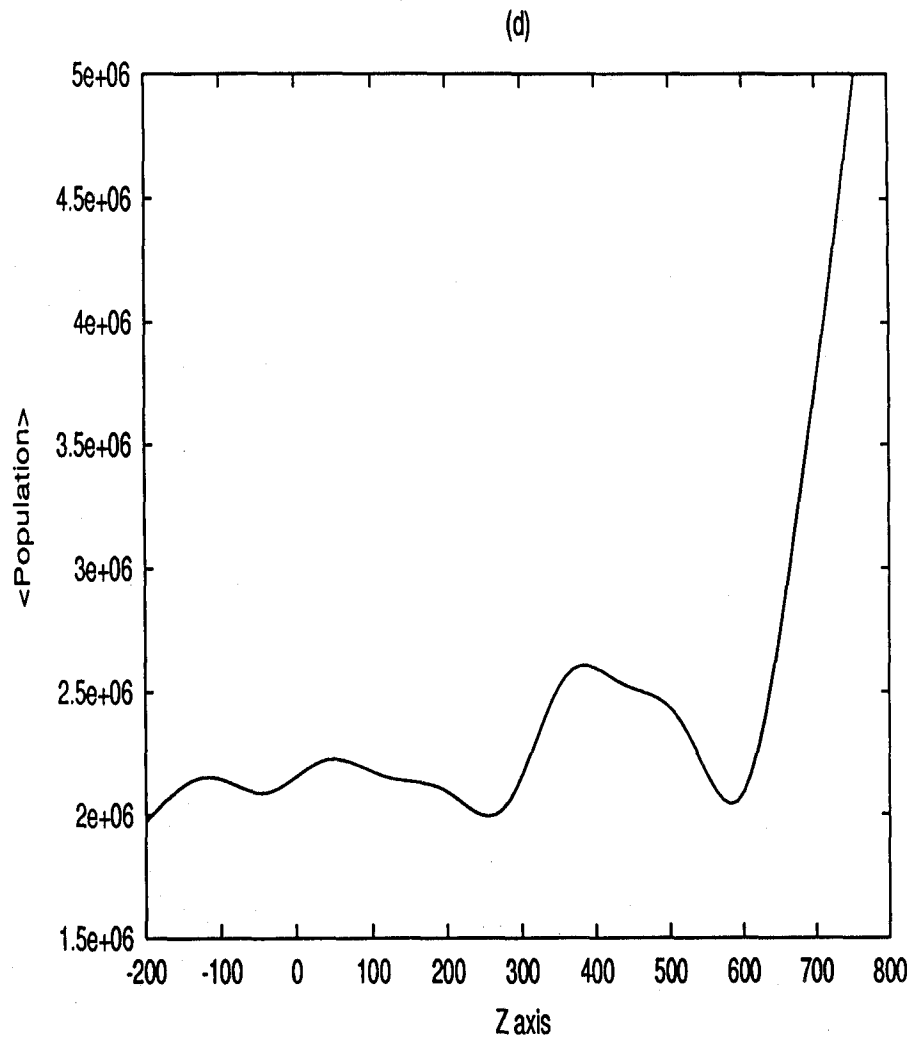


Figure 4.6: Population vs. Position along Z-axis for Titan -1:0 resonance simulation for $h = 750$, $\sigma = 0.4$

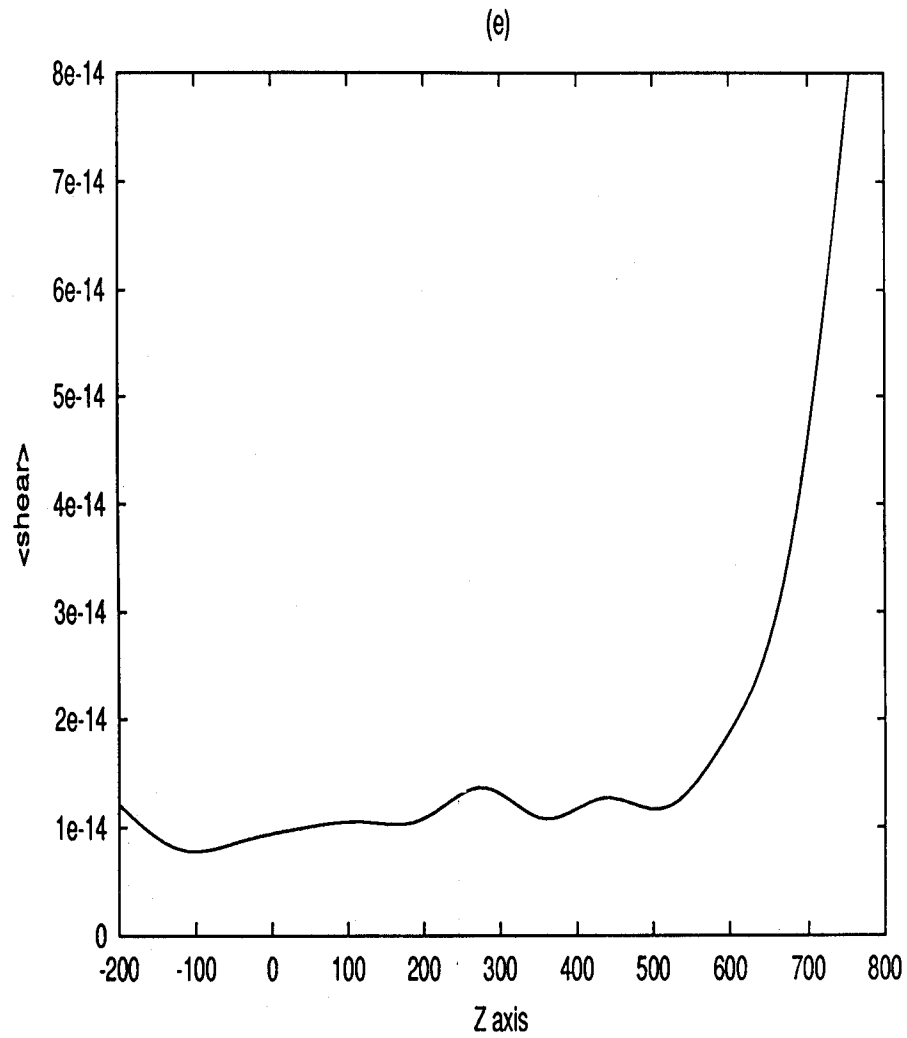


Figure 4.7: Shear vs. Position along Z-axis for Titan -1:0 resonance simulation for $h = 750$, $\sigma = 0.4 \epsilon$ fed in

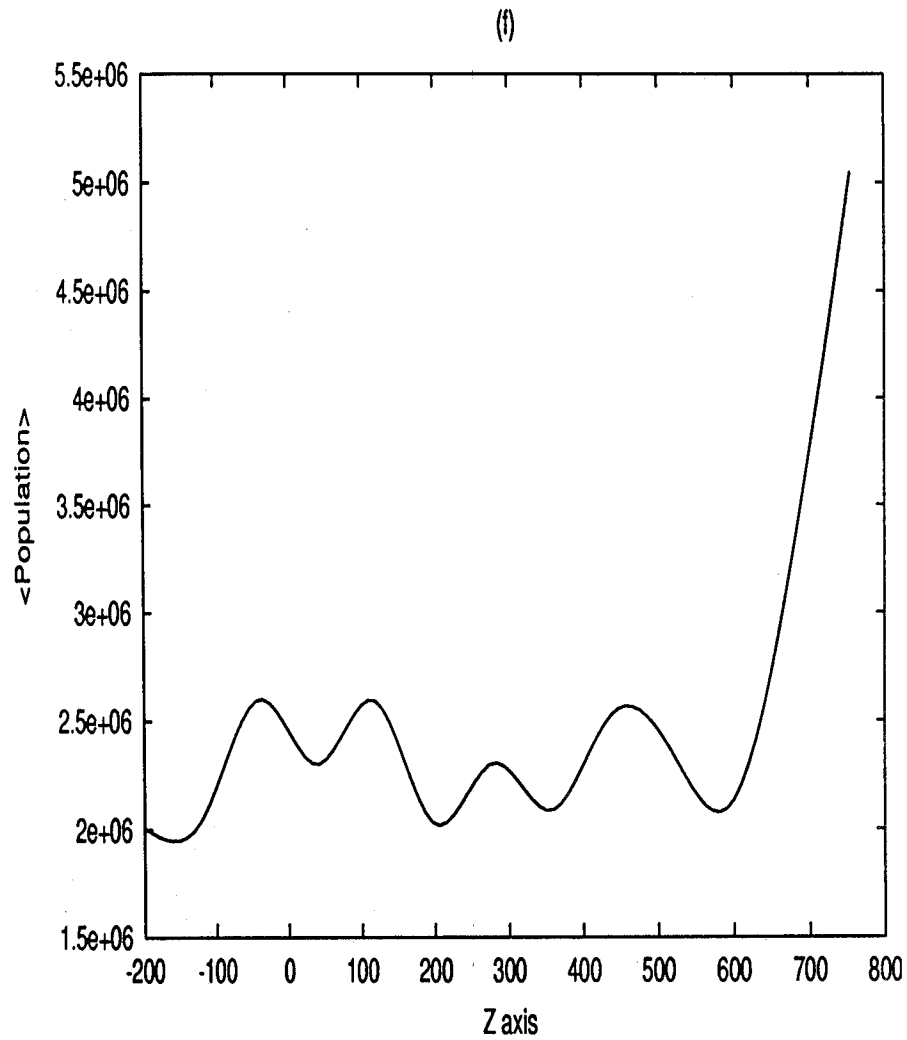


Figure 4.8: Population vs. Position along Z-axis for Titan -1:0 resonance simulation for $h = 750$, $\sigma = 0.4 \epsilon$ fed in

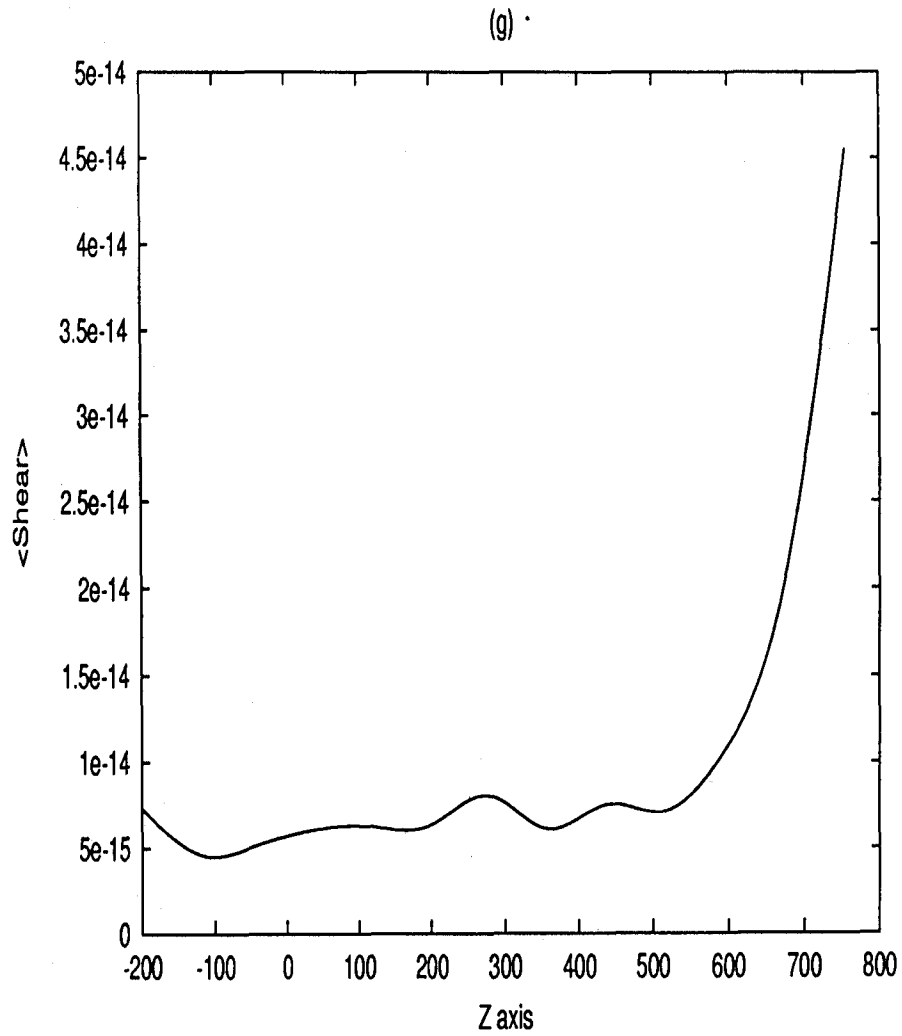


Figure 4.9: Shear vs. Position along Z-axis for Titan -1:0 resonance simulation for $h = 750$, $\sigma = 4.5$

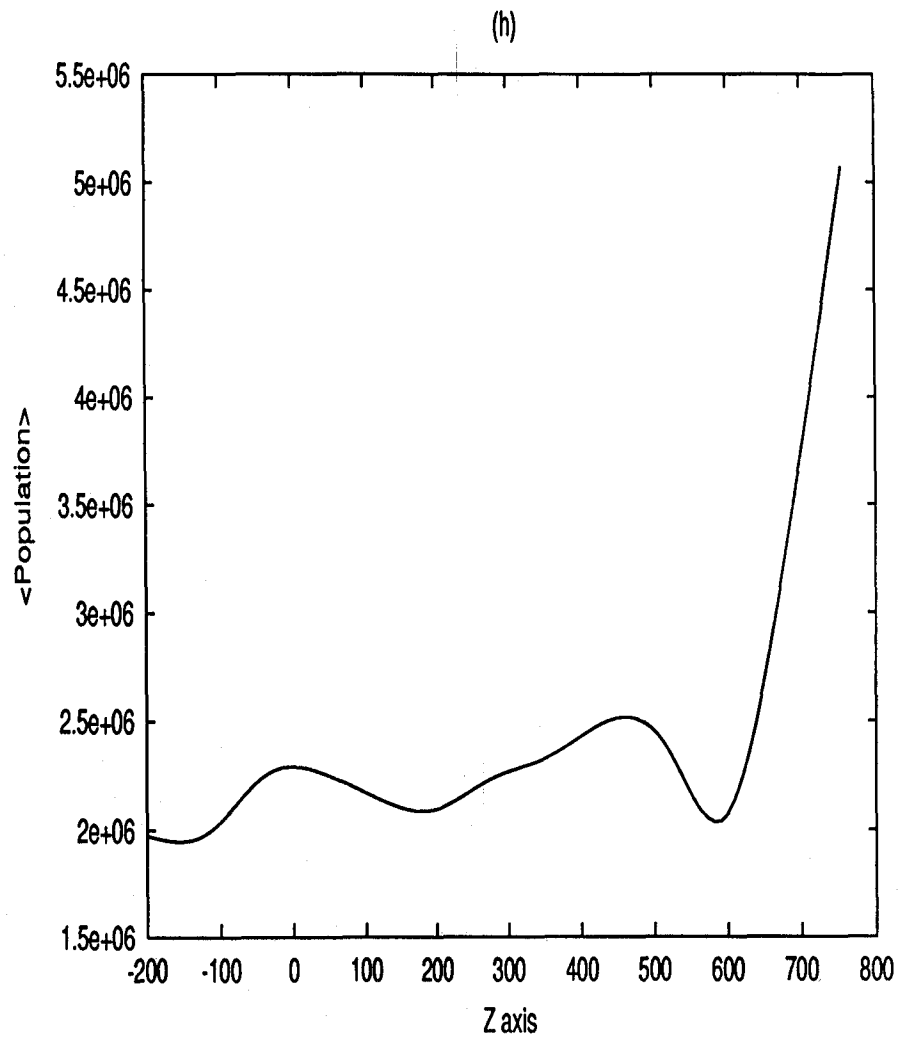


Figure 4.10: Population vs. Position along Z-axis for Titan -1:0 resonance simulation for $h = 750$, $\sigma = 4.5$

$$\Omega = 2.8338768600155213 \times 10^4$$

$$\omega = -2.8812219460613744 \times 10^{-4}$$

h	σ	ϵ	Shear
500.0	0.4	52810.03692481194	$6.0813370612990630 \times 10^{-7}$
500.0	4.5	15744.91099442046	$1.8835834639690321 \times 10^{-7}$
750.0	0.4	52810.03692481194	$3.9622382009817262 \times 10^{-7}$
(*) 750.0	0.4	120000.00	$1.5556055237445819 \times 10^{-7}$
750.0	4.5	15744.91099442046	$1.1931588214367842 \times 10^{-7}$
4000.0	0.4	52810.03692481194	$7.9709165468979398 \times 10^{-8}$

Table 4.1: Results of the analytical expressions considering only the hotness of the particles. Here (*) denotes that the value of ϵ was introduced by hand

the velocity and population as a function of the local vertical height. This naturally gives rise to a new source of shear and damping of the bending wave.

It is observed that complete dissipation of the bending wave at Titan -1:0 resonance takes place with 85km from the place of launching. Such a rapid dissipation requires a strong source of dissipation. We show that if the strongest component of shear is due to dv_x/dz_1 , then the damping takes place within 70 – 80km provided the total disk height is ~ 40 m. This has to be the strict upper limit of the vertical height, since additional normal shear should reduce the damping length to a even smaller value and thus bringing down λ_D corresponding to $h = 16$ m or even $h = 7.5$ m to the appropriate value which is observed.

The collision rate in Saturn's ring is a large uncertain factor. Because of the obvious nature of the vertical or horizontal oscillations, it is justified to assume that collision rate is roughly twice per orbit. However the normal shear in the Keplerian ring cannot be used without knowing the collision rates of the 'hot' rings. Our result thus avoids this complexity by using only vertical shear and giving the strict upper limit of the vertical height. One problem which needs to be addressed is that there are at least three parameters which are to be quantified very accurately: surface density σ , amplitude of the

bending wave ϵ and the vertical height h . Assuming $\sigma = 0.45\text{g/cm}^2$ and $\epsilon = 1200\text{m}$, which are very reasonable values we obtained these strict upper limit on h . In future, thorough study of the parameter space including the effect of the variation of the wavelength of the wave as a function of the distance from the launching site would be carried out. This would be reported by us in near future. Also from the binning of the analytical problem, it may be inferred that using the hotness is not the cause of smallness of the shear. The main forcing terms are basically sinusoidal and hence it may be argued that after a large number of tours in the orbit, these sinusoidal terms gets averaged out over the whole time period of the revolution. Hence after a large number of rotation, basically the effect of hotness prevails in the particle dynamics terms. So, analytical calculation using the hotness only may not be the fact of smallness. Rather, it may be argued that, binning may bring some error. Actually binning is done on the principle that we want to see how many times the particle has visited a particular area in the phase -space. The dimension of that elementary area becomes the size of the bin. This study, in a way, simulates the effect of population of particles at some particular region of finite dimension having some particular ranges of velocities. Hence as far as physics is concerned, this idea of calculation of shear and population has nothing wrong in it. The error, however, may creep in due to fixing of the dimension of the bin as there is no fixed formula to specify the dimension of region in the phase - space. In Chapter 5 we have studied the analytical expressions for the locus of the particles and then we determined the velocities and then we determined the value of shear without any binning for a range of heights (h) and surface mass density (σ).

Chapter 5

Analytical Study on Titan -1:0 resonance¹

5.1 Introduction

Voyager photopolarimeter experiment indicated that the thickness of the Saturn's ring is probably smaller than 200m at the outer edge of the A Ring [40]. When the oscillatory features in bending waves are identified with possible resonance events [68] and after a good fit of the ring profile the effective thickness is found, the thickness of the ring seems to be only a few tens of meters [12, 14, 59, 60]. One of the important new ingredient that has gone into measurement of thickness is a new source of shear which was found to be present during detailed numerical study of dynamics of particles inside the Saturn's ring [14]. This extra source of shear is found to effectively damp out the 5:3 bending wave within few tens of kilometers and since then is considered important [9, 53, 60] to describe particle dynamics inside a ring.

In the present paper, we write down the equations governing the particle dynamics and show that under reasonable assumption, one can solve the equations analytically. We compute the shear also from analytical consideration and average over a complete oscillation cycle to have an average shear. We then compute the damping length under various ring parameters (such as ring height and surface density)

¹communicated to *Icarus*

and show that the average shear could contribute to anomalously low damping length of the perturbations seen in Voyager data.

In the next Section, we present the basic equations of motion and explain the genesis of each of the terms. In §3, we present the solutions of the equations and compute the average shear analytically. In §4, we apply our result in various ring conditions. Finally, in §5, we draw our conclusions.

5.2 Model Equations

We choose the usual right handed Cartesian co-ordinate system (X, Y, Z) at a radial distance r from the center of the planet with the origin located on the equatorial plane of the planet with $X - Y$ plane coinciding with this plane. The X -axis points radially outward and Y -axis points toward the azimuthal direction. The frame is rotating around the planet with local Keplerian frequency $\Omega(r)$. Let the amplitude of the bending wave be ϵ . With this amplitude the midplane itself oscillates up and down. Sitting on the midplane, the particle oscillates up and down with amplitude h , the half-thickness of the ring. Let the coordinate of the origin of a Cartesian frame (X', Y', Z') which is oscillating with the midplane of the disk be (x^*, y^*, z^*) . In the absence of oscillations of the midplane, these two co-ordinate systems merge. A particle moving within the ring having coordinate (x, y, z) has a coordinate of $x_1 = x - x^*$, $y_1 = y - y^*$ and $z_1 = z - z^*$. If ω be the angular frequency of the propagating wave, then the phase of the midplane is $\phi^* = k_x x^* + k_y y^* - \omega t$ and that of the particle located at a point A (x, y, z) is $\phi = k_x x + k_y y - \omega t$. By definition, $\omega = (\Omega_p - \Omega)$ where, Ω_p is the pattern frequency (in the present case, angular frequency of the perturbing moon, with an opposite sign). Here, k_x and k_y are the x - and y - components of the wave vector \vec{k} . Let (x', y', z') be the co-ordinate of the particle in the (X', Y', Z') frame. Thus,

$$z' = h + \epsilon \cos \phi^*, \quad (5.1)$$

where, h is the half thickness of the ring. It is easy to show that the local normal at (x', y', z') on the midplane is given by,

$$\hat{n} = -\hat{i} \frac{\epsilon k_x \sin \phi^*}{W} - \hat{j} \frac{\epsilon k_y \sin \phi^*}{W} - \hat{k} \frac{1}{W}, \quad (5.2)$$

where, $W = (1 + \epsilon^2 k^2 \sin^2 \phi^*)^{1/2}$. From this one derives the following important relations,

$$x_1 = z_1 \epsilon k_x \sin \phi^*, \quad (5.3)$$

and

$$y_1 = z_1 \epsilon k_y \sin \phi^*. \quad (5.4)$$

If one ignores the oblateness of the planet, then the vertical frequency μ of the particle defined by,

$$\mu^2 = \frac{\partial^2 \phi_p}{\partial z^2}, \quad (5.5)$$

and the epicyclic frequency κ of the particle defined by,

$$\kappa^2 = \frac{1}{r^3} \frac{d}{dr} [(r^2 \Omega)^2], \quad (5.6)$$

are identical to the local Keplerian frequency Ω .

In general, there will be three forcing terms,

$$\vec{g} = \vec{g}_P + \vec{g}_M + \vec{g}_D, \quad (5.7)$$

where, subscripts P , M and D denote the acceleration due to the planet, the moon and the self-gravity of the ring. For simplicity, one can assume that the vertical motion is due to the planet and the moon only, so that the vertical component of the equation of motion is given by,

$$\ddot{z} = -\Omega^2 z + a \cos(k_x x + k_y y - \omega t). \quad (5.8)$$

The solution of this is,

$$z = -\frac{a}{\Omega^2 - \omega^2} \cos(k_x x + k_y y - \omega t). \quad (5.9)$$

This can be identified with the amplitude of the vertical movement of the midplane due to satellite forcing provided $\epsilon(\Omega^2 - \omega^2) = a$. Thus the forcing term due to the satellite is,

$$\vec{g}_m = \epsilon(\Omega^2 - \omega^2) \cos(k_x x + k_y y - \omega t). \quad (5.10)$$

Its components are to be added in the differential equation governing the motion of the particle.

The components of the equation of motion of the test particle are given by [14],

$$\frac{d^2x}{dt^2} = -2\Omega \frac{dy}{dt} + 3\Omega^2 x - \nu^2 x_1 - (\Omega^2 - \omega^2)\epsilon^2 \kappa_x \cos(\phi) \sin(\phi^*)/W, \quad (5.11)$$

$$\frac{d^2y}{dt^2} = 2\Omega \frac{dx}{dt} - \nu^2 y_1 - (\Omega^2 - \omega^2)\epsilon^2 \kappa_y \cos(\phi) \sin(\phi^*)/W, \quad (5.12)$$

$$\frac{d^2z}{dt^2} = -\Omega^2 z - \nu^2 z_1 + (\Omega^2 - \omega^2)\epsilon \cos(\phi)/W. \quad (5.13)$$

Here, $\nu^2 = 4\pi G\rho$ is the vertical oscillation frequency due to the self-gravity and ρ is the mass density of the ring matter. The first term of the R.H.S. of Eq. 5.11 comes from the well known Coriolis acceleration. The second term of that equation comes from the difference between the centrifugal acceleration of the particle and the centrifugal acceleration of the observer in the rotating reference frame. We consider the case when $\epsilon k \ll 1$, i.e., for wavelengths which are large compared to the amplitude of the bending wave. In this limit, $W \approx 1$ and $\phi = \phi^* + z_1 \epsilon k^2 \sin \phi^*$ and $\cos \phi \approx \cos \phi^* - \epsilon z_1 k^2 \sin^2 \phi^*$. Using this, the z -component of the equation is re-written as,

$$\frac{d^2 z_1}{dt^2} = -\alpha^2 z_1 - \epsilon^2 (\Omega^2 - \omega^2) z_1 k^2 \sin^2 \phi^*, \quad (5.14)$$

where, $\alpha^2 = \Omega^2 + \nu^2$. It is easy to transform the equation in terms of the phase ϕ^* by using $\partial/\partial t \equiv -\omega \partial/\partial \phi^*$ and $\partial^2/\partial t^2 \equiv \omega^2 \partial^2/\partial \phi^{*2}$. This yields,

$$\frac{\partial^2 z_1}{\partial \phi^{*2}} = -\frac{z_1}{\omega^2} \left[\alpha^2 + \frac{\epsilon^2 (\Omega^2 - \omega^2) k^2}{2} \right] + \frac{\epsilon^2 (\Omega^2 - \omega^2) z_1 k^2 \cos 2\phi^*}{2\omega^2}. \quad (5.15)$$

Close to the resonance orbit, $\Omega \sim \omega$ and the parameter,

$$\gamma^2 = \frac{\epsilon^2 k^2 (\Omega^2 - \omega^2)}{\omega^2} \quad (5.16)$$

could be treated as a perturbation parameter [14]. Defining,

$$\eta^2 = \frac{\alpha^2}{\omega^2} + \frac{\gamma^2}{2}, \quad (5.17)$$

The Eq. 5.15 becomes,

$$\frac{\partial^2 z_1}{\partial \phi^{*2}} = -\eta^2 z_1 + \frac{\gamma^2 \cos 2\phi^*}{2} z_1. \quad (5.18)$$

To obtain a complete solution, we expand z_1 in powers of γ^2 as,

$$z_1 = z_1^{(0)} + \sum_{i=0}^N \gamma^{2i} z_1^{(i)}. \quad (5.19)$$

Upon substitution in Eq. 5.18 and equating coefficients of the powers of γ^2 we obtain, up to powers of γ^4 , the solution of z as,

$$\begin{aligned} z = & \epsilon \cos \phi^* + h \sin \eta \phi^* - \frac{h\gamma^2}{16} \left[\frac{\sin(2+\eta)\phi^*}{1+\eta} - \frac{\sin(2-\eta)\phi^*}{1-\eta} \right] \\ & + \frac{h\gamma^4}{64} \left[\frac{\sin(4+\eta)\phi^*}{8(1+\eta)(2+\eta)} - \frac{\sin \eta \phi^*}{(1+\eta)(1-\eta)} - \frac{\sin(4-\eta)\phi^*}{8(1-\eta)(2-\eta)} \right] \end{aligned} \quad (5.20)$$

From Eqs. 5.11-5.12, we can now obtain the solutions for x ,

$$\begin{aligned} x = & h \sin(\Omega\phi^*/\omega) + \frac{\nu^2 \epsilon k_x h}{2\omega^2} \left[\frac{1 + \gamma^2/(16(1-\eta))}{\Omega^2/\omega^2 - (1-\eta)^2} \cos(1-\eta)\phi^* \right. \\ & - \frac{1 + \gamma^2/(16(1+\eta))}{\Omega^2/\omega^2 - (1+\eta)^2} \cos(1+\eta)\phi^* \\ & + \frac{\gamma^2/16 + \gamma^4/(512(2-\eta))}{(1-\eta)[\Omega^2/\omega^2 - (3-\eta)^2]} \cos(3-\eta)\phi^* \\ & + \frac{\gamma^2/16 + \gamma^4/(512(2+\eta))}{(1+\eta)[\Omega^2/\omega^2 - (3+\eta)^2]} \cos(3+\eta)\phi^* \\ & + \frac{\gamma^4/(512(1-\eta)(2-\eta))}{[\Omega^2/\omega^2 - (5-\eta)^2]} \cos(5-\eta)\phi^* \\ & \left. - \frac{\gamma^4/(512(1+\eta)(2+\eta))}{[\Omega^2/\omega^2 - (5+\eta)^2]} \cos(5+\eta)\phi^* \right] \end{aligned} \quad (5.21)$$

5.3 Computation of the Shear components

Numerical simulations [12, 14] tend to indicate that the shear due to variation of radial velocity component along vertical direction is significant.

Analytically this shear could be computed from $\langle \ddot{x} \rangle / \langle \dot{z} \rangle$:

$$\frac{\langle \ddot{x} \rangle}{\langle \dot{z} \rangle} = \frac{P}{Q}, \quad (5.22)$$

where,

$$\begin{aligned} P = & h\Omega\omega \left[\cos\left(\frac{2\pi\Omega}{\omega}\right) - 1 \right] \\ & - \frac{\nu^2 \epsilon k_x h}{2} \left[\left\{ \frac{1 + \gamma^2/16(1-\eta)}{\frac{\Omega^2}{\omega^2} - (1-\eta)^2} (1-\eta)^2 + \frac{1 + \gamma^2/16(1+\eta)}{\frac{\Omega^2}{\omega^2} - (1+\eta)^2} (1+\eta)^2 \right\} \right. \\ & \frac{(-\eta \sin 2\pi\eta)}{2\pi(1+\eta)(1-\eta)} + \left\{ \frac{1 + \gamma^2/16(1-\eta)}{\frac{\Omega^2}{\omega^2} - (1-\eta)^2} (1-\eta)^2 - \right. \\ & \left. \left. \frac{1 + \gamma^2/16(1+\eta)}{\frac{\Omega^2}{\omega^2} - (1+\eta)^2} (1+\eta)^2 \right\} \frac{(-\sin 2\pi\eta)}{2\pi(1+\eta)(1-\eta)} \right. \\ & + \left\{ \frac{\gamma^2/16 + \gamma^4/512(2-\eta)}{(1-\eta) \left\{ \frac{\Omega^2}{\omega^2} - (3-\eta)^2 \right\}} (3-\eta)^2 \right. \\ & + \left. \frac{\gamma^2/16 + \gamma^4/512(2+\eta)}{(1+\eta) \left\{ \frac{\Omega^2}{\omega^2} - (3+\eta)^2 \right\}} (3+\eta)^2 \right\} \frac{(-\eta \sin 2\pi\eta)}{2\pi(3+\eta)(3-\eta)} \\ & + \left\{ \frac{\gamma^2/16 + \gamma^4/512(2-\eta)}{(1-\eta) \left[\frac{\Omega^2}{\omega^2} - (3-\eta)^2 \right]} (3-\eta)^2 \right. \\ & - \left. \frac{\gamma^2/16 + \gamma^4/512(2+\eta)}{(1+\eta) \left[\frac{\Omega^2}{\omega^2} - (3+\eta)^2 \right]} (3+\eta)^2 \right\} \frac{(-\sin 2\pi\eta)}{2\pi(3+\eta)(3-\eta)} \\ & + \frac{\gamma^4/512(1-\eta)(2-\eta)}{\frac{\Omega^2}{\omega^2} - (5-\eta)^2} (5-\eta)^2 \left\{ \frac{-\eta \sin 2\pi\eta}{2\pi(5+\eta)(5-\eta)} \right. \\ & \left. \left. - \frac{\sin 2\pi\eta}{2\pi(5+\eta)(5-\eta)} \right\} \right], \end{aligned} \quad (5.23)$$

and,

$$\begin{aligned} Q = & \frac{-h\omega}{2\pi} \sin 2\pi\eta \\ & - \frac{h\gamma^2\omega}{8} \left[\frac{-\eta^2 \sin 2\pi\eta}{2\pi(1-\eta^2)(4-\eta^2)} + \left(\frac{2-\eta^2}{1-\eta^2} \right) \right] \\ & - \frac{-h\gamma^4\omega}{64} \left[\frac{(\eta^2+8) \sin 2\pi\eta}{8(1-\eta^2)(4-\eta^2)(16-\eta^2)} \right] \end{aligned}$$

$$- \left[\frac{\eta^2(\eta^2 - 10) \sin 2\pi\eta}{8\pi(1 - \eta^2)(4 - \eta^2)(16 - \eta^2)} - \frac{\eta \sin 2\pi\eta}{2\pi(1 - \eta^2)} \right]. \quad (5.24)$$

In above equations averaging is done over a complete cycle ϕ^* .

During excursion of the particle in epicyclic orbits inside the ring, it collides with a neighboring particle once in each orbit and in this process momentum is transferred. The mean distance between two colliding particles is either the epicyclic radius or the size of the particle, whichever is bigger.

This analytical model may be used for calculation of the damping length of the bending wave in the planetary rings. To calculate the damping length, the energy density of the wave is first calculated using

$$E_w = \frac{1}{2} \epsilon^2 \Omega^2 \quad (5.25)$$

and then the dissipation of the wave is calculated as,

$$\dot{E}_w = \nu_k \left(\frac{\partial \langle v_x \rangle}{\partial z_1} \right)^2, \quad (5.26)$$

where, the kinematic viscosity ν_k is given by,

$$\nu_k = \Omega \tau \max(R^2, R_{epi}^2). \quad (5.27)$$

Here, R is the size of the largest particle and R_{epi} is the amplitude of the epicyclic motion which is similar to half the thickness of the ring i.e., h . The group velocity is given by,

$$c_g = - \frac{\pi G \sigma}{\omega - m \Omega}. \quad (5.28)$$

The damping length is estimated from,

$$\lambda_D = \frac{E_w}{\dot{E}_w} c_g. \quad (5.29)$$

5.4 Results for various ring conditions

In this Section, we report some results of our calculation for rings of different characteristics considering Titan -1:0 resonance. The parameters we considered were the ring height h and the surface

mass density σ . Here, in Fig. 5.1, we plot curves of surface mass density σ vs damping length λ_D for half-thicknesses $h = 100\text{cms}, 150\text{cms}, 200\text{cms}, 250\text{cms}$. This figure illustrates the general analytical behaviour of the damping length varying with surface mass density. The figure also shows, in general, that there is a minima near $\sigma \sim 0.2\text{gm/cm}^2$ to 0.5gm/cm^2 . The observed damping length $\sim 85\text{km}$ is also shown which indicates that there is no analytical solution for higher value of surface mass density to have damping length of the wave $\sim 85\text{km}$. In the Fig. 5.2, we illustrate the zoomed nature of Fig. 5.1. The y-axis of the Fig. 5.2 has been taken in logarithmic form. It also illustrates the damping length of $85 \times 10^5\text{cms}$ line parallel to x-axis intersecting the curves for different half-thickness h at lower values of surface density. This indicates the surface density of the C-ring may be around 0.22gm/cm^2 to 0.3gm/cm^2 . The damping length is higher near $\sigma \sim 0.14\text{gm/cm}^2$. Preliminary results are reported in [4].

From the Figures it is clear that σ cannot be as large as 4.5 gm/cm^2 as reported in Rosen *et al.* [59] if the half height of the ring is $\sim 1 - 2.5\text{m}$ or so. From our analysis it is apparent that the *total* ring height for the C ring may be around $1 - 2.5\text{m}$ in order that the damping length agrees with the observed value of $\sim 85\text{km}$ or so [59].

5.5 Conclusion

Rosen *et al.* [59] inferred from their numerical modeling that the persistence of the wave for over 28 cycles indicated that the scale height of the C ring could not be more than 2 to 3 m. Even the radio occultation fitting indicated it would be rather $\leq 2.6\text{m}$ for damping length of the order of $\sim 85\text{km}$. Our analytical calculations show a good agreement with the observed results. We therefore believe that the new component of shear which was first introduced by [14] for Mimas 3:2 resonance, could be operating in Titan -1:0 resonance as well.

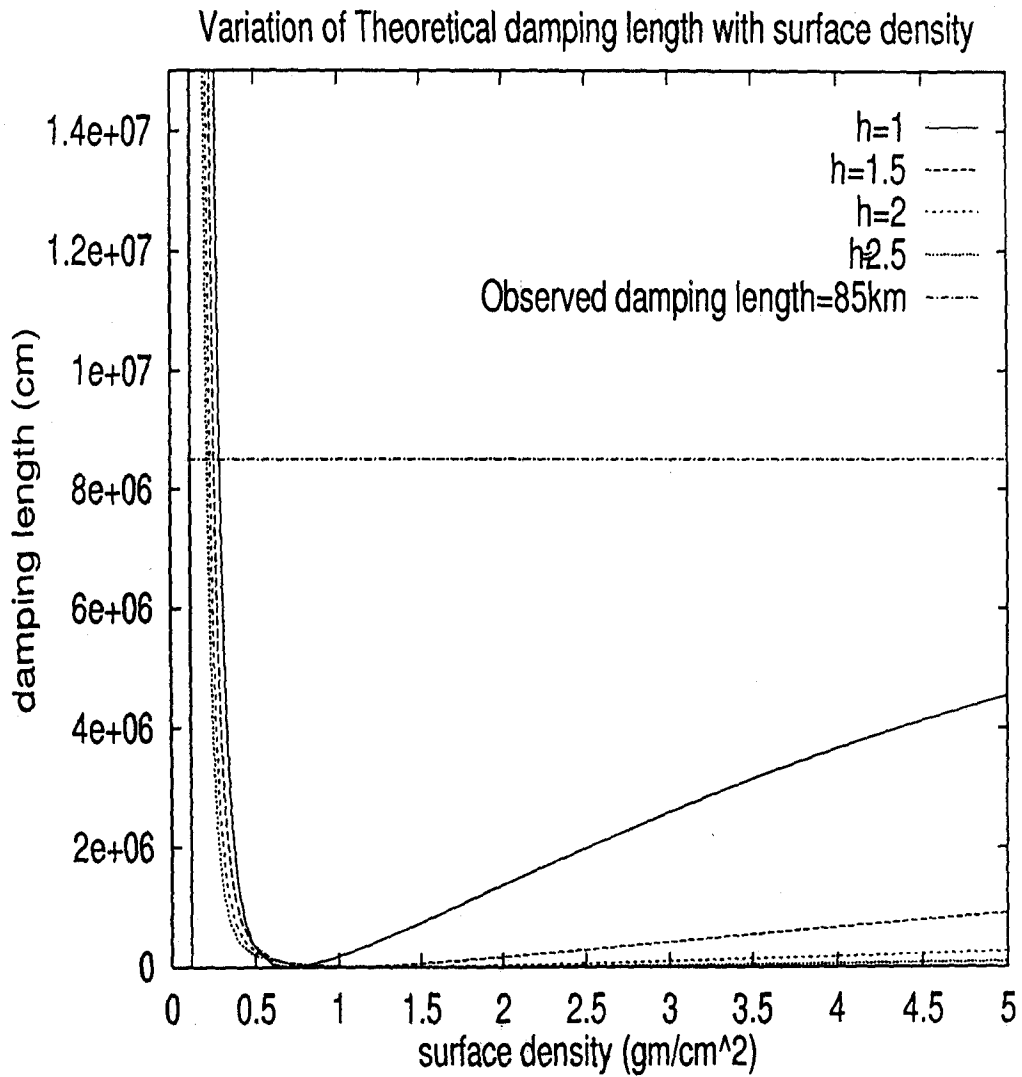


Figure 5.1: Surface mass density (σ) [gm/cm^2] vs damping length [cm] for different ring heights h . Observed damping length of 85km is shown for comparison.

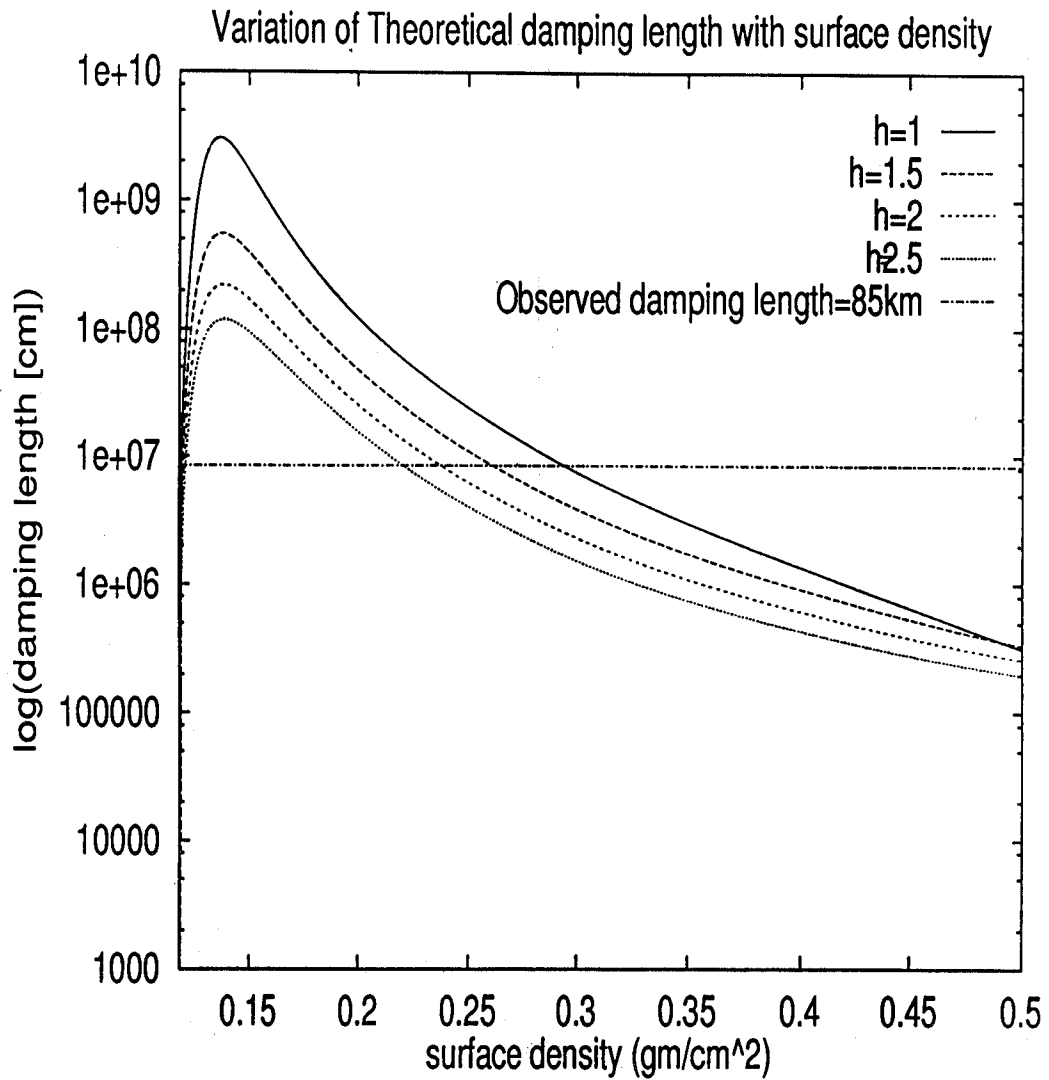


Figure 5.2: Surface mass density (σ) [gm/cm^2] vs $\log(\text{damping length [cm]})$ [cm] for different ring heights h . Observed damping length of 85km is shown for comparison.

Chapter 6

Conclusion

The spiral bending wave as observed in the planetary rings, especially for the case Saturn's ring provide an interesting method of probing the ring system to understand the dynamics of a particle in the planetary ring. Usually the bending wave is observed for particles of larger dimensions. Hence the study of effect of Lorentz force on the particles showing the bending wave is not viable. Therefore, it is only important to consider the effect of satellite forcing and the effect of self gravity with the planetary attraction and other collisional terms may be important to study the bending wave.

The effect of inter-particle collision may give rise to effect of viscosity leading to damping of the wave. However, both in our analytical and numerical study, we neglected the effect of inter-particle collision. We simply considered the effect of planetary attraction which was balanced by the effect of centrifugal force due to rotation of dust around the planet in the ring, the effect of satellite forcing and the effect of self gravity due to the whole disk itself. The result was amazing. In absence of any collisional terms, the result would show that the wave would last for atleast few cycles of rotation around the planet. However, the result showed that there exists some other kind of viscous shear in the particle model which forces the bending wave to damp after a few kilometers. The kinematic viscosity due to this type of damping was a measurable quantity. The effect of shear was strong enough to damp the bending wave at a distance which clearly matches with the observed data. This signifies that probably the effect of col-

lisional damping is weaker than the shear developed in our case.

The numerical simulation and the analytical work suggest that the damping length of the bending wave excited at the Titan -1:0 resonance of the C-ring would be around 85kms as observed by the Voyager provided the surface mass density is around $\sigma \sim 0.2\text{gm/cm}^2$ to 0.3gm/cm^2 and the ring thickness is around $2 - 5\text{m}$.

Bibliography

- [1] Aggarwal, H. R. and Oberbeck, V. R., 1974, Roche limit of a solid body, *Astrophys. J.*, **191**, 577 - 588
- [2] Alexander, A. F. O' D., 1962, *The planet Saturn, a history of observation, theory and discovery*, (London Faber & Faber)
- [3] Bhattacharyya Abhijit and Basu A. M., 1999, Non-linear vortices in planetary ionosphere", *Indian Journal of Physics B*, **73**, 6, 1999
- [4] Bhattacharyya Abhijit, Chakrabarti S. K., Theoretical study of constraints on the C ring parameters of Saturn at the Titan -1:0 resonance, No. 1046, 32nd Lunar and Planetary Science Conference, NASA Johnson Space Center, USA, Mar 12-16, 2001, (available now in INTERNET)
- [5] Bhattacharyya, Abhijit, Basu A. M. and Chakrabarti Sandip K., 2001, *Analytical Studies of Particle Dynamics in Planetary Rings, communicated to Icarus*
- [6] Bhattacharyya, J. C. and Bappu, M. K. V., 1977, Saturn-like ring system around Uranus, *Nature*, **270**, 503-506
- [7] Bondi, H., 1952, *Monthly Notices of Royal Astronomical Society (MNRAS)*, **112**, 195
- [8] Brahic, A., 1977, Systems of colliding bodies in a gravitational field: I Numerical simulations, *Astron. Astrophysics*, **54**, 895 - 907
- [9] Brophy, T.G. & Rosen, P.A., 1992, *Icarus*
- [10] Brahic, A. & Sicardy, B. 1981, *Nature*, **447**

- [11] Cameron, A. G. W., 1978, Physics of the primitive solar accretion disk, *Moon Planets*, **18**, 5 - 40
- [12] Chakrabarti, Sandip K. and Bhattacharyya, Abhijit, Constraints on the C ring parameters of Saturn at the Titan -1:0 resonance, 2001, *Monthly Notices of Royal Astronomical Society (MNRAS)*, **326**, L23-L26, 2001
- [13] Chakrabarti, S. K. 1988, *J. Astrophys. Astr.*, **9**:243
- [14] Chakrabarti, S. K. 1989, *Mon. Not. R. Astr. Soc.*, **238**:1381-1394
- [15] Cherepashchuk, A. M., 1981, *Stars and stellar systems* (Ed. D. Ya. Martynov), Nauka, Moscow, 38
- [16] Cook, A. F. and Franklin, F. A., 1964, Re-discussion of Maxwell's Adams prize essay on the stability of Saturn's rings, *Astron. J.*, **69**, 173 - 200
- [17] Cuzzi, J. N., Lissauer, J. J. and Shu, F. H., 1981, Density waves in Saturn's ring, *Nature*, **292**, 703 - 707
- [18] Cuzzi, J.N. et al. in *Planetary Rings*, (Eds.) R. Greenberg and A. Brahic (Univ. of Arizona Press, 1984)
- [19] Darwin, G. H., 1889, Saturn's Rings, *Harpers New Monthly Magazine*, **79**, 66-76
- [20] Dobrovalskis, A. R., 1982, Internal stresses in Phobos and other triaxial bodies, *Icarus*, **52**, 136 - 148
- [21] Franklin, F. A. and Colombo, G., 1970, A dynamical model for the radial structure of Saturn's rings, *Icarus*, **12**, 338-347
- [22] Franklin, F. A., Colombo, G. and Cook, A. F., 1971, A dynamical model for the radial structure of Saturn's rings, *Icarus*, **15**, 80-92
- [23] Fridman, A. M. and Ozernoy, L. M., 1991, Testing in AGN Paradigm, *Proc. 2nd Ann. Oet. Ap. Conf.*, Maryland

- [24] Fridman, A. M. and Gor'kavyĭ, N. N. , 1992, Chaos, Resonance and collective dynamical phenomena in the Solar system (Ed. S. Ferraz-Mello), Kluwer, Dordrecht, 75
- [25] Fujimoto, M., 1968, In non-stable phenomena in galaxies, Proc. IAU Symp. no. **29**, 453 - 463
- [26] Gor'kavyĭ, N. N. and Fridman, A. M., 1985, Sov. Astron. Lett., **11**, 264
- [27] Goldsborough, G. R., 1921, Phil. Trans. Roy. Soc., London, 222, 101
- [28] Goldreich, P. and Tremaine, S., 1978, The velocity dispersion in Saturn's rings, *Icarus*, **34**, 227 - 239
- [29] Goldreich, P. and Tremaine, S., 1979, The Excitation of density waves at the Lindblad and corotation resonances by an external potential, *Astrophys.J.*, **233**, 857-871
- [30] Goldreich, P. and Tremaine, S., 1978, The formation of Cassini division in Saturn's rings, *ICARUS*, **34**, 240-253
- [31] Goldreich, P. and Tremaine, S., 1982, The dynamics of planetary rings, *Ann. Rev. Astron. Astrophys.*, **20**, 249 - 283
- [32] Greenberg, R. *et al*, 1977, Size distributions of particles in planetary rings, *Icarus*, **30**, 769 - 779
- [33] Greenberg, R, *et al*, 1978, Planetesimals to Planets: Numerical simulation to collisional evolution, *Icarus*, **35**, 1 - 26
- [34] Harris, A. W., 1978, The formation of outer planets, *Lunar Planet. Sci.*, IX, 459 - 461
- [35] Harris, A. W., 1978, Satellite formation, II. *Icarus*, **34**, 128 - 145
- [36] Hayle, J. and Smarr, L., 1988, Numerical Astrophysics (Eds J. Centrella *et al*, Jones and Bartlett, Boston MA
- [37] Huygens, C., 1659, *Systema Saturnium* : In Oeuvres Completes de Christiaan Huygens, XV, The Hague 1925, 294-296

- [38] Jewitt, D. C. and Danielson, G. E., 1981, The Jovian ring, *J. Geophys. Res.*, **86**, 8691 - 8697
- [39] Jeffreys, H., 1947, *Monthly Notices of Royal Astronomical Society (MNRAS)*, **107**, 260
- [40] Lane, A. L. et al. 1982, *Science*, **265**, 537
- [41] Laplace, P. S., Marquis de, 1802, *Mechanique Celeste*, translated by N. Bowditch (Boston, 1832 : Hilliard, Gray, Little and Wilkins), vol III, sec 46, 512
- [42] Laue, A. L. *et al*, 1982, Photopolarimetry from Voyager 2: Preliminary results on Saturn, Titan and rings, *Science*, **215**, 537 - 543
- [43] Lin, D. N. C. and Papaloizou, J., 1980, On the structure and evolution of the primordial solar nebula, *Monthly Notices of Royal Astronomical Society (MNRAS)*, **191**, 37- 48
- [44] Lin, C. C. and Shu, F. H., 1964, *Astrophysical J.*, **140**, 646
- [45] Lin, C. C., and Shu, F. H. 1968, *Astrophysics and General Relativity*, Ed. Chrétien *et al*, New York: Gordon & Breach
- [46] Lin, C. C. and Lau, Y. Y., 1979, Density wave theory of spiral structure of galaxies, *Studies Appl. Math.*, **60**, 97 - 163
- [47] Lynden-Bell, D. and Pringle, J. E., 1974, The evolution of viscous disks and the origin of the nebular variables, *MNRAS*, **168**, 603 - 637
- [48] Mark, J. W-K, 1976, *Astroph. Jour.*, **206**, 418
- [49] Marouf, E. A., Tyler, G. L., Zebker, H. A., Simpson, R. A. and Eshleman, V. R., 1983, Particle size distributions in Saturn's rings from Voyager-1 radio occultation, *ICARUS*, **54**:189-211
- [50] Marouf, E. A., Tyler, G. L. and Rosen, P. A. 1986, Profiling Saturn's rings by radio occultation, *ICARUS*, **68**:120-166

- [51] Mizuno, H. 1980, Formation of the giant planets, *Prog. Theor. Phys.*, **64**, 544 - 557
- [52] Müller, G., 1893, Helligkeitsbestimmungen der grossen Planeten und einiger Asteroiden, *Pub. d. Astrophys. Obs. zu Potsdam*, **8**, 193-389
- [53] Nicholson, P.D. & Dones, L., 1991 *Rev. Geophys.*, **29**, 313
- [54] Nicholson, P. D. and Jones, T. J., 1980, IAU Circular No. 3515
- [55] Osterbrock, D. E. and Cruikshank, D. P., 1983, J. E. Keeler's discovery of a gap in the outer part of the A ring, *Icarus*, **53**, 165-173
- [56] Owen, T. *et al*, 1979, Jupiter's rings, *Nature*, **281**, 442 - 446
- [57] Pringle, J. E., 1981, *Ann. Rev. Astron. Ap.*, **19**, 137
- [58] Roche, R. A., 1847, *Akad. des Sciences et letters de Montpellier, Mem de la Section des Sciences*, **1**, 243 - 262
- [59] Rosen, P. A. and Lissauer, J. J., 1988, The Titan -1:0 nodal bending wave in Saturn's ring C, *Science*, **241**, 690 - 694
- [60] Rosen, P.A., Tyler, G.A. & Marouf, E.A. and Lisauer, J.J. *Icarus*, **93**, **25**, 1991
- [61] Safronov, V. S., 1972, *Evolution of protoplanetary cloud and formation of the Earth and Planets (Jerusalem: Israel Prog. for Sci. Trans.) NASA TT F-677*
- [62] Seeliger, H. von, 1887, *Zur Theorie der Beleuchtung der grossen Planeten, insbesondere des Saturn*, *Abhandl. Bayer. Akad. Wiss.*, **Kl. II**, **16**, 405-516
- [63] Seeliger, H. von, 1895, *Theorie der Beleuchtung staubformigen kosmischen Massen insbesondere des Saturn-ringes*, *Abhandl. Bayer. Akad. Wiss.*, **KL. II**, **18**, 1-72
- [64] Shakura, N. I. and Sunyaev, R. A., 1973, *Astron. Astrophys.*, **24**, 337

- [65] Showalter, M. R. *et al*, 1985, Discovery of Jupiter's Gossamer ring, *Nature*, **316**, 526 - 528
- [66] Showalter, M. R. *et al*, 1987, Jupiter's ring system: New Results on structure and particle properties, *Icarus*, **69**, 458 - 498
- [67] Showalter, M.R. and Nicholson, P. D., 1990, Saturn's rings through a microscope: Particle size constraints from the Voyager PPS scan, *Icarus*, **87**, 285 - 306
- [68] Shu, F. H., Cuzzi, J. N. and Lissauer, J. J. 1983, Bending waves in Saturn's rings, *ICARUS*, **53**:185-206
- [69] Shu, F. H., Milione, V. and Roberts, W. W., 1973, Non-linear gaseous density waves and galactic shocks, *Astrophys. J.*, **183**, 819 - 841
- [70] Shu, F. H. 1984, Waves in Planetary Rings, *Planetary Rings*, Ed. Brahic, A. and Greenberg, R., University of Arizona Press, Tucson
- [71] Sicardy, B. *et al* 1982, *A & A*, **108**, 296
- [72] Smith, B. A. *et al*, 1979, The Jupiter system through the eyes of Voyager 1, *Science*, **204**, 951 - 971
- [73] Toomre, A., 1964, On the gravitational stability of a disk of stars, *Astrophys. J.*, **139**, 1217 - 1238
- [74] Tyler, G. L., Eshleman, V. R., Anderson, J. D., Levy, G. S., Lindal, G. F., Wood, G. E. and Croft, T. A., 1981, Radio science investigations of the Saturn system with Voyager-I: Preliminary results, *Science*, **212**:201-206
- [75] Tyler, G. L. Marouf, E. A., Simpson, R. A., Zebker, H. A. and Eshleman, V. R., 1983, The microwave opacity of Saturn's rings at wavelengths of 3.6 and 13 cm from Voyager-1 radio occultation, *ICARUS*, **54**:160-188
- [76] Tyler, G. L., 1987, *Proc. IEEE*, **75**, 1404
- [77] Van Helden, A., 1973, The Academia del Cimento and Saturn's ring, *Physis*, **15**, 237-259

- [78] Woodward, P. R., 1975, On the non-linear time development of gas flow in spiral density waves, *Astrophys. J.*, **195**, 61 - 73